Lawrence Berkeley Laboratory
UNIVERSITY OF CALIFORNIA

CHEMICAL BIODYNAMICS DIVISION

SPECTROSCOPIC AND MAGNETIC PROPERTIES OF THE COMPLEXES OF THE HEME OCTAPEPTIDE FROM CYTOCHROME C

Esther Koo Yang
(Ph.D. thesis)

November 1979

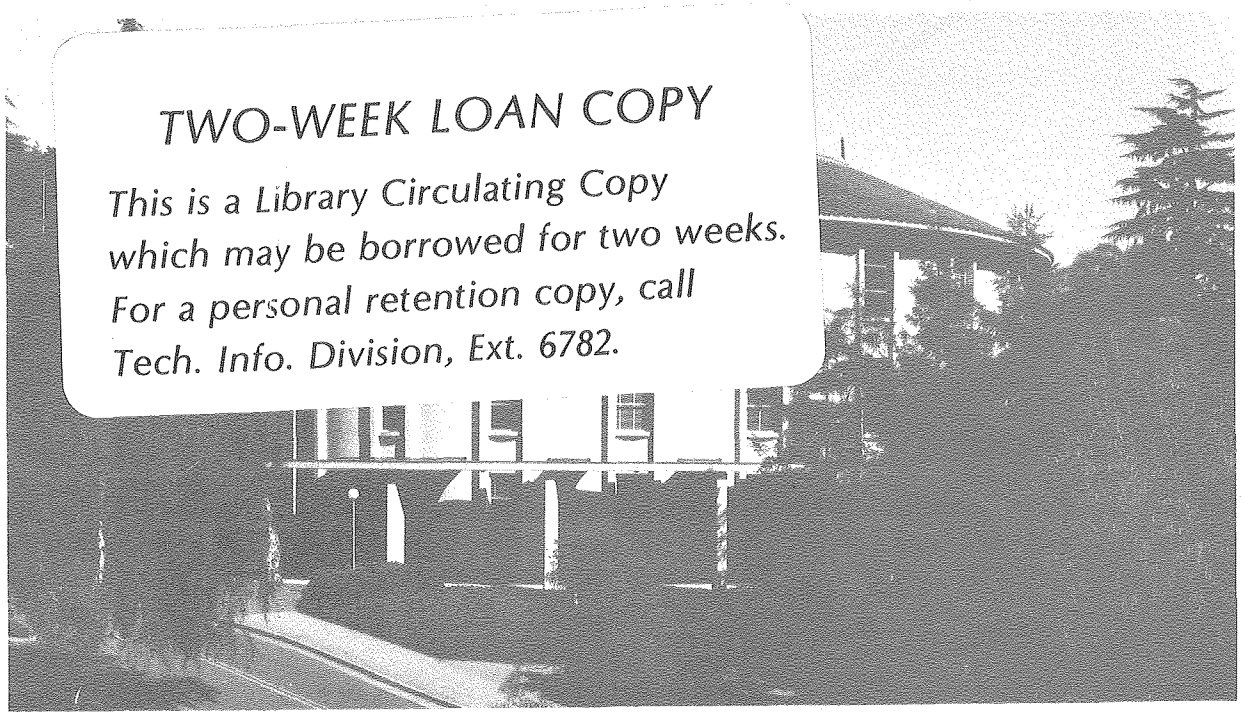

Prepared for the U.S. Department of Energy under Contract W-7405-ENG-48

DISCLAIMER

SPECTROSCOPIC AND MAGNETIC PROPERTIES OF THE COMPLEXES OF THE HEME OCTAPEPTIDE FROM CYTOCHROME C

Esther Koo Yang

Lawrence Berkeley Laboratory
University of California
Berkeley, California

This work was prepared with the support of the U. S. Department of Energy under Contract W-7405-ENG-48.

SPECTROSCOPIC AND MAGNETIC PROPERTIES OF THE COMPLEXES OF THE HEME OCTAPEPTIDE FROM CYTOCHROME C

by

Esther Koo Yang

ABSTRACT

Detailed ligand binding effects have been examined in a model system of cytochrome c, the N-acetylated ferric heme octapeptide (N-H8PT) directly isolated from horse heart cytochrome c. The room temperature absorption and magnetic circular dichroism (MCD) spectra of the complexes of N-H8PT with various external ligands such as F^-, H_2O, OH^-, N_3^-, imidazole (Im) and CN^- are found to behave generally as predicted from ligand field considerations. These results are consistent with the paramagnetic susceptibility measurements. There is a direct correlation between the Soret absorption band position, β band intensity or the Soret MCD intensity and susceptibility.

The N-acetylated methionine complex of the N-H8PT, which shares identical axial coordination as the parent molecule, however, exhibits thermal equilibrium of spins between high and low spin states, while cytochrome c exists in the purely low spin state. The presence of thermal spin equilibrium in the model complex is not due to incomplete methionine binding nor bis-methionine complex formation nor carboxyl ligation. Temperature dependence of paramagnetic susceptibility of the methionine complex yields

ΔH° = -7.6 kcal/mole and ΔS° = -25.9 e.u. for a high spin to low spin transition demonstrating a compensation effect between the two thermodynamic parameters. The low temperature ESR spectrum of the methionine complex indicates a low spin ground state with g values at 2.91, 2.31 and 1.51 which are distinct from the g values of cytochrome c. The axial (Δ) and rhombic (V) distortion parameters in the t_{2g} set of orbitals correspond to 1200 cm^{-1} and 780 cm^{-1}, respectively.

From these results, a model is proposed to account for the uniqueness of the methionine complex: a change in Fe-S distance may play a role in regulating the redox properties of cytochrome c.

DEDICATION

To my mother and my lovely daughter, Michelle.

ACKNOWLEDGEMENTS

I am deeply indebted to my research director, Professor Kenneth Sauer who has taught me the art of scientific research through encouragement, warm understanding and criticism. I would especially like to express my deep gratitude for the immense patience he has shown me to the completion of this thesis. I thank him for the support during my preparation for parenthood. Above all, I appreciate him for allowing me the independence which inspired me to gain scientific maturity and creativity.

I would like to thank Professor Larry Vickery for the many fruitful suggestions and guidance throughout this work.

I would also like to thank my dear friend, Anne McGuire who shared with me all the tears and laughs during our graduate life. I like to thank Nonon Kafka, Kyong Yoon and all of my fellow graduate students for their friendship. I am also thankful to Chuck Dismukes and Richard Friesner for many discussions on the theoretical aspects of hemeprotein chemistry. I am indebted to Marshall Tuttle who with his superb typing skill made the completion of this thesis possible. I must also thank my husband Duck, for his support and care in difficult times.

TABLE OF CONTENTS

CHAPTER I

INTRODUCTION

CHAPTER I

Biological systems in which metal ions are essential for activity are common. Among them the iron-porphyrin containing complexes are of special importance because they are ubiquitous in nature. In addition to that, hemeproteins are involved in a wide variety of physiological functions such as oxygen transport and storage, substrate reduction, oxidation and hydroxylation reactions, and electron transport. Oxygen transport in most mammals is carried out via reversible binding of oxygen to reduced hemoglobin molecules, Fe(II), which are found in red blood cells. Oxygen storage is the function of myoglobin which can release oxygen at lower partial pressures of oxygen than hemoglobin. Cytochromes are involved in electron transfer processes. The electron transfer proceeds via changing the redox state of the iron between ferric (Fe(III)) and ferrous (Fe(II)) forms. The chemical potential energy gained during the transfer of an electron from one redox component to another may be used in the energy transduction process which appears in the form of oxidative phosphorylation in mitochondria. Cytochromes are found in electron transport chains of photosynthesis, microsomal drug metabolism and many other energy conserving mechanisms of various micro-organisms (1). One other major class of hemeproteins are the catalases. They include oxidases and peroxidases which utilize molecular oxygen or hydrogen peroxide in their catalytic reactions to oxidize,

reduce or hydroxylate substrates. Cytochrome c oxidase is a fine example of this category. It reduces oxygen to a water molecule while oxidizing the substrate which is cytochrome c. An interesting point one can find is that hemeproteins are equipped with the ability to undertake such diverse functions even though they share more or less the same prosthetic group(s) at the active site. In this regard, detailed understanding of the structural features associated with each catalytic function seems extremely helpful in advancing our knowledge of hemeproteins.

The aim of this thesis work is to examine the structure-function relations in one class of hemeproteins, cytochromes. Naturally the main question concerns the structural factors associated with the regulation of the redox properties of cytochromes. Is it the intrinsic ability of the heme group? Is it the manner in which the heme is interacting with the remainder of the protein molecule? Or how significant is the specific folding of the protein? It is most likely the composite effect of many subtle changes. For example, even within the same type of cytochromes, namely type c, the observed mid-point potential may vary between -50 mv and +400 mv (1,2). This suggests that subtle structural variation at the heme group and its immediate local environment must be extremely effective in changing the mid-point potential. For instance, the mid-point potential is a sensitive function of pH which alters conformation and effective charge of the enzyme (3,4). pH may also change the nature of the axial ligand(s). In cytochrome c,

chemical modification of the amino acid side chains only in the deepest part of the heme crevice is known to affect the redox properties (5). If the structure of the heme chromophore is examined, the central iron ion is hexacoordinated. Four of the ligands are provided by the pyrrole nitrogens of a planar porphyrin ring and the remaining two axial ligands, by the amino acid side chains of the protein in which one of the axial ligands may be a water molecule. The magnetic state of the iron which is in large part determined by the chemical identity of the axial ligands is known to play a significant role in regulating the redox properties. A change in the spin state from a low spin (S = 1/2) to high spin (S = 5/2) state may induce a shift of reduction potential by differentially altering the importance of the π acceptor power of the ligand which leads to a higher reduction potential and the electron donor power of the ligand which gives rise to a lower reduction potential (2). In addition, model studies show that at least +160 mv shift is expected for the ligand change from histidine to methionine even though both ligands are of low spin type (6). This is in good accordance with the fact that most of b type cytochromes, i.e. bis-imidazole complex, indeed exhibit lower reduction potential than type c cytochromes as in mitochondria or photosynthetic apparatus in chloroplasts. Many data on the effect of axial ligands on redox potential are available, but more elaborate molecular mechanisms of electron transfer still remain to be investigated.

My approach is first to characterize as thoroughly as possible the electronic and magnetic properties of the heme group through detailed ligand binding studies, and to find meaningful correlation between the heme group and its immediate protein environment. Cytochrome c is particularly convenient for this purpose since the electronic structure of the heme group is already known fairly accurately and the high resolution x-ray analysis (7) as well as the primary amino acid sequence (8) have been studied. Indeed, cytochrome c is one of the most widely characterized heme-proteins. In order to simplify the problem, a model system is chosen which mimics closely the native heme environment without having any extensive protein conformation. The model system is the heme peptide fragment directly isolated from horse heart cytochrome c which was first isolated by Tuppy and Pelius in 1955 (9). Described in this chapter are the physico chemical properties of cytochromes, in particular cytochrome c. Chapter II includes the theoretical basis for the techniques applied in the investigation of the electronic and magnetic properties. In Chapter III, isolation and characterization of the heme peptides, and their aggregation properties [as studied by circular dichroism (CD) spectra) are discussed. Chapter IV describes the optical behavior of the various complexes of the heme octapeptide with externally added ligands, which consist of absorption and magnetic circular dichroism (MCD) spectral properties. Since magnetic properties are intimately related to electronic structures,

the magnetic methods are powerful means of studying biological molecules which contain unpaired electrons. In the last chapter, discussion is focused on the magnetic properties of iron which are monitored by the two complementary techniques, namely direct measurement of room temperature paramagnetic susceptibility and sub-zero temperature electron spin resonance (ESR) measurements.

Cytochrome c

Cytochrome c is the most widely occurring and thoroughly characterized of all heme proteins found in cells from mammals to invertebrates and yeast (1). Cytochrome c was named and first described in the classical work of Keilin (10,11). Cytochromes in general can be classified into four main groups which are distinguishable by their prosthetic heme groups as shown in Figure 1.

1. cytochrome a: cytochromes in which the heme group contains a long formyl side chain (Figure 1a). The heme is held into the protein mostly by non-specific hydrophobic interaction.
2. cytochrome b: The heme group is iron protoporphyrin IX, protoheme (Figure 1b). Again hydrophobic interaction is the dominant force between the heme and protein.
3. cytochrome c: The heme group (protoheme) is covalently linked to the protein via two cystinyl thioether bridges at the vinyl side chain sites (Figure 1c). Today only thioether linkages are known.

Figure 1. Taken from R. Lemberg and J. Barrett, "Cytochromes", Academic Press, London and New York, 1973.

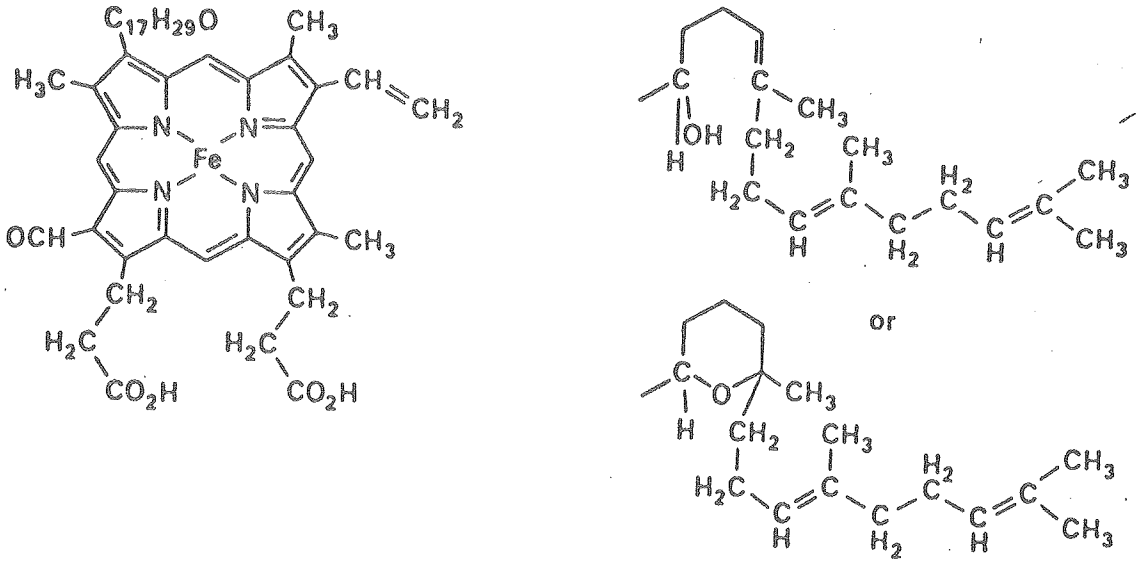

FIG. 1a. Haem *a* (Cytohaem *a*)

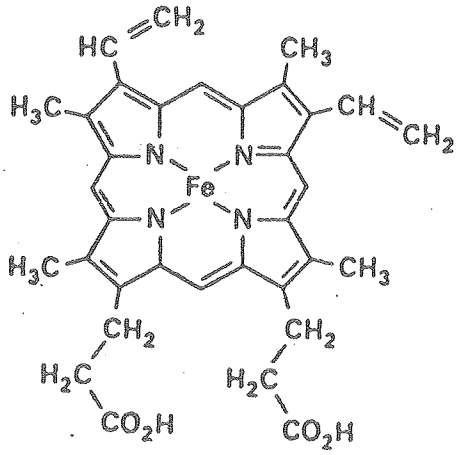

FIG. 1b. Protohaem (Cytohaem *b*).

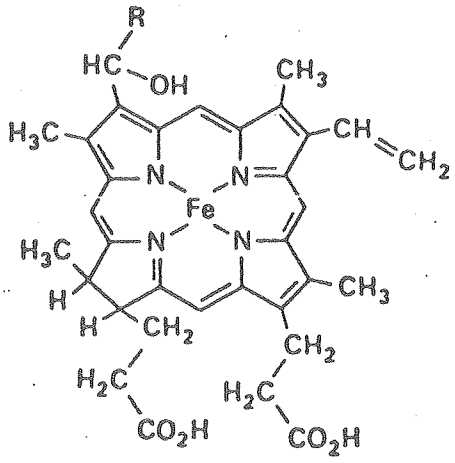

FIG. 1d. Cytohaem *d*.

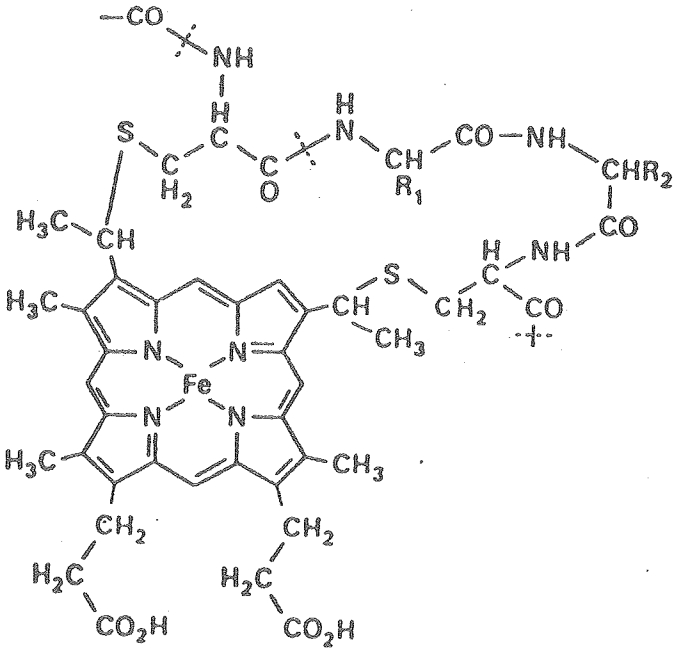

FIG. 1c. Haem *c* (Cytohaem *c*).

4. cytochrome d: The heme group is iron dihydroporphyrin, chlorin (Figure 1d).

Spectroscopically these hemeproteins may be distinguished by the position of the α band of the bis-pyridine hemochromogen [Fe(II)] spectra: 580-590 nm for cytochromes a, 556-558 nm for cytochromes b, 549-551 nm for cytochromes c and 600-620 nm for cytochromes d. This is due to the tendency to shift the absorption maxima to longer wavelength by electrophilic side chains. To extend the specification, some of the newly found cytochromes are designated as, for example, cytochrome b_{562} (*Escherichia coli*) where the subscript indicates the α band position and parenthesis, its source. However, names such as cytochrome f (type c) or A_2 (type d) are so widely used that they are still in use. And no alternative names are given to cytochromes o and P-450, cytochromes cc' or c' which are bacterial in origin and represent the heme group in which one of the axial coordinations differs from a typical cytochrome c (1). These compounds show a more hemoglobin-like spectrum and react easily with external ligands with which cytochrome c does not react. Cytochrome c oxidase (cytochrome aa_3) is regarded as type a even though it also contains two copper ions. Strictly speaking, cytochrome c has no clearly definable prosthetic group since the heme is built into the protein by covalent linkages. With all these exceptions, one can still classify most cytochromes according to the heme group. The structure of the protoheme which is also the prosthetic group of hemoglobin, myoglobin, catalases,

horse radish peroxidase and cytochrome c peroxidase is well known and was proven as early as 1926 by Fischer (12) who succeeded in synthesizing the heme.

Cytochromes are essential components of cellular respiration, photosynthesis and anaerobic dark processes of bacteria such as nitrate reduction and sulfate reduction. Figure 2 shows the sequence of electron flow in the respiratory chain components in the inner membrane of mitochondria (13). NADH collects electrons from many different substrates through the action of NAD-linked flavoprotein dehydrogenases. Other respiratory substrates may also be dehydrogenated by flavin-linked dehydrogenases, such as succinate dehydrogenase and acyl-CoA dehydrogenase, which funnel electrons into the chain via ubiquinone (UQ). The sequence from NADH to oxygen is now fairly well established: electrons flow from lower reduction potential to higher reduction potential which is down hill in free energy change. Apparently, decline in free energy during the passage of an electron from NADH to oxygen is enough to synthesize several ATP molecules, by which the energy can be conserved. The three sites (I, II and III) in Fig. 2 indicate the site of ATP synthesis. The role of cytochrome c is to shuttle electrons between cytochrome c reductase (cytochrome c_1) and cytochrome c oxidase (cytochrome aa_3) at which molecular oxygen is reduced to water. Cytochrome c is a peripheral protein, and thus is easily isolable under a mild condition, while all the other cytochrome components in a respiratory chain are membrane bound. Great

Figure 2. Taken from A.L. Lehninger, "Biochemistry", Worth Publishers Inc., New York, 1972.

Mitochondrial Respiratory Components

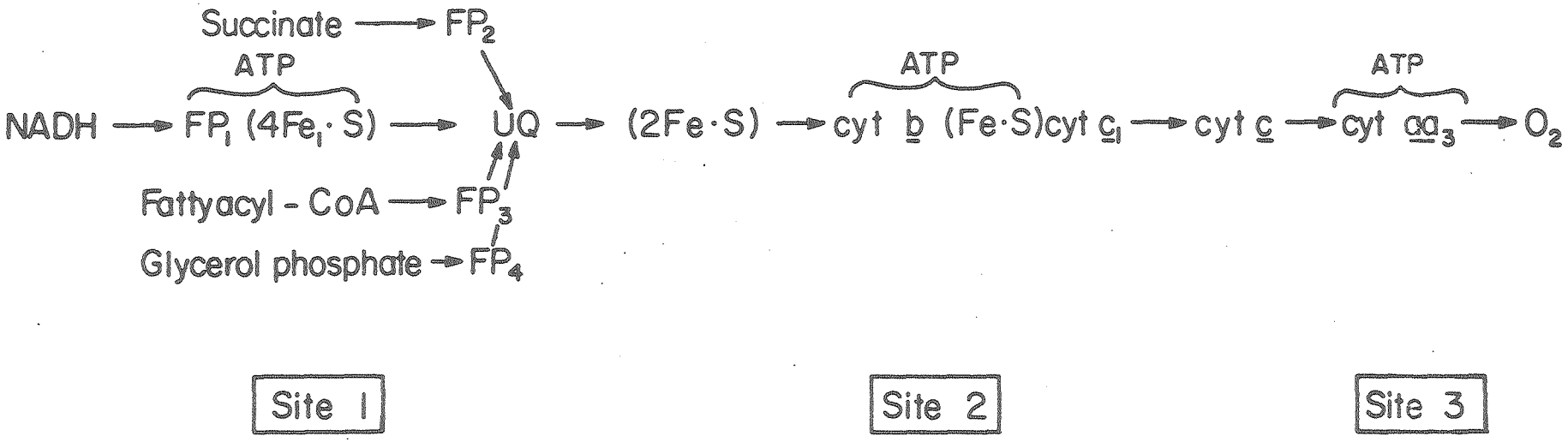

EY 23

solubility in concentrated ammonium sulfate solution allows removal of the more easily precipitated protein impurities. Because of remarkable stability to drying and heat, cytochrome c was isolated in nearly pure state by Keilin (14) and Theorell (15) as early as 1935. Cytochrome c is not auto oxidizable and does not react with CO (16). The mid-point reduction potential of eukaryotic cytochrome c is +255 mv at pH 7. The molecular weight of cytochrome c from eukaryotic cells ranges between 12,000 and 13,000, and it consists of 104 amino acid residues. Figure 3 shows the diagramatic representation of mammalian cytochrome c obtained based upon a recent high resolution x-ray analysis (7). In Fig. 3a, the amino acid sequence and folding of the protein are given, which include the site of two thioether bridges. In addition the two axial ligands, histidine 18 and methionine 80 are indicated. The single polypeptide chain of 104 amino acid residues is wrapped around the heme in two halves; the residues 1 to 47 to the right and 48 to 91 to the left of the heme, which provide the heme crevice with one edge exposed to the solvent medium. Residues 92 to 104 form an α helix that rises over the top rear of the molecule. No disulfide bridges are present. The dark circles represent residues that are buried in the interior of the molecule while attached black dots mark residues whose chains pack against the heme. Arrows from tryptophan 59 and tyrosine 48 to the buried propionic acid group represent hydrogen bonds. Figure

Figure 3. Taken from R.E. Dickerson et al., J. Biol. Chem. 246, 1511 (1971).

Cytochrome c

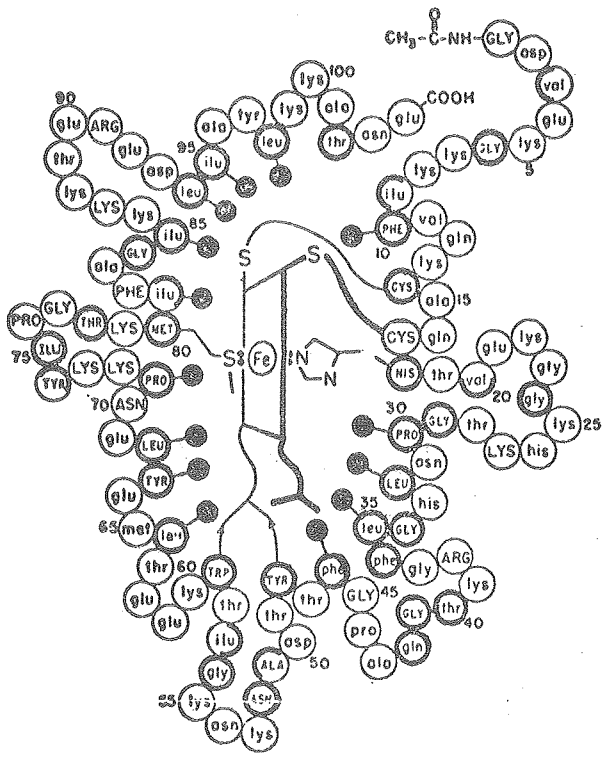

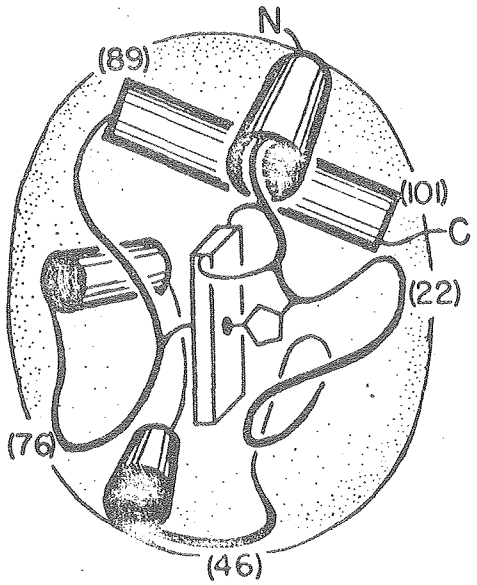

EY 22

3b depicts the region of α helical straps as cylinders. The numbers in parenthesis indicate residue numbers. The α helix content is estimated to be 10% as a lower limit from the polypeptide circular dichroism spectral results. As can be seen, the heme is enclosed by the hydrophobic residues which are invariant in many species. This is reasonable since the hydrophobic residues may play an essential role in providing the proper heme environment. One of the most distinct features of cytochrome c is the high lysine content - 19 residues are found in horse cytochrome while only 12 acidic residues are observed. In fact cytochrome c is a basic protein with an isoelectric point near pH 10 (17). Furthermore, acidic and basic groups are segregated as patches on the molecular surface and these regions are found to remain similarly charged in many species even if the individual residues may vary. In most globular proteins, the charged groups that are not directly involved in catalytic sites play a role in maintaining an optimum pK for the molecule by a proper balance between acidic and basic groups. In cytochrome c, segregation of charge seems necessary since it has to interact with several macromolecules like the reductase, oxidase and membrane itself. Macromolecular binding sites may be recognized by the distribution of surface charge. For instance, the basic lysyl side chains are essential for binding of oxidase. If the lysyl residues are chemically modified such that its basicity becomes lost, the electron

transfer from cytochrome c to oxidase also becomes inhibited (18). Some conformational change is evident upon reduction and oxidation of cytochrome c. Several evidences include 1) the sixth ligand exchange with external ligand such as cyanide is easier in the oxidized state, 2) the reduced protein is less susceptible to trypsin hydrolysis, 3) the reduced protein is more stable to heat, and 4) the nuclear magnetic resonance (NMR) spectra are also different in the two states. All suggest a more compact structure of the reduced cytochrome c with the heme crevice closed or blocked. The effects of solvent perturbation, denaturation by urea, ionic strength and pH indicate that cytochrome c exists in a number of conformational states that may best be differentiated by absorption and optical rotatory dispersion (ORD) or circular dichroism (CD) spectral features (19). For ferricytochrome c, between pH 2.8 and 8.5, little change in protein conformation is observed. Below pH 2.5, the protein unfolds, the methionine ligand is replaced by a chloride ion if the low pH is achieved by the addition of hydrochloric acid, and even the imidazole ligand may be replaced or at least protonated. At this low pH, if the ionic strength is increased, however, some of the α-helical content is recovered. Methionine ligand may also be replaced by lysine with a pK value of 9.3 (20). And in the extreme alkaline region (pH > 12.5) the denaturation effect appears similar to the one observed at the low pH. The loss of methionine ligand that may be monitored by disappearance of an

absorption at 695 nm is directly correlated with the loss in enzymatic activity (21-23). This implies that the methionine ligand must play an essential part in maintaining a correct reduction potential of cytochrome c, or the electron transfer actually occurs via the methionine ligand. An interesting observation is that cytochrome c contains several aromatic rings which tend to occur in parallel pairs throughout many different species (Fig. 3a) for example, tryptophan 59 and tyrosines 67 and 74 to the left and phenylalanine 10 and tyrosine 97 to the right. The right side leads to histidine 18 and left side to methionine 80 residues. These aromatic side chains are thought to provide chain flexibility (18) to allow passage of an electron from the surface to the iron which is known as the "Winfield" mechanism of electron transfer (24).

REFERENCES

1. R. Lemberg and J. Barrett, "Cytochromes", Academic Press, London and New York, 1973.

2. R.J.P. Williams, FEBS Letters, 79, 229 (1977).

3. Y.P. Myer and H.A. Harbury, Annals New York Academy of Sciences, p. 685, 1967.

4. H.A. Harbury and P.A. Loach, J. Biol. Chem. 235, 3640 (1960).

5. A. Pande, A.F. Saturno and Y.P. Myer, Biophysical Journal, Abstracts, 23rd Annual Meeting, p. 125a, 1979.

6. T. Mashiko, J.-C. Marchon, D.T. Musser, C.A. Reed, M.E. Kastner and W.R. Scheidt, J. Am. Chem. Soc. 101, 3653 (1979).

7. R.E. Dickerson, T. Takano, D. Eisenberg, O.B. Kallai, L. Samson, A. Cooper and E. Margoliash, J. Biol. Chem. 246, 1511 (1971).

8. E. Margoliash and A. Schejfer, Adv. Protein Chem. 21, 113 (1966).

9. H. Tuppy and S. Paléus, Acta Chem. Scand. 9, 353 (1955).

10. D. Keilin, Proc. Roy. Soc. London, B, 98, 312 (1925).

11. D. Keilin, Proc. Roy. Soc. London, B, 100, 129 (1926).

12. H. Fischer and H. Orth, "Die Chemie des Pyrrols" Pyrrolfarbstoffe II, Erste Hälfte. Akademische Verlagsgesellschaft, Leipzig, 1937.

13. A.L. Lehninger, "Biochemistry", Worth Publishers, Inc., New York, 1972.

14. D. Keilin, and E.F. Hartree. Proc. Roy. Soc. London, B, 122, 298 (1937).

15. H. Theorell, J. Am. Chem. Soc. 63, 1820 (1941).

16. H. Theorell and A. Akeson, J. Am. Chem. Soc. 63, 1804, 1812, 1818 (1941).

17. E. Racker, "Membranes of Mitochondria and Chloroplasts" edited by E. Racker, Van Nostrand Reinhold Company, New York, p. 127, 1970.

18. R.E. Dickerson, T. Takano, O.B. Kallai and L. Samson, "Structure and Function of Oxidation-Reduction Enzymes" Vol. 18, 69, Pergamon Press, 1970.

19. R. Mirsky and P. George, Biochem. 56, 222 (1966).

20. D.O. Lambeth, K.L. Campbell, R. Zand, and G. Palmer. J. Biol. Chem., 248, 8130 (1973).

21. E. Schechter and P. Saludjian, Biopolymers 5, 788 (1967).

22. W.A. Eaton and R.M. Hochstrasser, J. Chem. Phys. 46, 2533 (1967).

23. M.T. Wilson and C. Greenwood, Eur. J. Biochem. 22, 11 (1971).

24. M.E. Winfield, J. Mol. Biol. 12, 600 (1965).

CHAPTER II

ELECTRONIC STRUCTURE AND MAGNETIC PROPERTIES OF HEMEPROTEINS

CHAPTER II

INTRODUCTION

Spectroscopic properties of hemoproteins or iron porphyrins are much more complex than those of other metalloporphyrins owing to extensive mixing between porphyrin π and iron $d\pi$ orbitals. Interpretation of the electronic spectra of hemoproteins thus requires thorough understanding of the electronic structure of porphyrin and magnetic properties of iron. This chapter provides the theoretical basis for interpreting the hemoprotein spectra.

The skeletal structure of porphyrin consists of four pyrrole groups linked by methine bridges into a planar ring structure. The side chain assignment for protoporphyrin IX, a common prosthetic group in heme proteins, is given in Fig. 1. The porphyrin macrocycle contains eleven conjugated double bonds but only nine of these are required to form a fully conjugated cyclic polyene (thick trace of Fig. 1a) (1). If the two nitrogen atoms involved are regarded as equivalent to methine groups, this 18-atom, 18-electron ring system satisfies the Hückel rule, $4n+2$, for aromaticity. This conjugation can not be used as a model for metal porphyrins, however. The well resolved x-ray structural analysis of porphyrins to nickel derivatives shows that the lengths of four C-C bonds from ring I and III (arrows in Fig. 1a) are distinctively longer than in a corresponding aromatic system (2). Different bond lengths would have to be introduced, which is not characteristic of having full aromaticity.

Figure 1.

a) The "outer" conjugation path of the metal porphyrin. It passes through a total four α,β-pyrrole bonds (arrows).

b) The "inner" conjugation path of metal porphyrin, in which only the atoms in contact with the metal atom are included.

a

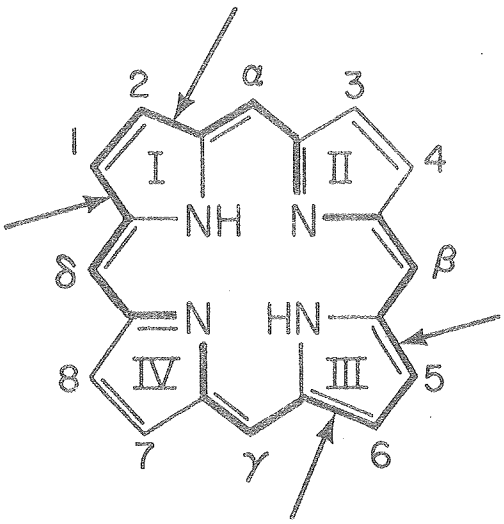

b

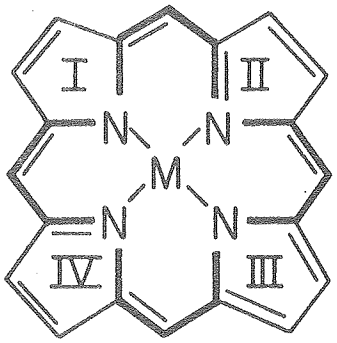

Porphine: 1,2,3,4,5,6,7,8,α,β,γ,δ: H

Protoporphyrin IX: 1,3,5,8: methyl
2,4: vinyl
6,7: propionic acid
α,β,γ,δ: H

XBL 787-4073

According to the x-ray results, a more appropriate model appears to be the one with the inner conjugation system (thick trace of Fig. 1b) which consists only of atoms in contact with the central metal ion. In this model, all the bond lengths are equal and are close to those of aromatic compounds. However, from the formal standpoint, this is not a cyclic polyene: it consists of 16 atoms and 6 π double bonds. It is best characterized as the porphyrin dianion in which the four nitrogen atoms are replaced by methine groups and two electrons of the metal ion are also included. The aromaticity of this model, first proposed by Gouterman, (3,4) is discussed by Corwin, et al (5).

Most hemoproteins contain iron protoporphyrin IX as the chromophore (the sidechain assignment is shown in Fig. 1). Addition of aromatic sidechains such as vinyl groups affects the electronic structure of porphyrin due to their electron donating nature. In cytochromes of type c, these vinyl side chains are broken because the heme is thioether bonded to the protein at the two vinyl sites (6). The central iron ion in hemoproteins is hexacoordinated; four ligands are provided by the nitrogens of pyrrole groups and the two axial ligands may come from protein amino acid side chains, or one may be a small molecule like water. In cytochromes, the axial ligands are thought to play a significant physiological role in electron transport. The chemical nature of the axial ligands controls the spin state of iron

which reflects magnetic properties of the unfilled outer shell d orbital electrons. The iron atom may exist in high, intermediate or low spin ground state in either redox state depending on the net effective ligand field environment. At room temperature where the protein is physiologically active, however, a large number of hemoprotein derivatives exhibit thermal equilibrium between high and low spin states. In iron porphyrins, the effective ligand field strength within the heme plane is much stronger than that out of the plane (7). The x-ray structural analysis shows that the iron-to-ligand bond length is typically shorter within the heme plane than in the axial direction (2). Thus the axial ligands seem to provide a fine control for obtaining thermal equilibrium of spins. This fine tuning of thermal equilibrium of spins is thought to play a role in regulating the function of hemoproteins (8). The physical origin of this phenomenon is discussed on the basis of ligand field theory. Complexes involving the intermediate spin ground state or quantum-mixed-spin ground state are much less well characterized. In contrast to thermal mixture of spin states in which protein molecules exist in two magnetically distinguishable pure spin states, a protein molecule having a quantum admixture of spin states corresponds to a single magnetic species with magnetic properties distinct from either pure spin states. In one class of hemoproteins, i.e. bacterial cytochromes c', the ground spin state has been claimed by Meltempo, et al (9,10) to be the quantum-mixed state between high and

intermediate spin states. Magnetic properties of iron may be monitored by the direct measurement of paramagnetic susceptibility or by the low temperature electron spin resonance (ESR). Both techniques measure the Zeeman effect of the degenerate states of iron in the applied magnetic field. The theoretical basis for the two methods is discussed in detail. Magnetic circular dichroism also measures the Zeeman splitting of the degenerate states of iron in the applied magnetic field but the virtue of this technique is its association with the electronic transitions of porphyrin. Because there is extensive mixing between iron $d\pi$ and porphyrin π orbitals, the singlet ground state of porphyrin reflects the spin degenerate ground state of iron. This leads to the paramagnetic MCD effect due to the thermal distribution of spins according to Boltzmann factors among the spin multiplets of the ground state. Current views on the origin of Soret MCD of ferric hemoproteins are discussed.

ABSORPTION SPECTRA OF HEMOPROTEINS

A. Electronic Structure of Porphyrins

Free Electron Model

The electronic spectrum of porphyrin can be successfully explained by a simple model in which all 18 π electrons are treated as being free to circulate in a ring (Fig. 1a) (11). In this model, each electron is given orbital angular momentum that can be attributed to circulation about the porphyrin ring.

Because circulating to the left or to the right are equal in energy in the absence of magnetic and electric fields, this leads to a simple energy level diagram shown in Fig. 2, where the energy levels are labeled by their angular momentum, ℓ. The ground state has a closed shell with no net angular momentum. Two doubly degenerate singlet electronic transitions are possible as indicated by the arrows with a resultant angular momentum of $\pm$ 1 if the transition takes place between energy levels having the corresponding quantum numbers with the same sign, or $\pm$ 9 if the sign changes. The former transition is "allowed" according to Hund's rule while the latter is "forbidden". Hund's rule also indicates that for a given multiplicity, the lowest energy states have the greatest angular momentum: the model predicts an intense transition at high energy and a weak transition at lower energy which correspond to Soret and visible absorption bands, respectively.

Four Orbital Model

More quantitative interpretation of the electronic spectrum of porphyrin can be obtained using a four orbital model proposed by Gouterman (4). The model considers excitations only from the two highest filled orbitals to the two lowest empty orbitals. The molecular orbitals are calculated under the D_{4h} point group using the extended Hückel model in which all valence orbitals of each atom involved in a 16-membered ring shown in Fig. 1b are included.

Figure 2.

a) Orbital energy levels.

b) Transition energies.

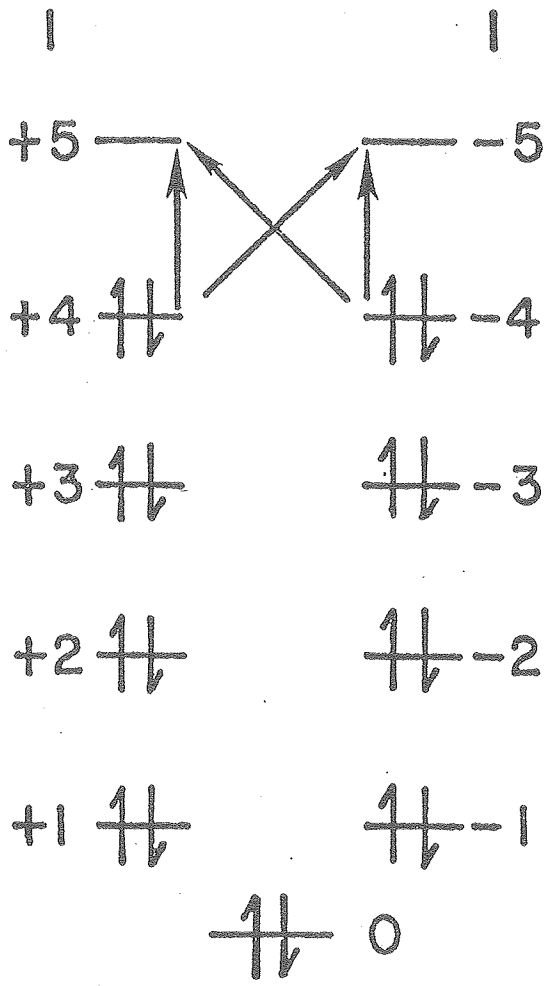

ORBITAL ENERGY LEVELS

(a)

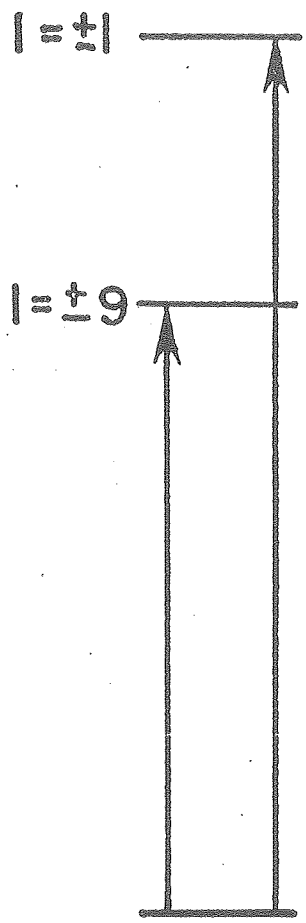

TRANSITION ENERGIES

(b)

XBL 7610-4841 A

(For metalloporphyrins, the 3d, 4s and 4p orbitals of a metal ion are also included in MO calculation.) The resultant symmetry assignments for the highest filled orbitals in D_{4h} are A_{1u} and A_{2u} and for the lowest empty orbitals, e_g are shown in Fig. 3. The A_{1u} and A_{2u} orbitals are nearly degenerate in energy which allows two doubly degenerate electronic excitations of nearly same energy and of same symmetry, E_u (the arrows in Fig. 3). This leads to strong configuration interaction and results in two new doubly degenerate transitions which arise from addition or subtraction of the transition dipoles. The model predicts a very intense absorption band at high energy, the Soret band, and a weak band at low energy, Q band. Two bands appear in the visible region because 0-1 vibronic component (Q_{0-1}) on the high energy side of the 0-0 transition (Q_{0-0}) becomes active. Q_{0-0} and Q_{0-1} are commonly referred to as α and β bands, respectively.

The free electron model is incapable of including metal ions except as small perturbations, because it deals with π electrons of the porphyrin only. On the other hand, the four orbital model can accomodate valence orbitals of metal ions in the bases set atomic orbitals and thus is capable of predicting the extent of d orbital mixing into porphyrin π orbitals. In most cases, the energies of porphyrin π orbitals have been shown to be well separated from those of

Figure 3. Electronic transitions in a four orbital model.

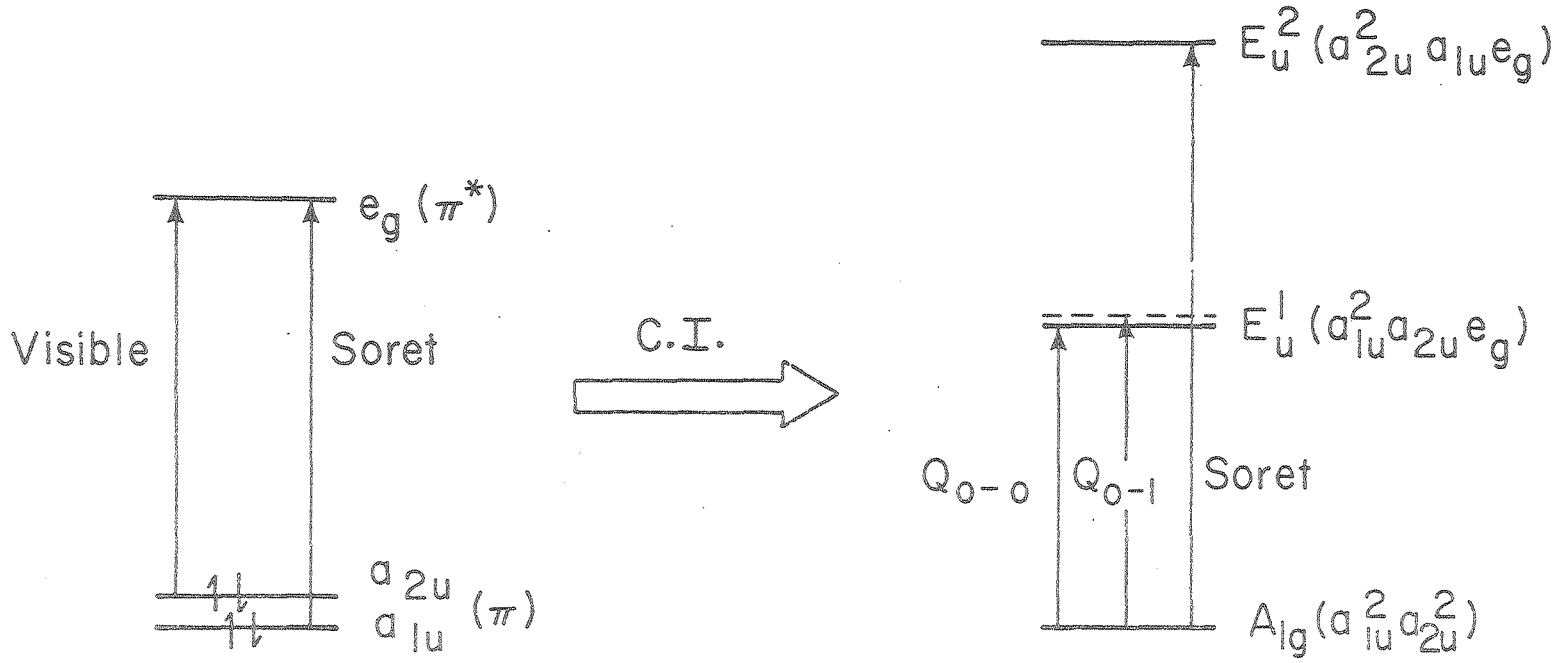

Single electron energy level of a four orbital model

D_{4h}

Molecular energy levels of a four orbital model

D_{4h}

XBL 786-4003

the d orbitals such that little mixing occurs. However, iron and manganese porphyrins are exceptions. There is extensive mixing between iron $d\pi$ and porphyrin π orbitals of these metalloporphyrins, which complicates interpretation of the absorption spectra. The success of Gouterman's model is in its ability to predict both the position and intensity of the absorption bands in metalloporphyrins.

B. Ligand Field Theory of a d^5 System (Fe^{+3})

The ligand field theory is essentially the refinement of the crystal field theory. In the crystal field model, the influence of ligand atoms on the central ion for a given coordinate cluster is treated as being purely electrostatic (12,13). The crystal field strength does not depend on the nature or positions of the ligand atoms associated with the metal ion but only on the effect of interaction potentials on the electrons of the central ion. By contrast, the ligand field theory covers all aspects of the manner in which a metal ion is influenced by its nearest neighbor atoms, including the strength of the metal-ligand bond, stereochemistry and coordination number. In practice, however, the ligand field theory is of little use unless certain approximations are made. The progression from treating the ligand atoms as point charges through point dipoles to a simple molecular orbital model still leaves the quantitative calculation of the ligand field effect unsatisfactory. Thus, the ligand field effects will be explained from the crystal field approach. For example, whether or not all the ligands are identical, we use the term "octahedral" to refer to a coordination cluster in which six

ligands are located at the vertices of a regular octahedron.

Transition metal complexes possess unfilled outer shell 3d orbital electrons which constitute the basis for their observed spectral and magnetic properties. In Fig. 4 is shown a single electron d orbital energy diagram in different crystal field environments. In the free ion case, the five d orbitals are degenerate in energy. When the metal atom is placed in an octahedral coordination sphere, O_h, where the crystal field strength is equivalent in each direction (x, y and z), the five-fold degenerate d orbitals are split into two levels: t_{2g} and e_g states. The t_{2g} set includes d_{xy}, d_{xz} and d_{yz} orbitals and the e_g set contains $d_{x^2-y^2}$ and d_{z2}. The latter lies higher in energy because the orbitals pointing in the direction of the ligands experience greater electron repulsion. Typically the energy separation between the two levels corresponds to about 10,000 cm^{-1} which is commonly referred to as the crystal field energy, Δ (12). As the O_h symmetry is lowered to D_{4h}, in which the axial crystal field is different from the in-plane field, the d orbitals are split further into four levels. In the case of hemoproteins where the axial field is much weaker than that in-plane (tetragonal), d_{z2} lies lower than $d_{x^2-y^2}$ while d_{xz} and d_{yz} lie higher than d_{xy}, as illustrated in Fig. 4. When the D_{4h} symmetry is even further reduced to D_{2h}, where inequivalency in x and y directions is induced due to rhombic distortion, the degenerate e_g state (d_{xz} and d_{yz}) is split.

Figure 4. Single electron d orbital energy levels in different ligand fields.

Single Electron d Orbital Energy Diagram

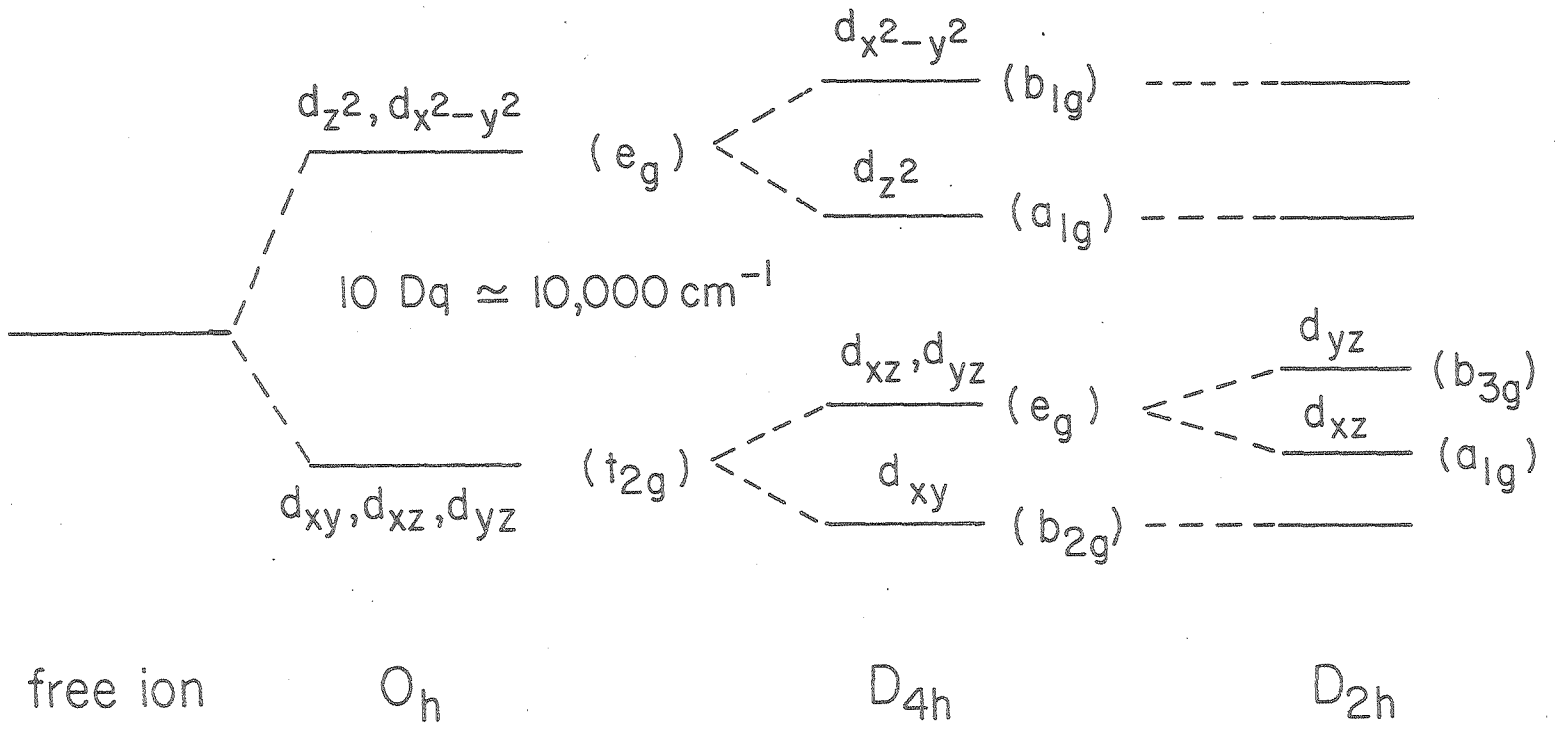

XBL 787-4054

Ferric ion (Fe^{3+}) has five d orbital valence electrons, d^5, which may exist in different spin states depending on the crystal field strength. Figure 5 (top figure) shows the energy correlation diagram between weak and strong crystal field limits for d^5 in O_h symmetry (12). Weak crystal field environment refers to a situation where the electron repulsion (or pairing) energy exceeds the crystal field energy. In such a case the ground state will have the highest spin multiplicity, following Hund's rule. In other words, the maximum number of unpaired electrons is achieved; i.e., the total spin is S = 5/2, which is called the high spin state. Because each orbital contains one electron, there will be no net orbital angular momentum; thus, the ground state has $^6A_{1g}$ symmetry in O_h. In the strong crystal field limit, the electron repulsion energy is overcome by the large crystal field energy. The electrons are now forced to pair up leaving only a single unpaired electron in the ground state. It is evident then, that the total spin becomes S = 1/2, which is called the low spin state, and the ground state symmetry corresponds to $^2T_{2g}$. Most hemoproteins exist in either a high or low spin ground state, but a significant number of hemoprotein derivatives exhibit thermal spin equilibrium between high and low spin states near room temperature (14). Such a phenomenon can occur when the net effective ligand field

Figure 5. Top: Energy Correlation Diagram for d^5 in O_h and T_d*. Bottom: Tanabe-Sugano Diagram for d^5 in O_h*.

Energy Correlation Diagram for d^5 in O_h and T_d*

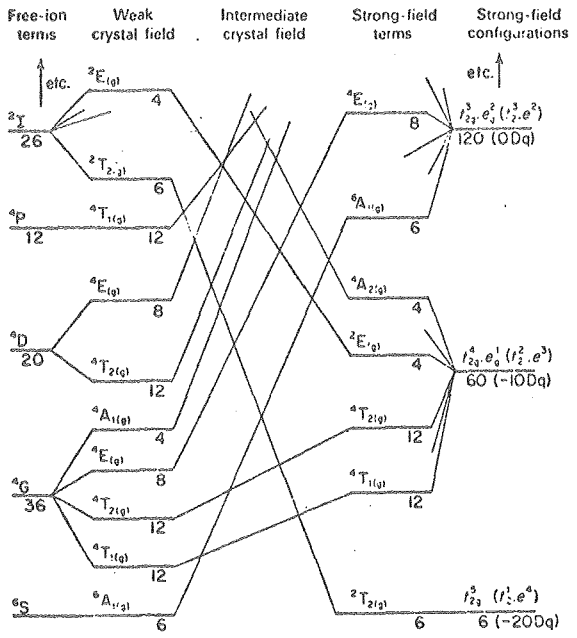

Tanabe-Sugano Diagram for d^5 in O_h*

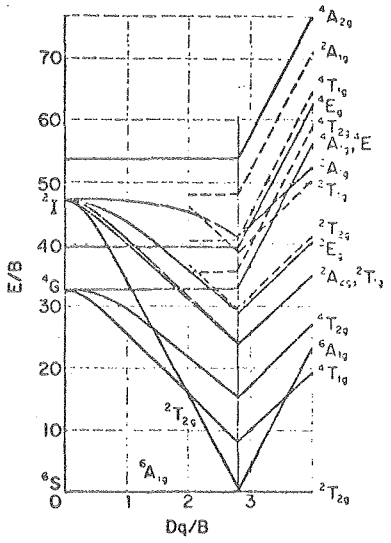

*B.N. Figges, Introduction to Ligand Fields, John Wiley & Sons, 1967, Chap. 7

XBL 786-4014

strength lies near the high and low spin crossover point. The bottom part of Fig. 5 is a Tanabe-Sugano diagram which describes the relation between the energies of states and the crystal field strength more quantitatively than does the top figure (12). Dq corresponds to the crystal crystal field splitting (Δ = 10 Dq) and B, to the Racah electron repulsion parameter. In this figure it is clear that in the intermediate field range where the high and low spin states cross each other, the lowest excited state above the high spin ground state is the low spin state and *vice versa*. Thus, the only requirement for obtaining thermal spin equilibrium is to have the energy separation between the ground and excited states in the order of kT near room temperature.

The intermediate spin state (S = 3/2) or the quantum mechanically admixed spin states in which the wavefunction is a true combination between S = 5/2 and S = 3/2 or S = 3/2 and S = 1/2, are much less well known. They have only rarely been invoked as a possible explanation for some atypical hemoprotein magnetic phenomena. The stability of the S = 3/2 ground state is still questionable. Griffith (15) proposed in his simple model that the relative energy levels of the S = 3/2 and S = 5/2 states depend entirely on the energy level of the $d_{x^2-y^2}$ antibonding orbital in the heme plane. The model suggests that, if bringing one electron down from $d_{x^2-y^2}$ becomes energetically favorable, then

bringing another electron down from d_{z^2} is even more energetically favorable. In other words, the S = 1/2 state is always more stable than the S = 3/2 state. Recently, however, Meltempo and Moss (10) have criticized Griffith's argument and claimed that the stable intermediate spin ground state is obtainable if the variable iron position with respect to the heme plane is considered. They suggest that the energy levels of $d_{x^2-y^2}$ and d_{z^2} are not necessarily independent of each other, while Griffith assumes that changing axial ligands would not have any effect on the energy level of $d_{x^2-y^2}$. In view of the x-ray results, Meltempo and Moss's model for the high, intermediate and low spin energy levels for single-electron d orbitals corresponds to the diagram shown in Figure 6. The x-ray analysis of ferrimyoglobin, which is in the high spin state in its native form, and of the ferrimyoglobin-cyanide derivative, which is in the low spin state, have shown that in the high spin state the iron is displaced out of the heme plane toward the proximal histidine ligand by about 0.4 Å, while it is in the plane in the low spin state. Thus, the position of the intermediate spin iron is proposed to be in between the high and low spin positions. Quantum mechanical mixing of spin states occurs via spin-orbit interaction, in which case the selection rule $\Delta S=0,\pm1$ must be satisfied first. This indicates that between S = 1/2 and S = 5/2, there will be no first order mixing of the wavefunctions. In other words, no

Figure 6. Correlation between the spin state and the position of iron atom. The low spin iron is in the plane, the high spin iron is out of the plane and the intermediate spin iron is in between the two positions.

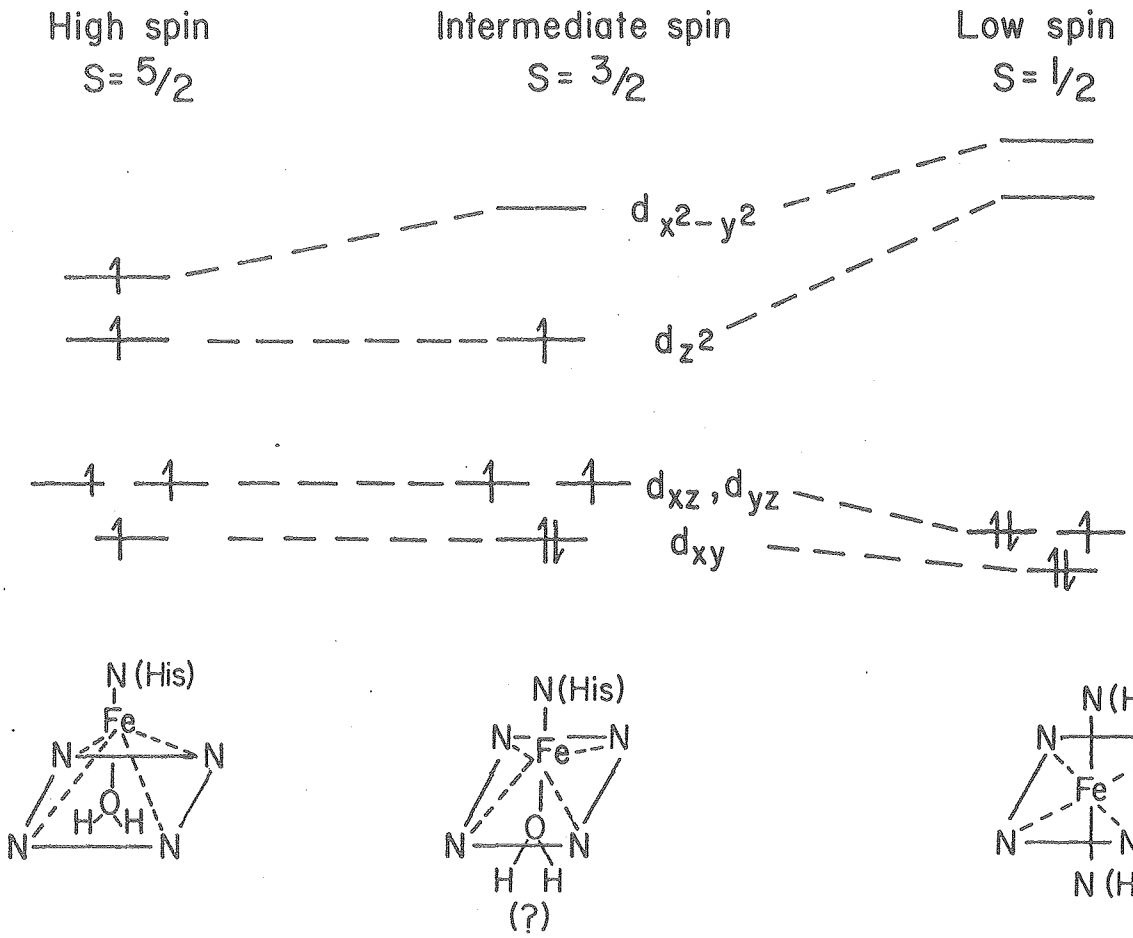
High spin
S= 5/2
Intermediate spin
S= 3/2
Low spin
S= 1/2
$d_{x^2-y^2}$
d_{z^2}
d_{xz}, d_{yz}
d_{xy}
N (His)
Fe
N
O
H
(?)

XBL 787 -4074

quantum mechanical mixing is expected to occur between those two spin states. An additional requirement for obtaining quantum mechanical mixing of spin states is to have the energy separation between the unperturbed pure spin states in the order of the spin orbit coupling constant, which is about 400 cm^{-1} in ferric heme complexes.

C. Absorption Spectra of Hemoproteins

The absorption spectra of ferric hemoproteins are complex to interpret because many overlapping bands appear in the visible region due to extensive interaction between iron $d\pi$ and porphyrin π orbitals. Figure 7 shows the molecular energy diagram of a typical high spin hemoprotein whose absorption spectrum is even more complex than the low spin form. For a high spin heme, in addition to the Soret and visible transitions, several charge transfer (CT) transitions are possible in the visible region. Although the exact assignment of these transitions is not known with certainty, it is generally thought that there are two allowed CT transitions of E_u symmetry resulting from porphyrin π to $d\pi$ excitation, as indicated by the arrows in Fig. 7. The particular porphyrin π orbitals involved are also not known with certainty, but they are most likely the same porphyrin π orbitals that are involved in the $\pi \rightarrow \pi^*$ transition: A_{1u} and A_{2u}. Consistent with the polarized crystal spectra of myoglobin, which exists mostly in the high spin state, the two CT transitions are in-plane (xy) polarized (16). Because the

Figure 7. Electronic transitions of ferric iron porphyrin in weak crystal field.

Weak Crystal Field

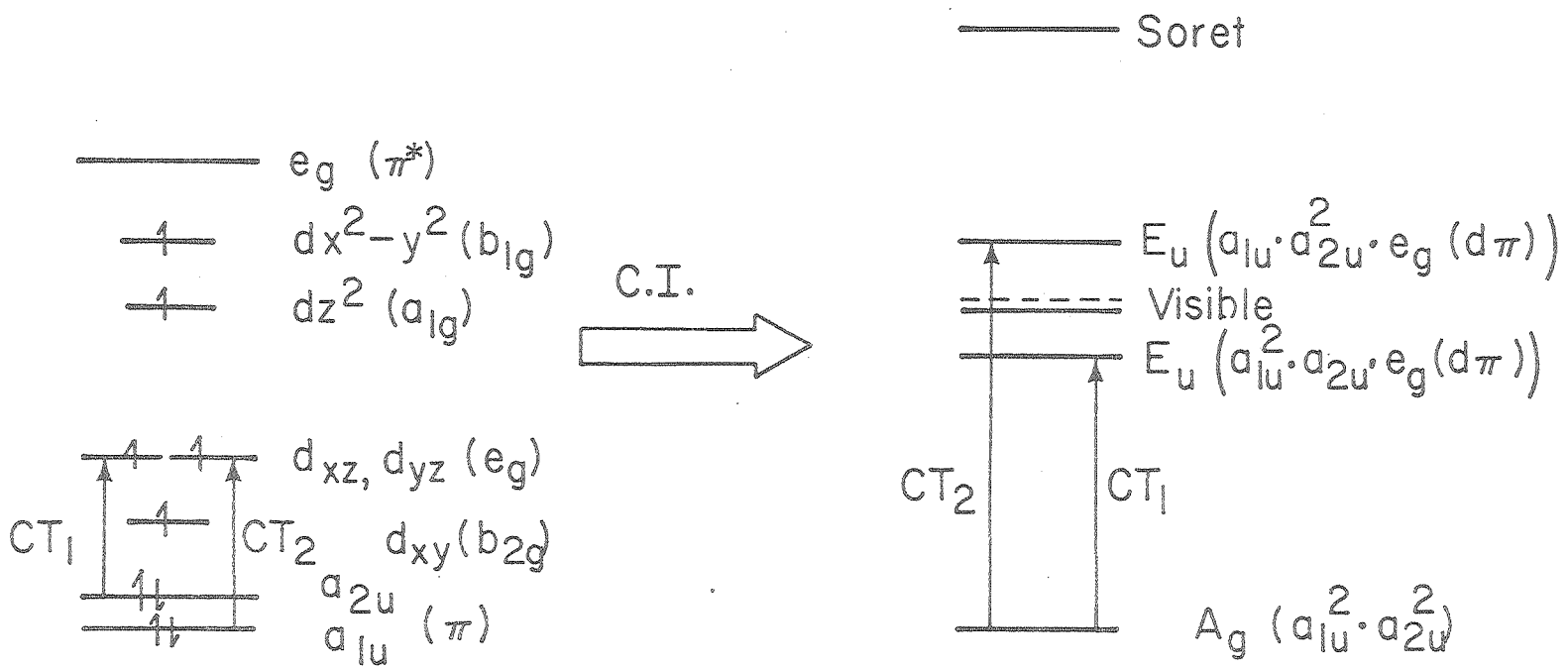

Single electron energy levels

D_{4h}

Molecular energy levels

D_{4h}

XBL 786-4004

CT excitations show identical symmetry and are sufficiently close in energy to the visible band (Q_{0-0}), they can mix via configuration interaction. As a result, the CT bands borrow intensity from the visible band. Their position and intensity are thus strongly dependent on the nature of the axial ligands, which determines the relative energy separation between porphyrin and iron π orbitals. Another allowed CT transition in the visible region is from the porphyrin A_{2u} orbital to the iron d_{z^2} orbital. The excited state of this transition is of A_{2u} symmetry and is z polarized. Its intensity, however, is expected to be rather small, because there is no other z-polarized transition from which it can borrow intensity. It is probably buried underneath the strong porphyrin bands. A typical high spin absorption spectrum consists of four in-plane polarized transitions in the visible region in addition to the Soret transition. The two in the middle are not well resolved but they correspond to Q_{0-0} (α) and Q_{0-1} (β) bands while the two on the high and low energy side of the Q band region are the mixed in-plane CT transitions. In the low spin case, the d orbital energy levels relative to the porphyrin π orbitals are such that the CT bands are not close in energy to the porphyrin $\pi \rightarrow \pi^*$ bands. The xy-polarized CT transitions of E_u symmetry like the ones in high spin hemes fall in the infrared (IR) region. This indicates that there will be little or no

configuration interaction and, as a consequence, the α and β bands should remain strong and well resolved. Sometimes, a weak z-polarized transition appears in the near IR region between 620 and 700 nm of low spin heme complexes such as cytochrome c, myoglobin-azide and hemoglobin-azide. In the case of cytochrome c, the band at 695 nm is believed to be a charge transfer transition from the axial ligand (sulfur or methionine) to iron (17,18). However, an alternative explanation that it can also be a CT transition from the porphyrin A_{2u} to the iron d_{z2} is given for the azide complexes.

According to Meltempo and Moss, (10) the intermediate spin hemoprotein should give rise to more or less the same spectral characteristics as the high spin complex. As shown in Fig. 6, the energy level of dπ orbitals does not change when the spin state changes from S = 5/2 to S = 3/2. This suggests that the CT transitions should occur at nearly the same energy as in the high spin case. The extent of configuration interaction, however, is expected to be slightly different. The relative energy levels of porphyrin π orbitals are different in the two spin states due to different degrees of doming of the heme plane. In other words, the optical spectra are not capable of distinguishing the intermediate or quantum mechanically admixed spin state between S = 5/2 and S = 3/2 from the pure high spin state.

It is worth noting that in Gouterman's (19) model for high spin hemes, the iron displacement out of the heme plane is a requirement, consistent with the x-ray results. According to his model, low or intermediate spin states should occur with the iron position in the heme plane. This, however, does not agree with Meltempo and Moss's model for the intermediate spin state where the iron lies between the high and low spin positions.

Magnetic Circular Dichroism of Hemoproteins

A. Introduction to MCD

Magnetically induced optical activity arises from the well known Faraday effect, where the electronic transitions between the levels split by the applied magnetic field are preferentially allowed by the left or right circularly polarized light. In contrast to natural optical activity in which the presence of molecular dissymmetry is a requirement, magnetically induced optical activity is present in all substances placed in a properly oriented magnetic field (20-22). Analogous to natural circular dichroism (CD), and optical rotatory dispersion (ORD), magnetic circular dichroism (MCD) measures the difference of the extinction coefficients for left (LCP) and right (RCP) circularly polarized light, i.e. $\varepsilon_L - \varepsilon_R$, while magnetic optical rotatory dispersion (MORD) measures the rotation of the plane polarized light in terms of the difference in refractive indices, i.e. $n_L - n_R$. This chapter will focus on the application of MCD since it is much better characterized and more convenient to measure experimentally than MORD.

The theory of MCD has evolved through a joint effort of several workers. The most rigorous treatment is given by Stephens (23). His approach introduces the magnetic field perturbations explicitly to the conventional semiclassical theory of the electric-dipole approximations. The theory is successful in including the zero field splitting induced by spin-orbit coupling and/or by vibronic interactions (Jahn-Teller effect). The electric-dipole approximations which are developed by Buckingham and Stephens (20) are essentially extensions of the classical theory of optical activity for transparent regions into absorption regions. The expression for magnetic optical activity may be given in terms of three experimentally distinguishable band components; A, B and C term effects.

$$(\varepsilon_L - \varepsilon_R) \propto [f_1 A + f_2(B + C/kT)] \qquad (1)$$

where f_1 and f_2 are line shape functions. The effect of magnetic field is to split all of the degenerate levels into equally spaced Zeeman components with $E_{M_J} = g\beta H M_J$, where M_J corresponds to the angular momentum in the direction of the applied field specified by J, the total angular momentum of a molecule; H is the intensity of the field; β, the Bohr magneton and g, the "spectroscopic" splitting factor. If spin-orbit interaction is neglected, g corresponds to 1 for a singlet-singlet electronic transition. Figures 8 and 9

illustrate the f_1 and f_2 spectral band shapes mentioned above (Eq. 1). In Fig. 8a, the energy level diagram shows the case in which the ground state is orbitally and spin non-degenerate (J=0) while the excited state is orbitally degenerate (J=1). J=1 state will be split by the magnetic field into M_J=0 and ±1. A very important physical phenomenon is that circularly polarized light has a well defined z component of angular momentum: M_J=+1 and M_J=-1 may be specifically associated with the left and right circularly polarized light, respectively. Thus the selection rule indicates that the transitions to M_J=+1 and M_J=-1 are allowed only in LCP and RCP light, respectively. In the applied magnetic field, the absorption spectra for RCP and LCP light will be shifted from the absorption maximum in the absence of the field by $-g\beta H$ and $+g\beta H$, respectively. The Zeeman splitting is, in general, much smaller than the absorption band width; thus, the absorption spectrum does not usually exhibit an observable splitting. But the resultant MCD band shape resembles the first derivative of the absorption band, as shown in Fig. 8b. The magnitude of peak-to-trough splitting will depend on the magnetic field strength and the angular momentum of the excited state. Figure 9a shows the reverse situation where the ground state is degenerate and is specified by J=1. When the ground state is degenerate, the dominant effect arises from thermal distribution of molecules among the Zeeman sublevels. Since the selection rule indicates that the high energy transition from M_J=-1

Figure 8. Magnetic circular dichroism where the excited state is orbitally degenerate and the ground state is non-degenerate.

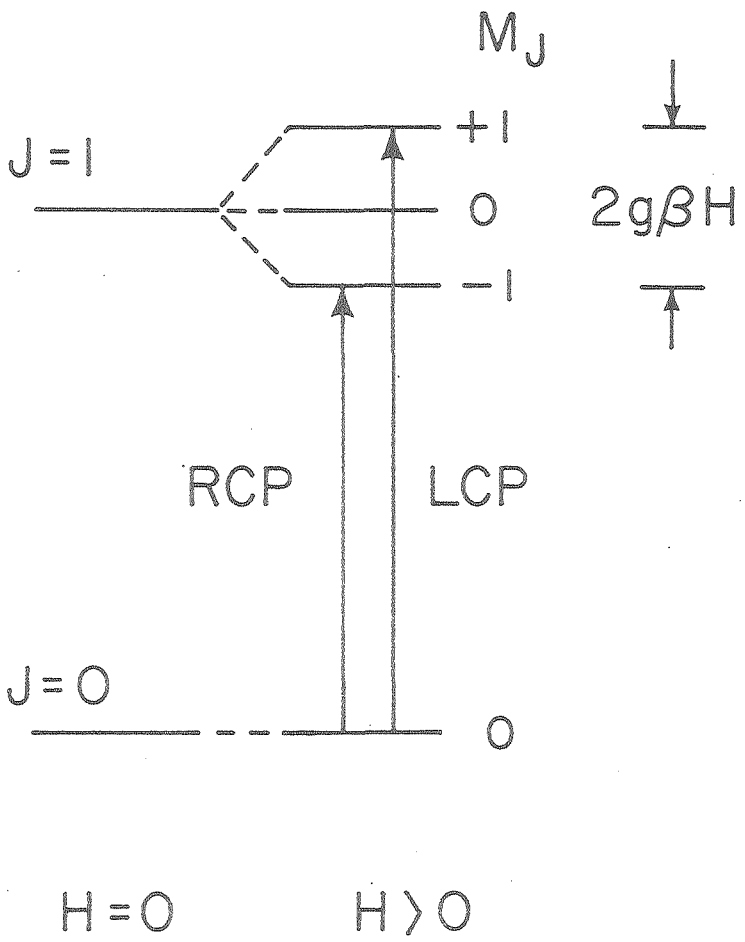

a

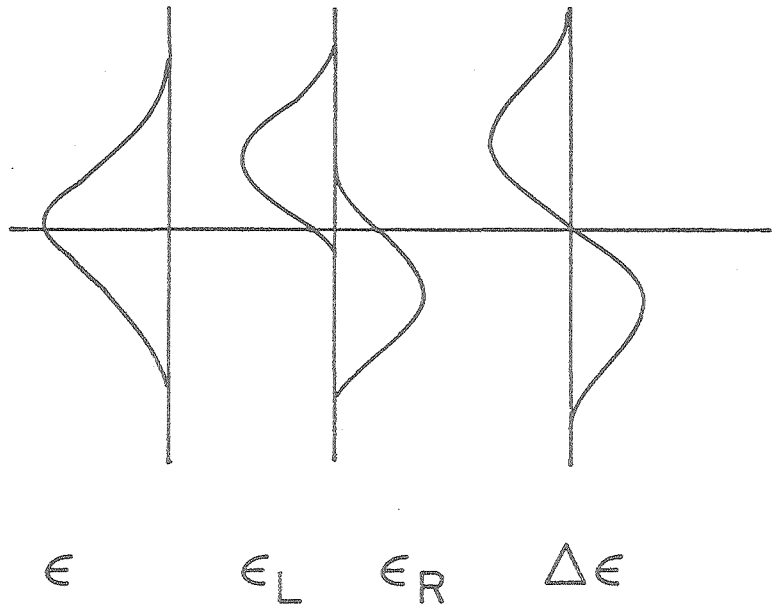

b

XBL 787-4070

Figure 9. Magnetic circular dichroism where the ground state is degenerate and the excited state is non-degenerate. Left circularly polarized light is absorbed more strongly according to Boltzmann statistics.

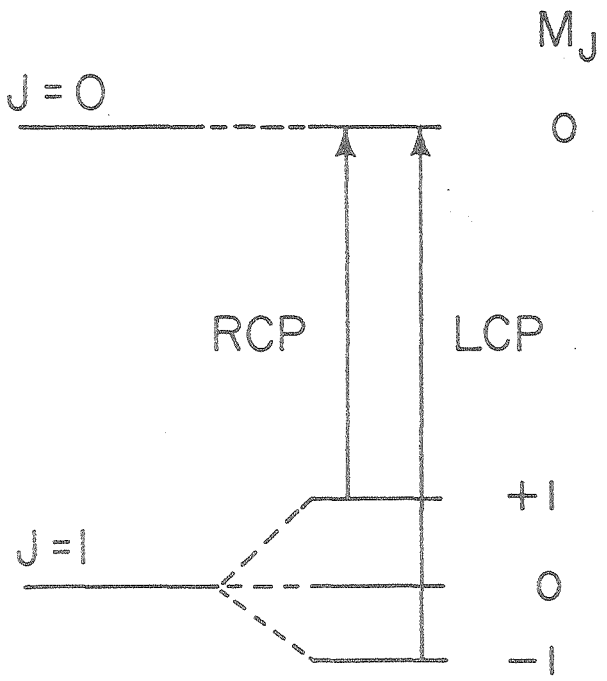

(a)

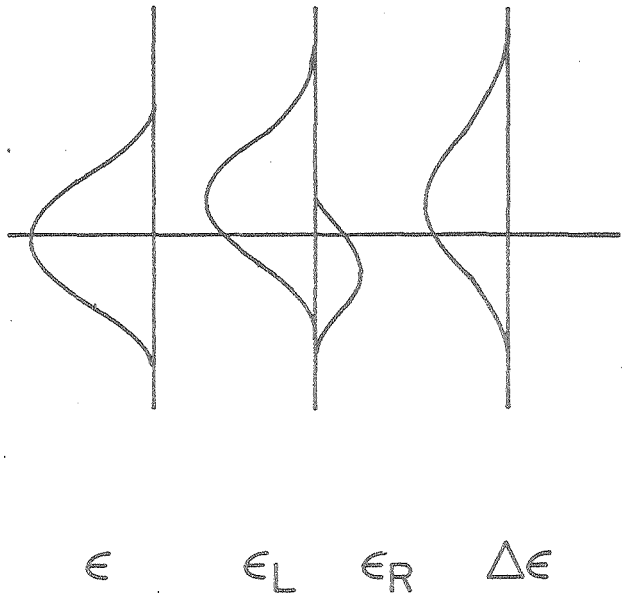

(b)

XBL 787-4071

to J=0 is associated with the LCP light and since M_J=-1 state is more populated than M_J=+1 state by a Boltzmann factor, the absorption band for the LCP light will be more intense and lie higher in energy than that for the RCP light. The resultant MCD band shape will be a skewed positive absorption (Fig. 9b). The first derivative MCD band shape (f_1), more commonly referred to as an A term, can arise from either the degenerate ground or the excited state. However, in the degenerate ground state, the A term effect is rarely emphasized due to population differences and transition probability differences among the sub-levels. The absorption MCD band shape (f_2), is the result of B and C term effects. A B term describes the mixing between the states induced by the magnetic field, while a C term reflects degeneracy of the ground state. The latter can be easily differentiated from the former by temperature dependent MCD measurements.

B. MCD Spectra of Ferric Hemoproteins

MCD offers much promise for assigning the electronic structure of the heme group, because the technique is intrinsically sensitive to distinguishing the redox and spin state changes of iron, independently of each other. Porphyrin alone or low spin ferrous hemochrome yields an MCD spectrum that consists predominantly of A term effects and some B term effects (24). In both the Soret and visible electronic transitions the excited state configuration corresponds to the doubly degenerate E_u state (A_{1u},A_{2u}→e_g) while the ground state

is orbitally non-degenerate. This means that only the excited state is split by the external magnetic field giving rise to the first derivative band shape A term dispersion (Fig. 8). As in absorption spectra, however, insertion of an iron into porphyrin induces additional MCD spectral bands. The paramagnetic nature of iron becomes reflected in the $\pi \rightarrow \pi^*$ electronic transitions of porphyrin. Spin-orbit interaction arising from the delocalization of iron d orbital electrons to porphyrin π orbitals is thought to be the major mechanism by which the paramagnetism of iron is manifested in the MCD spectra (25). Figures 10 and 11 illustrate schematically the origin of Soret MCD for the low spin and high spin states of ferric iron porphyrins, respectively (25,26). The electronic configurations of the ground and excited states are described as a composite of the porphyrin π and iron d^5 systems. In the low spin case the ground state corresponds to $^2E_g[(A_{1u}^2 \cdot A_{2u}^2) \cdot (b_{2g}^2 \cdot e_g^3)]$ while the excited state corresponds to $^2E_u[(A_{1u}^1 \cdot A_{2u}^2 \cdot e_g^1) \cdot (b_{2g}^2 \cdot e_g^3)]$. The parentheses on the left indicate the configuration of the porphyrin part and on the right, that of the iron in D_{4h} symmetry. In low spin hemoproteins such as cytochrome c, however, the ground state is actually orbitally non-degenerate. The reason is because the lowest three d orbitals of iron, i.e. b_{2g} and e_g (Fig. 4), are mixed by spin-orbit coupling which removes the degeneracy of e_g orbitals of iron. As a consequence the ground state is described as a product wavefunction between the porphyrin π system and the lowest Kramers doublet of the low spin iron.

Figure 10. Molecular energy diagram in the presence of spin-orbit coupling and magnetic field interaction, and corresponding magnetic circular dichroism of low spin heme for the Soret region.

Molecular Energy Diagram for Low Spin Heme

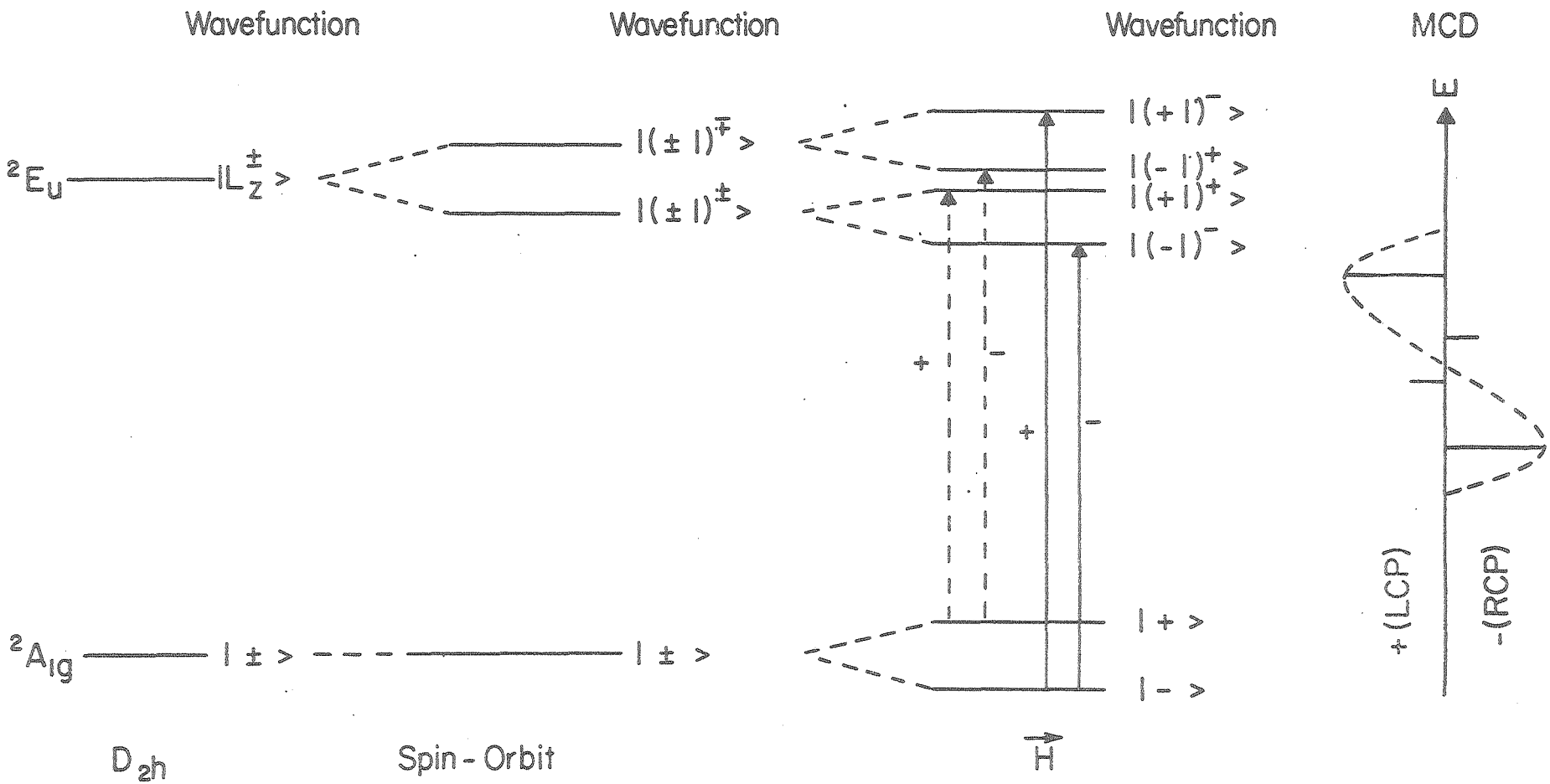

Figure 11. Molecular energy diagram in the presence of spin-orbit coupling and magnetic field interaction, and corresponding magnetic circular dichroism of high spin heme for the Soret region.

Molecular Energy Diagram for High Spin Heme

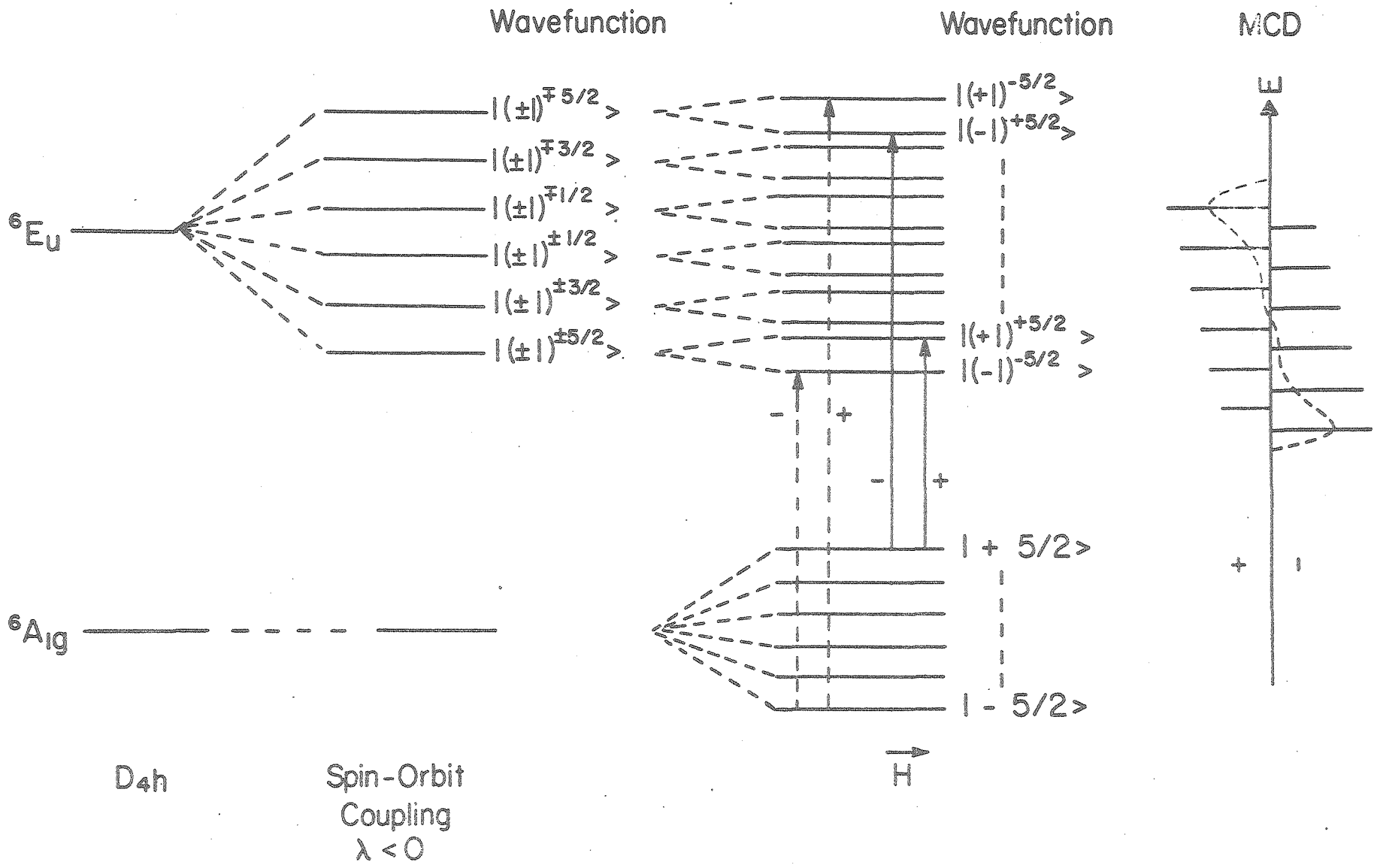

In Fig. 10 the ground state wavefunction is represented as $|\pm\rangle$ where $\pm$ indicates a Kramers doublet. The excited state wavefunction is given by $|L_z^{\pm}\rangle$ where L_z is the excited state orbital moment of the Soret transition, i.e. ± 1. Spin-orbit interaction between the spin magnetic moment of iron and the orbital motion of porphyrin π electrons splits the excited state into two doublet states. For iron porphyrin complexes this zero-field splitting is found to be much greater than the Zeeman splitting. In addition the sign of the spin-orbit coupling constant is known to be negative for S = 1/2 which suggests that the lowest energy component of a multiplet corresponds to the parallel orientation of the orbital and spin moments. Thus $|(\pm 1)^{\pm}\rangle$ is a degenerate state in which the orbital angular momentum induced upon excitation is in the direction of the resultant momentum of spin-orbit coupling at the iron, and $|(\pm 1)^{\mp}\rangle$ is a degenerate state in which the orbital angular momentum is counter to the iron angular momentum. Each degenerate state exhibits a Zeeman splitting in the applied magnetic field. The arrows with + and - signs indicate transitions associated with the left and right circularly polarized light, respectively, according to the selection rule. From this, the appearance of paramagnetic C term effects of opposite sign can be easily understood, as shown in the lower portion of Fig. 10. The transitions from the $|-\rangle$ state which is more populated by a Boltzmann factor, $\exp(-2g\beta HS_z/kT)$, are shown with greater intensity. At reduced temperatures, the Soret MCD intensity is expected to

increase as a function of 1/T if the intensity is assumed to be directly proportional to the population difference. When spin-orbit coupling is neglected, however, this C term effect disappears and only the A term remains, because + and - absorptions mostly cancel each other. The low spin hemoprotein complexes exhibit Soret MCD spectra as predicted from the simple stick diagram shown in Fig. 10. Sometimes additional MCD features appear on the high energy side of the Soret transition which introduces asymmetry to the first derivative band shape. This is most likely due to B term effects arising from the vibronic side bands.

The high spin hemoproteins exhibit very weak MCD. Although no quantitative treatment has been given in the literature, the stick diagram illustrated in Fig. 11 may account for the origin of weak MCD at least semi-quantitatively. The symmetry assignment of the ground state is $^6A_{1g}[(A_{1u}^2 \cdot A_{2u}^2) \cdot (b_{2g}^1 \cdot e_g^2 \cdot A_{1g}^1 \cdot b_{1g}^1)]$ and the excited state is $^6E_u[(A_{1u}^1 \cdot A_{2u}^2 \cdot e_g^1) \cdot (b_{2g}^1 \cdot e_g^2 \cdot A_{1g}^1 \cdot b_{1g}^1)]$. It is clear that the first order spin-orbit interaction will not split the ground state degeneracy, because there is no orbital moment but the spin moment. The excited state on the other hand will be split into six doublet states. The corresponding wavefunctions are given in Fig. 11 assuming that the spin-orbit coupling constant (λ) is still negative. If λ were positive, the lowest energy component within the multiplet would be the one with $|(\pm 1)^{\mp 5/2}>$. As shown in the lower portion of Fig. 11 MCD of the high spin heme consists of twelve individual lines. The shape of the spectrum will

depend largely on the extent of spin-orbit interaction which determines the spacing between the individual lines and on the sign of the spin-orbit coupling constant. In iron porphyrin complexes, two mechanisms of spin-orbit coupling are believed to contribute to the splitting of degenerate states. The first mechanism describes the appearance of the non-zero spin density of iron on the porphyrin orbitals with non-zero orbital moment. This leads to the normal splitting with $\lambda > 0$; the lowest energy component corresponds to the anti-parallel arrangement of the orbital and spin magnetic moments. The second mechanism is one in which the spin magnetic moment of iron interacts with the orbital motion of porphyrin π electrons. For this type of interaction λ is negative. The real sign of spin-orbit coupling will then depend on which of the above two mechanisms happens to be dominant. In the high spin case it is difficult to determine whether λ is positive or negative, because the observed MCD is very weak and the bands are superimposed. The stick diagram shown in Fig. 11 illustrates that the MCD spectrum will consist of weak C terms on the high and low energy ends. Most of the MCD effect will be cancelled out, since the intensity of the + and - absorptions is about the same.

Magnetic Susceptibility

Magnetic susceptibility measures magnetic induction in a substance when it is placed in a magnetic field; i.e., it represents the bulk magnetic property of a molecule (27).

Magnetic induction, B, is simply defined as the sum of the applied field and the induced field, such that

$$B = H + \Delta H$$

If the molecule is isotropic the magnetic induction is given by

$$B = H + 4\pi I$$

where I is the intensity of magnetization. The volume susceptibility, κ, is then related to I by

$$\kappa = I/H$$

In general, the mass susceptibility, χ_g, is used, which is given by

$$\chi_g = \kappa/\rho$$

where ρ is the density of the substance. The molar susceptibility, χ_M, is then

$$\chi_M = \chi_g \times M$$

where M is the molecular weight.

A measured magnetic susceptibility contains contributions from both molecular paramagnetism and diamagnetism. All molecules exhibit diamagnetism which arises from orbital motion of paired electrons in the applied field. In such a case the induced magnetic dipoles lie antiparallel to the

direction of the magnetic field so that the intensity of magnetization is negative and consequently χ_g is negative. Diamagnetic susceptibilities of atoms in molecules are additive within reasonable limits. This is a very useful quality in determining the diamagnetic susceptibilities of ligand atoms and counter-ions in transition metal complexes. The diamagnetic susceptibility expression for a molecule may be written as

$$\chi_{mol}^{dia} = \sum_i n_i \chi_i + \sum \varepsilon$$

where n_i indicates the number of atoms of a given element in the molecule, χ_i, atomic susceptibility of the element and ε, constitutive corrections such as the existence of π bonds. Because the additivity of χ_i was establashed by Pascal, χ_i is commonly referred to as Pascal's constant. Molecular paramagnetism is a consequence of the interaction of orbital- and/or spin-angular momenta of unpaired electrons with the applied field. The observed paramagnetic susceptibility defines the effective magnetic moment, μ_{eff}, as

$$\mu_{eff}^2 = \frac{3kT}{N\beta^2} \cdot \chi_M$$

where β is the Bohr magneton ($\beta = eh/4\pi mc = 0.927 \times 10^{-27}$ erg gauss^{-1}) N, Avogadro's number; k, Boltzmann's constant and T, temperature. If μ_{eff} is temperature independent, χ is inversely proportional to temperature, which is known as Curie's Law, $\chi = c/T$ where c is the Curie constant. So far, only magnetically dilute and isotropic molecules have been

considered. However, even single crystals, except those belonging to the cubic class, are magnetically anisotropic; thus, the susceptibility must be described by three orthogonal principal crystal susceptibilities. For solution samples then the observed susceptibility is the average susceptibility:

$$\chi = \frac{\chi_x + \chi_y + \chi_z}{3},$$

$$\mu_{eff} = \left[\frac{\mu_x^2 + \mu_y^2 + \mu_z^2}{3}\right]^{1/2}$$

The bulk magnetic interaction of a substance may be described as arising from changes in the energy levels of an ensemble of atoms when it is subjected to a magnetic field. A quantum mechanical treatment seeks to find new energy levels of individual atoms in the magnetic field and to derive the susceptibility expression from the thermal distribution of N atoms among all possible states, according to Boltzmann statistics. The derivation of a general equation for such a system is due to H.J. Van Vleck. Thus, it is generally referred to as Van Vleck's equation (28). There are two important assumptions made in his derivation; (1) the system is magnetically isolated so that no magnetic interaction between atoms has been considered, and (2) the energy of the ith level of the atom in the magnetic field may be expressed as a power series. This means that the energy of the ith level of the atom is given by

$$\omega_i = \omega_i^{(0)} + \omega_i^{(1)}H + \omega_i^{(2)}H^2 + \ldots.$$

where $\omega_i^{(0)}$ is the energy of the ith level in the absence of the field and $\omega_i^{(1)}$ and $\omega_i^{(2)}$ are the first and second order Zeeman coefficients respectively. The intensity of magnetization may then be related to the rate of change of energy of the molecule in the magnetic field, i.e.

$$I_i = -\frac{\partial \omega_i}{\partial H} = -\omega_i^{(1)} - 2\omega_i^{(2)} H - \ldots .$$

and its susceptibility, χ_i, to

$$\chi_i = I_i/H$$

The first assumption implies that there will be no field dependence of the susceptibility which indicates that the terms beyond the second order Zeeman effect must be neglected. This simplifies the expression to a great extent. For an ensemble of N atoms, χ_M will be the sum of individual intensity of magnetization multiplied by the Boltzmann factor divided by the field:

$$\chi_M = \frac{\frac{N}{H} \sum_i [-\omega_i^{(1)} - 2\omega_i^{(2)} H] \exp(-\omega_i/kT)}{\sum_i \exp(-\omega_i/kT)}$$

The first order term, $\omega_i^{(1)}$, represents the magnetic field perturbation of a degenerate level i which leads to splitting of the level into a set of equally spaced components separated by $g\beta H$. The second order term, $\omega_i^{(2)}$, arises from mixing of the non-degenerate levels by the magnetic field. The net effect is to lower or raise the levels involved in mixing without any changes in degeneracy. $\omega_i^{(1)}$ is typically

in the order of a few cm^{-1}; that is, much smaller than kT except at very low temperatures. This further simplifies the Van Vleck equation. Since $\exp(-\omega_i/kT) = \exp(-\omega_i^{(0)}/kT) \times [(1-H\cdot\omega_i^{(1)}/kT)\cdot(1-H^2\cdot\omega_i^{(2)}/kT) \ldots.]$,

$$\chi_M = \frac{N \sum_i [(\omega_i^{(1)})^2/kT - 2\omega_i^{(2)}] \exp(-\omega_i^{(0)}/kT)}{\sum_i \exp(-\omega_i^{(0)}/kT)}$$

The Zeeman coefficients are related to the wavefunctions by the magnetic dipole operator. In classical electrodynamics the magnetic dipole moment is given by the sum of orbital and spin moments. Likewise the magnetic dipole operator may be given by

$$\mu_z = (L_z + 2S_z)\beta$$

where the direction of quantization is in z. Then,

$$\omega_i^{(1)} = \langle\psi_i|L_z+2S_z|\psi_i\rangle\beta$$

$$\omega_i^{(2)} = \frac{\sum_j \langle\psi_i|L_z+2S_z|\psi_j\rangle\cdot\langle\psi_j|L_z+2S_z|\psi_i\rangle\beta^2}{\omega_i^{(0)} - \omega_j^{(0)}}$$

Ferric hemeproteins and their derivatives exhibit spin degenerate ground states; therefore, the first order term is expected to dominate ths susceptibility. If we neglect the second order effect and assume $\omega_i^{(0)} = 0$, then the susceptibility may simply be given by

$$\chi_M = \frac{N \sum_i (\omega_i^{(1)})^2/kT}{\sum_i \exp(-\omega_i^{(0)}/kT)}$$

Furthermore, if the wavefunctions are specified by the orbital and spin angular momentum quantum numbers in the magnetic field, M_L and M_S, then each $\omega_i^{(1)} = (M_L+M_S)\beta$, which yields

$$\chi_M = \frac{N\beta^2}{kT(2L+1)(2S+1)} \begin{vmatrix} [L+2S]^2 + \ldots\ldots\ldots + [-L+2S]^2 \\ +[L+2(S-1)]^2 + \ldots\ldots + [-L+2(S-1)]^2 \\ \vdots \\ +[L+2(-S)]^2 + \ldots\ldots [-L+2(-S)]^2 \end{vmatrix}$$

Evaluation of this gives (27)

$$\chi_M = \frac{N\beta^2}{3kT}[L(L+1) + 4S(S+1)]$$

The effective magnetic moment, which is an empirical parameter, is then directly related to $[L(L+1) + 4S(S+1)]^{1/2}$. Thus far L and S are treated independently of each other. In the presence of spin-orbit interaction; however, L and S are not good quantum numbers anymore. Thus a new quantum number J must be introduced which is a vector sum of L and S. J is not colinear with the magnetic dipole operator; an additional parameter, g, is included in the magnetic dipole expression such that

$$\mu_{eff} = g[J(J+1)]^{1/2}$$

and g is defined as

$$g = \frac{3}{2} + \frac{S(S+1) - L(L+1)}{2J(J+1)}$$

In transition metal complexes, the d orbital degeneracy which accounts for the orbital moment is usually removed by crystal field interaction. This leads to quenching of the orbital moment. In such a case it is a common practice to regard the observed magnetic moment as arising from the spin moment only:

$$\mu_{eff} = 2[S(S+1)]^{1/2}$$

The number of unpaired electrons at the paramagnetic center can then be evaluated. The ground state symmetry of iron in high spin hemeproteins is $^6A_{1g}$, and the first excited state, $^4A_{2g}$, which lies about 2000 - 3000 cm^{-1} above the ground state is not thermally accessible. The observed μ_{eff} is indeed very close to the spin only value. The low spin ground state symmetry is assigned to ^2E_g which suggests that even if spin-orbit interaction removes the orbital degeneracy, there will be a residual of the orbital moment via "mixing in" of the low lying orbitally degenerate excited states. In fact the low spin magnetic moment is close to $\sqrt{5}$ rather than the spin only value of $\sqrt{3}$. If there exist thermally accessible degenerate excited states in addition to the degenerate ground state, then the second order effect can not be neglected. In this case no simplification of Van Vleck's equation is possible, and we may expect a complicated temperature-dependent susceptibility. A deviation from the Curie law will lead to the observation of a temperature-dependent magnetic moment.

Careful application of Van Vleck's equation to temperature dependence of the susceptibility will thus assign the ground state symmetry and provide information about the excited states as well.

Electron Spin Resonance

A. Introduction to Electron Spin Resonance

Electron spin Resonance (ESR) is extremely specific in its application because only those systems which contain unpaired electrons such as transition metal ions, free radicals and free electron centers will give rise to an ESR signal. Like any other resonance method, ESR spectroscopy monitors the net absorption of energy from a radiation field when molecules change their energy state (29-31). Essentially it measures the electron Zeeman energy of a paramagnetic species in the magnetic field. As discussed earlier, the magnetic dipole of an electron consists of an orbital part and a spin part. A spin moment is a purely quantum mechanical effect and can not be described accurately by classical analogs while the orbital moment can be easily derived from a classical electrodynamics point of view. The magnetic moment of molecules with unpaired electrons is dominated by the spin moment, thus ESR spectra are usually interpreted by means of a spin Hamiltonian rather than the actual Hamiltonian for the system. Any orbital angular momentum contribution is allowed for by making the g values deviate from the free electron value, 2.00232. The quantum mechanical

spin magnetic moment operator is given by

$$\mu_z = -g\beta S_z$$

where the direction of quantization is z. Here no hyperfine interaction is considered. The corresponding spin Hamiltonian is then

$$\mathcal{H}_s = -\mu_z H = g\beta H S_z$$

Since the two possible electron spin eigenvalues are ±1/2, the Zeeman energy, E, corresponds to

$$E = \pm\frac{1}{2} g\beta H$$

Here, if the energy of radiation matches the separation of the Zeeman energy at a certain magnetic field, H_γ, the resonance condition is met:

$$h\omega = g\beta H_\gamma$$

It is evident that information that one obtains from an ESR experiment is contained in the g values, which reflect the extent of spin-orbit interaction. Most molecules are highly anisotropic, which means that the energy levels are dependent on the direction of the applied field with respect to the principal axes of symmetry of the molecule, x, y and z (32).

As a result in general three principal g values, g_x, g_y and g_z, are expected to be observed. However, this anisotropy of g values can be averaged out in solution samples where molecular tumbling is fast. The anisotropy may also be partially removed by symmetry in the molecule. For example, if the molecule contains a single three-fold or higher axis of symmetry along z, then x and y are equivalent. In such a case, $g_x = g_y \neq g_z$, which are commonly designated as $g_\perp$ and $g_\parallel$.

ESR Spectra of Hemeproteins

ESR spectroscopy has been exclusively applied to ferric hemeproteins although other valence states may be paramagnetic. Ferric hemeproteins yield two most commonly observed classes of EPR spectra; namely, those characteristic of high spin and low spin states. Typical low spin ESR spectra consist of highly anisotropic g values, which immediately suggests two things: (1) the symmetry of the heme group, which is generally regarded as D_{4h}, may have been reduced to D_{2h}, and (2) there may be a large orbital angular momentum contribution. The low spin heme EPR spectra may be best analyzed by a positive hole model proposed by Weissbluth (33). The model assumes that the three t_{2g} orbitals are completely isolated from the remaining two e_g orbitals by a strong octahedral field (Fig. 2). Then five valence electrons will occupy t_{2g} orbitals such that one electron configuration corresponds to $(d_{xy})^2(d_{xz})^2(d_{yz})$, which can be represented alternatively as $(d_{yz})^+$, a positive hole in d_{yz}. The states of such a

system will be determined by asymmetric ligand field interaction and spin-orbit coupling (34). Spin-orbit coupling mixes the three d orbitals and spin systems, which gives rise to Kramers doublets. Figure 12 illustrates the energy levels and orbitals viewed as hole states. The eigenfunctions corresponding to the lowest Kramers doublet may be given as a linear combination of T_{2g} spin orbitals:

$$|+> = a|\xi\alpha> - ib|\eta\alpha> - c|\zeta\beta>$$
$$|-> = -a|\xi\beta> - ib|\eta\beta> - c|\zeta\alpha>$$

where ξ, η and ζ are orbital wavefunctions corresponding to d_{yz}, d_{xz} and d_{xy}, respectively. The ESR transition arises from this doublet when it is split by the magnetic field. For an anisotropic system the energy splitting along axis j is $\Delta E_j = g_j \beta H$, where j = x, y or z. From this the principal g values may be expressed in terms of the wavefunction coefficients by

$$g_x = 2[a^2 - (b+c)^2]$$
$$g_y = 2[(a+c)^2 - b^2]$$
$$g_z = 2[(a+b)^2 - c^2]$$

Or, if the principal g values are known from an ESR measurement one can estimate the coefficients. Then from the known eigenfunctions and the relation $a^2 + b^2 + c^2 = 1$, the eigen energies may be calculated. If the energy of d_{yz} positive hole, E_{yz}, is assumed to be zero, then the energy of the ground Kramers

Figure 12. d orbital energy levels of a t_{2g} set viewed as hole states in strong ligand field, which show the origin of a low spin ESR.

A Positive Hole Model in Strong Ligand Field S = 1/2

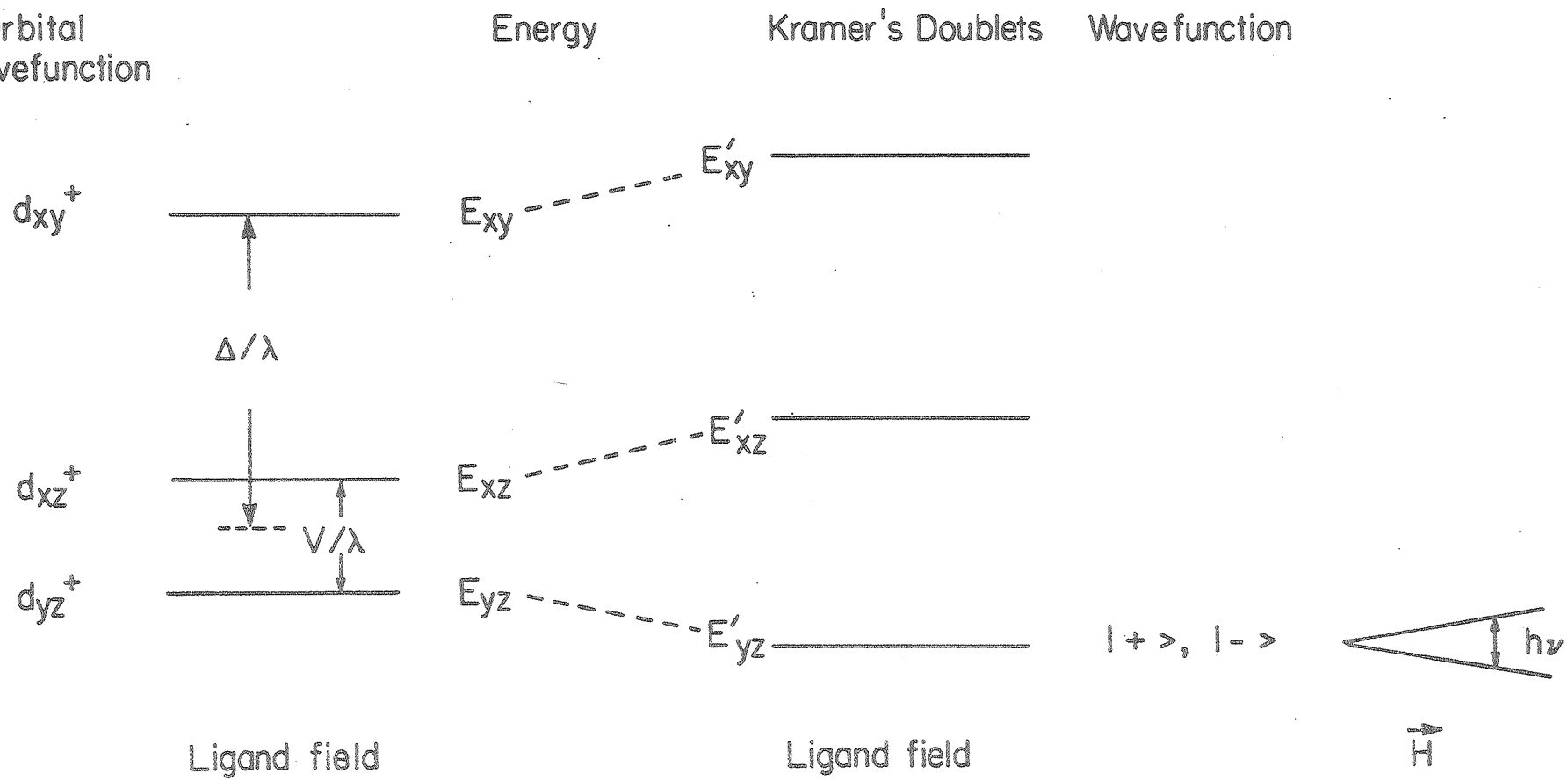

EY 13

doublet, E'_{yz}, corresponds to

$$E'_{yz} = -\frac{b+c}{2a} = \frac{g_x}{g_z+g_y} - \frac{1}{2}$$

and E_{xz} and E_{xy} correspond to

$$E_{xz} = E'_{yz} + \frac{a+c}{2b} = \frac{g_x}{g_z + g_y} + \frac{g_y}{g_z - g_x}$$

$$E_{xy} = E'_{yz} + \frac{a+b}{2c} = \frac{g_x}{g_z + g_y} + \frac{g_z}{g_y - g_x}$$

where the eigen energies are given in units of spin-orbit coupling constant, λ. It is clear that the axial distortion Δ/λ, will be $E_{xy} - \frac{1}{2} E_{xz}$ and rhombic distortion, V/λ, will be E_{xz}. The above correlation is, however, only a first-order approximation, because no orbital reduction via covalent bonding is taken into account. Indeed, consistently greater orbital contribution to the ground $^2T_{2g}$ term has been found. Griffith (15) claims that this can be due to mixing in of the excited states such as the $t_{2g}^4 e_g$ configuration, but no theory has been worked out in detail.

High spin heme ESR spectra are characterized by $g_{\|}=2$ and $g_{\perp}=6$ signals almost without exception (33). This immediately indicates the presence of strong axial symmetry. In weak crystal field, the ground term is $^6A_{1g}$, and the lowest lying excited states are $^4A_{2g}$ and ^4E_g in D_{4h} point group (Fig. 13). Spin-orbit coupling mixes these excited states into the ground state which leads to axial zero field splitting. When the local symmetry of iron is reduced by a rhombic field, ^4E becomes split into E_x and E_y components which results in

Figure 13. d orbital energy diagram in weak crystal field which indicates the axial (Δ_1,Δ_2) and rhombic (Δ_x,Δ_y) distortion parameters and the origin of a high spin ESR.

Weak Crystal Field
S = 5/2

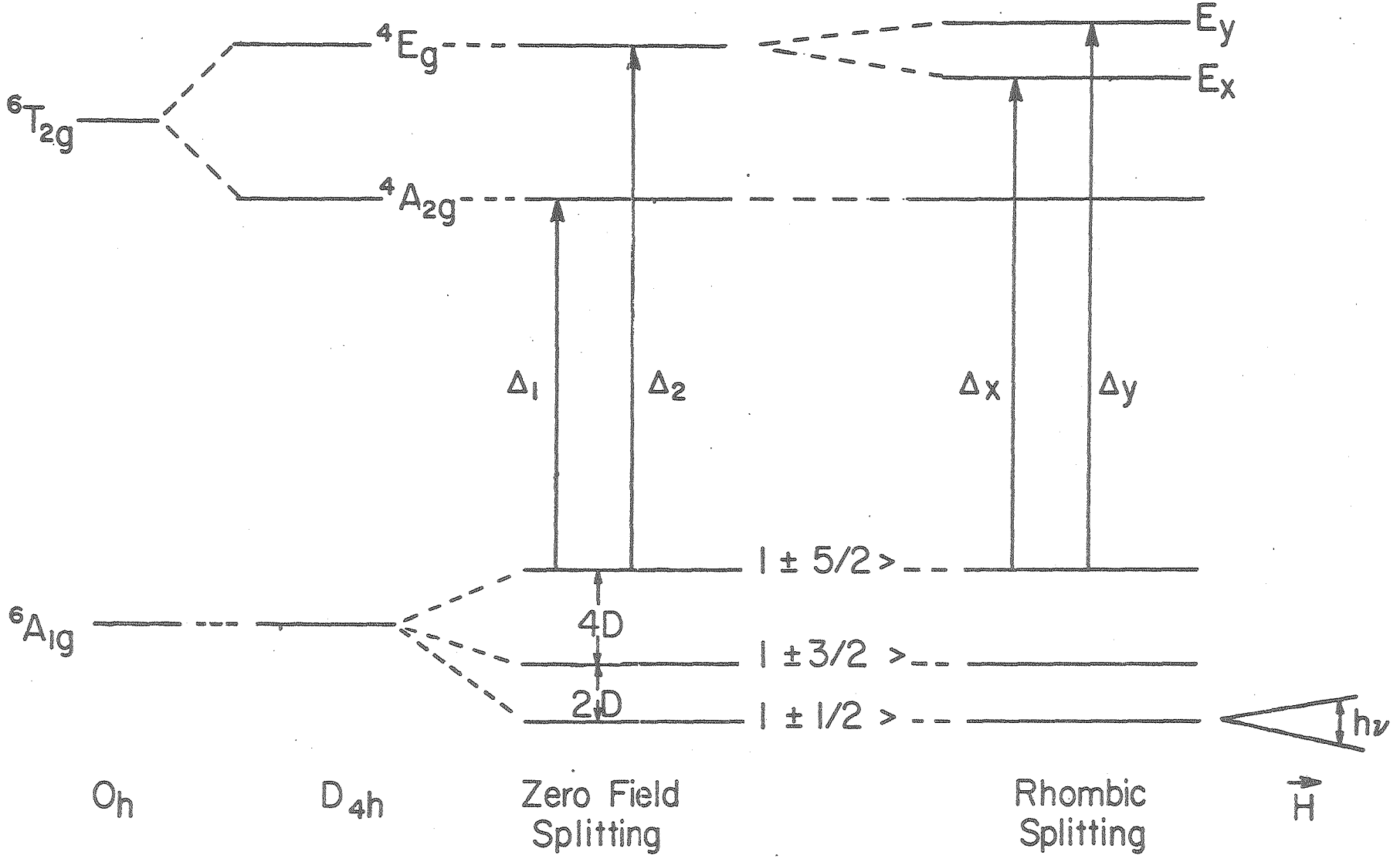

EY 12

rhombic splitting of $g_\perp = 6$ signal. In such a case, the spin Hamiltonian for the total interaction may be written as

$$\mathcal{H}_S = g_\parallel \beta H_z S_z + D[S_z^2 - \frac{1}{3} S(S+1)] + E[S_x^2 + S_y^2]$$

where D and E are axial zero field and rhombic field splitting parameters, respectively, and $S(S+1) = S_x^2 + S_y^2 + S_z^2$. D and E may be defined in terms of crystal field energy and spin-orbit coupling constant as

$$D = \frac{\lambda}{5} \left(\frac{1}{\Delta_1} - \frac{1}{\Delta_2}\right)$$

$$E = \frac{\lambda^2}{10} \left(\frac{1}{\Delta_x} - \frac{1}{\Delta_y}\right)$$

where Δ_1, Δ_2, Δ_x and Δ_y are as indicated in Fig. 13. The zero field splitting removes the sextet spin degeneracy into three Kramers doublets with $S_z = \pm 5/2$, $\pm 3/2$ and $\pm 1/2$. According to the above spin Hamiltonian $S_z = \pm 5/2$ and $S_z = \pm 3/2$ states are separated from the lowest doublet, $S_z = \pm 1/2$, by 6D and 2D, respectively. The ESR transition is from the lowest Kramers doublet. When the magnetic field is along z, the projection of $S_z = \pm 1/2$ state on the field is normal, i.e. $g_\parallel = 2$. When the field is perpendicular to the direction of quantization, however, the interaction of $S_z = \pm 1/2$ state with the field becomes exceedingly large, which will induce the value of $g_\perp$ to deviate from the free electron value. In general when $D > g\beta H$, $g_\perp = 2\delta + 1$.

Under certain conditions, the separation of energy between $^4A_{2g}$ and $^6A_{1g}$ states of high spin iron can be very small. Indeed, in *Chromatium* cytochrome c', $^4A_{2g}$ is known to be the ground state (10). If this energy separation is in the order of spin-orbit coupling constant, a large amount of mixing of the two quantum mechanical states is expected and the ground state wavefunction will be of the form

$$|\pm> = a \cdot |^6A_{1g} \pm 1/2> + b \cdot |^4A_{2g} \pm 1/2>$$

with $a^2+b^2 = 1$. Accordingly,

$$g_1 = a^2 \cdot 6 + b^2 \cdot 4$$

In other words, when the ground state of iron exists in a quantum mechanically admixed state, the g_1 value will lie between that for the pure $S_z = 1/2$ components of $^6A_{1g}$ ($2S+1 = 6$) and $^4A_{2g}$ ($2S+1 = 4$) states.

REFERENCES

1. J.-H. Fuhrhop, Angew. Chem., Int. Ed. 13, 321 (1974).

2. J.L. Hoard, Science 174, 1295 (1971).

3. M. Gouterman, J. Chem. Phys. 30, 1139 (1959).

4. C. Weiss, H. Kobayashi and M. Gouterman, J. Mol. Spectrosc. 16, 415 (1965).

5. A. Corwin, Ann. N.Y. Acad. Sci. 206, 201 (1973).

6. R.E. Dickerson, T. Takano, D. Eisenberg, O.B. Kallai, L. Samson, A. Cooper, and E. Margoliash, J. Biol. Chem. 246, 1511 (1971).

7. A. Tasaki, in "Probes of Enzymes and Hemoproteins" (B. Chance, T. Yonetani and A.S. Mildvan, eds.) p. 247. Academic Press, 1971.

8. A. Tasaki, in "Probes of Enzymes and Hemoproteins", Vol. II, (B. Chance, T. Yonetani and A.S. Mildvan, eds.) Academic Press, 1971.

9. M.M. Meltempo, T.H. Moss and M.A. Cusanovich, Biochim. Biophys. Acta 342, 290 (1974).

10. M.M. Meltempo and T.H. Moss, Quarterly Reviews of Biophysics 9, 181 (1976).

11. W.T. Simpson, J. Chem. Phys. 17, 1218 (1949).

12. B.N. Figgis, "Introduction to Ligand Fields", Interscience Publishers, John Wiley & Sons, 1967.

13. H. Eyring, J. Walter and G.E. Kimball, "Quantum Chemistry", John Wiley, 1944.

14. T. Iizuka and M. Kotani, Biochim. Biophys. Acta 194, 351 (1969).

15. J.S. Griffith, Proc. Roy. Soc. (London) A 235, 23 (1956).

16. P. Day, D.W. Smith and R.J.P. Williams, Biochem. 6, 1563 (1967).

17. B.R. Sreenathan and C.P. Taylor, Biochem. Biophys. Res. Commun. 42, 1122 (1971).

18. C.C. McDonald, W.D. Phillips and S.N. Vinogradov, Biochem. Biophys. Res. Commun. 36, 442 (1969).

19. M. Zerner, M. Gouterman, H. Kobayashi, Theor. Chem. Acta 6, 363 (1966).

20. A.D. Buckingham and P.J. Stephens, Ann. Rev. Phys. Chem. 17, 399 (1966).

21. B. Briat and C. Djerassi, Nature 217, 918 (1968).

22. P.N. Schatz and A.J. McCaffery, Quart. Rev. Chem. Soc. 23, 552 (1969).

23. P.J. Stephens, Ann. Rev. Phys. Chem. 25, 201 (1974).

24. L. Vickery, T. Nozawa and K. Sauer, J. Am. Chem. Soc. 98, 351 (1976).

25. L.A. Livshitz, A.M. Arutyunyan and Y.A. Sharnov, J. Chem. Phys. 64, 1276 (1976).

26. H. Kobayashi, Adv. Biophys. 8, 191 (1975).

27. F.E. Mabbs and D.J. Machin, "Magnetism and Transition Metal Complexes", Chapman and Hall, 1973.

28. J.H. Van Vleck, "The Theory of Electric and Magnetic Susceptibilities", Oxford University Press, 1965.

29. A. Carrington and A.D. McLachlan, "Introduction to Magnetic Resonance", Harper and Row, New York, 1967.

30. P.F. Knowles, D. Marsh and H.W.E. Rattle, "Magnetic Resonance of Biomolecules", John Wiley and Sons, Inc., 1976.

31. J.R. Bolton, "Biological Applications of Electron Spin Resonance", (H.M. Swartz, J.R. Bolton and D.C. Berg, eds.) John Wiley and Sons, Inc., 1972.

32. J.E. Wertz and J.R. Bolton, "Electron Spin Resonance", p. 135, McGraw-Hill, New York, 1972.

33. M. Weissbluth, "Hemoglobin", Springer-Verlag, New York, 1974.

34. C.P.S. Taylor, Biochim. Biophys. Acta 491, 137 (1977).

CHAPTER III

PREPARATION AND CHARACTERIZATION OF N-ACETYLATED HEME OCTAPEPTIDE: N-H8PT

CHAPTER III

A. INTRODUCTION

Appropriate model systems of hemoproteins can be of great value in studies concerning the elucidation of structure-function relationships in the parent molecules. Porphyrins and iron porphyrins, in particular, have received close attention because of their structural analogy to the prosthetic groups of hemoproteins (1-7). However, their intrinsic low solubilities and aggregation properties in aqueous solutions have been a serious problem for obtaining any meaningful information. It is especially true with regard to the details of ligand binding effects on hemes and heme analogs, because most of the studies have been carried out in non-aqueous solvent systems. Use of non-aqueous solvent medium, although it removes the aggregation problem, remains undesirable because the active sites of hemoproteins are at least partially exposed to water in the native state.

For cytochromes of type c, the two representative model compounds are hemin c and heme peptides of mammalian cytochrome c (8-17). Hemin c contains two cystinyl thioether linkages at the vinyl sites of protoporphyrin IX characteristic of the parent molecule. The addition of thioether bonds to porphyrin not only greatly enhances water solubility but also yields a typical type c hemochrome absorption spectrum; the position of the Q_{o-o} transition lies higher in energy than that of normal iron protoporphyrin IX. This is due to

reduction in the size of porphyrin π system. Extensive investigation has been performed on the optical and thermodynamic characteristics of ligand binding on hemin c in aqueous solutions (18). However, hemin c still dimerizes readily even at a dilute concentration; i.e., in the order of 10^{-6}M. In addition, it does not form mixed axial coordinate complexes such as cytochrome c where sulfur of methionine and nitrogen of histidine residues are known to be the axial ligands. The better models are the heme peptides directly isolated from the native enzyme by the action of protease or chemical means (11,14,15). The length of the peptides may vary from five to sixty five. More commonly used and extensively characterized are the heme undeca- and octapeptides of horse heart cytochrome c (Fig. 1), first prepared by Tuppy and Pelius (9) and later by Harbury and Loach (10). These model systems are unique in that the fifth axial coordination site is intrinsically occupied by the imidazole of the peptide histidyl residue. Furthermore, the hemes are covalently bonded to the peptide as in hemin c. Thus, the principal difference from its parent molecule is the absence of methionine ligand and the protein moiety. These heme oligopeptides are readily soluble over a wide range of pH, an additional advantage for studying aqueous solution properties. The absorption spectral and the pH-dependent redox properties of some of the nitrogenous complexes as well as heme peptides themselves have been

Figure 1. Amino acid sequence of the heme undeca- and octapeptides of horse heart cytochrome c.

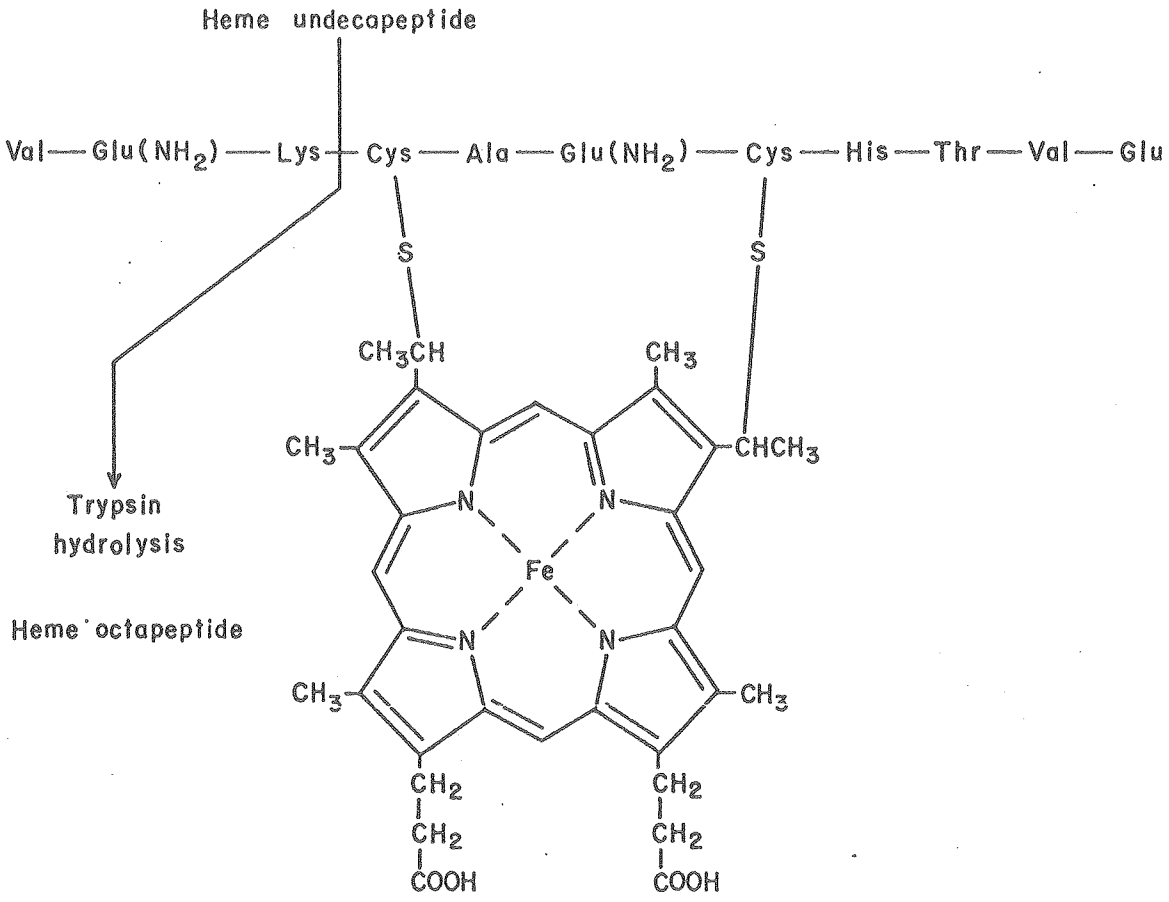
Heme undecapeptide
Val—Glu(NH2)—Lys—Cys—Ala—Glu(NH2)—Cys—His—Thr—Val—Glu
S
S
CH3CH
CH3
CH3
CHCH3
N
N
Fe
N
N
CH3
CH3
CH2
CH2
COOH
CH2
CH2
COOH
Trypsin
hydrolysis
Heme octapeptide

XBL751-5026

investigated in detail previously (10,11,19,20). In these studies there were indications of concentration-dependent intermolecular heme interactions between the heme peptides, later verified by Urry and Pettegrew (21,22) in their optical and circular dichroism (CD) studies in the Soret region. The effect of aggregation is found to be manifest as exciton splitting of the Soret transition. In addition, the observed hypo- or hyperchromism that arises from large dispersion force interactions between the hemes at high concentrations is found to reflect the geometric heme orientations within the aggregates. This may facilitate determination of the heme arrangements in multi-heme proteins such as cytochrome oxidase, hemoglobin and cytochrome cc'. One obvious mechanism of aggregation is to form a tight dimer where the free N-terminal amino group of one peptide participates as a sixth ligand to the second heme molecule. In the heme undecapeptide (H11PT), intermolecular coordination is also possible via the ε-amino group of the lysyl residue (Fig. 1). In fact, more recent studies concerning pH-dependent kinetic measurements and magnetic properties have shown that the H11PT undergoes lysine residue-induced aggregation via the ε-amino group with a pK value of 7.6, while the N-terminal α-amino group mediated aggregation occurs with a pK value of 5.8 (23,24). At low heme concentrations, where heme peptides are mostly monomeric species, attempts were also made to identify the unknown ligands of cytochrome c before the x-ray structure became known (12,13).

Although previous studies illustrate versatile applicability of heme peptides as model compounds of various hemoproteins, they do not include extensive characterization of monomeric heme peptides at high concentration, which may be obtained by blocking the free amino group. For our magnetic and electron spin resonance measurements discussed in Chapter V, it is important that ligand induced aggregation such as that mentioned above is removed even at high concentration. Described in this chapter are the methods for the preparation of the N-acetylated ferric heme octapeptide from horse heart cytochrome c. Also included is its detailed optical and CD spectral characterization.

B. ISOLATION AND N-ACETYLATION OF FERRIC HEME OCTAPEPTIDE

Materials

Horse heart cytochrome c (Type IV grade) was obtained from Sigma and used without further purification. Pepsin and trypsin twice crystallized products were also from Sigma and used without further purification. Acetic anhydride was from Matheson, Coleman and Bell, sodium acetate and ammonium sulfate, from Baker and Adamson, and trichloroacetic acid, from Mallinckrodt. Other reagents were of analytical grade.

Methods

Absorption spectra were recorded on a Cary 118 Spectrometer and CD spectra on an instrument which is described elsewhere (25). Amino acid analyses were performed using a Beckman Multichrome

Liquid Column Chromatograph 120C. The heme concentration was determined from the absorbance at 406 nm of the imidazole complex, which exhibits $\varepsilon_M = 128 \times 10^3\ M^{-1}cm^{-1}$ at pH 7.0 (13).

The isolation procedure was essentially that used by Harbury and Loach (10). A solution containing 2.0 g cytochrome c and 40 mg pepsin in a total volume of 200 ml at pH 1.5 was incubated for 10 hours at 20°C with slow stirring. Additional 40 mg pepsin was added, the pH was restored to 1.5, and the product was precipitated at 3°C by ammonium sulfate addition to a final concentration of 4.1 M (near saturation). The solution was then centrifuged at 7.7 kg for 15 minutes at 3°C. The precipitates were dissolved in 110 ml, 0.01 M NH_4OH, and to that was added slowly with stirring 500 ml of 4.2 M ammonium sulfate solution at 3°C. After 20 minutes, 19.5 ml of 1.2 M trichloroacetic acid was added and the precipitates were collected by centrifugation again at 7.7 kg, 3°C and redissolved in 40 ml of 0.01 M NH_4OH. After dialysis for 12 hours at 3°C against 10^{-3}M NH_4OH with frequent changes of NH_4OH solution during the period, the sample solution was subjected to lyophilization.

A partition column which was 2 cm in diameter and 40 cm long was prepared as follows: crude Hyflo Super-Cel was washed twice in 6N HCl with stirring followed by thorough washing with distilled water. The solution was filtered and dried at 115°C. To 39 g of dried Hyflo Super-Cel, 24 ml of the aqueous phase of a mixture n-butanol/acetic acid/water

(4 : 1 : 5) was added followed by 105 ml of the non-aqueous phase. The slurry was used to pack the column. The lyophilized heme fragments were then dissolved in 4.0 ml of the non-aqueous phase and loaded on the column. It was eluted with the non-aqueous phase at a rate of 4 ml/hr and the main colored band was collected into tubes with 3 ml each. The chromatogram obtained by absorbance reading at 625 nm confirmed the presence of a single component. The tubes in the tail region of the chromatogram were discarded. The purified H11PT so obtained was extracted into the aqueous phase by addition of 3.5 M NH_4OH. Several repeated extractions were combined to give a total volume of 4.4 ml; the final pH was 8.7. The sample solution was dialized against 10^{-3}M NH_4OH for 5 hours with at least four changes of NH_4OH solution during the period, and against distilled water for 3 hours. The resulting material was lyophilized.

Conversion of the H11PT to H8PT was carried out as follows: After 200 mg of the H11PT was dissolved in 90 ml of 5 x 10^{-3}M NH_4OH, 21 mg of twice crystallized trypsin was added and the solution was incubated for 12 hours at 36°C with slow stirring. The pH of the solution was monitored to follow the rate of hydrolysis. At the end of incubation, another 11 mg of trypsin was added and the incubation continued for an additional 12 hours at 36°C. No pH change was observed towards the end of second incubation period indicating the completion of hydrolysis. The solution was boiled at 100°C for 5 minutes and subjected to lyophilization. The crude

product of the H8PT was then purified by partition chromatography according to the method described above. The resulting material was dialized against 10^{-3}M NH_4OH and against water, then was lyophilized again.

Acetylation of the N-terminal amino group of the H8PT was carried out by the method of Fraenkel-Conrat (26). A mixture containing equal volumes of heme solution (60 mg/1.5 ml) and saturated sodium acetate solution was treated by slow addition of an amount of acetic anhydride approximately equal to the weight of the H8PT at 0°C. The mixture was allowed to react for 3 hours at 0°C. The modified H8PT was then purified twice on a Bio Gel P-2 column (1.5 cm x 15.0 cm) equilibrated with 0.1 M phosphate buffer, pH 7.0 and dialized abainst 5 x 10^{-3} M phosphate buffer, pH 7.0 followed by distilled water. The final sample solution was lyophilized and stored at -20°C. For amino acid analysis, the following procedure was used. 1 mg of the heme peptide, which was enough to provide 0.02 to 0.6 micromoles of each constituent amino acid, was dissolved in 1.0 ml of glass-distilled 6N HCl. The solution was transferred into a test tube with a narrow neck, 1 to 3 mm in diameter, at a point about 1.5 cm from the end of the tube, frozen in dry ice/acetone bath and connected to a high vacuum pump line. It was evacuated for 20 minutes while keeping the solution frozen, and the tube was sealed at the narrow neck with a torch. The sample was allowed to hydrolyze

for 22 hours in a 110°C oven. After cooling, the top of the tube was removed and the precipitates containing heme residues were removed by centrifugation. The HCl in the hydrolyzate was evaporated to dryness under vacuum in a closed desiccator with a dish of NaOH pellets. The dried film of hydrolyzed sample was dissolved in 2.0 ml buffer, pH 2.2 for the analysis.

C. RESULTS AND DISCUSSION

Amino acid analyses of the H11PT and H8PT gave results in good agreement with those reported by Harbury and Loach (10) and are consistent with the known composition of the peptides (Table I). It is significant that in the H8PT preparation, lysine content is reduced to 2%, indicating essentially complete trypsin hydrolysis. Complete N-acetylation of the H8PT was verified by thin layer chromatography on a silica gel plate using the non-aqueous phase of a mixture n-butanol/acetic acid/water (4 : 1 : 5) as a solvent system. The N-acetylated H8PT (N-H8PT) showed no trace of the unmodified form. The R_f values for the H8PT and N-H8PT were approximately 42 and 57, respectively, which agree very well with the reported values (20).

Figures 2 and 3 show concentration dependent variations of the visible absorption and Soret circular dichroism spectra of the ferric H8PT at neutral pH, 20°C before and after N-acetylation. For the absorption spectra, concentration and path length were reciprocally changed to maintain the heme

TABLE I

AMINO ACID ANALYSIS

Residue	Peak Area/Average Area	
	H11PT	H8PT
Ala	0.96	1.04
Glu (NH_2), Glu	3.12	2.10
His	1.04	0.96
Thr	0.87	0.86
Val	1.91	1.05
Lys	1.10	0.02
Cys (2)	0.89	0.67
Others		
Asp	0.08	0.06
Ser	0.02	0.04
Gly	0.08	0.08
Ile	0.03	0.05
Leu	0.04	0.06
Tyr	0.03	0.03
Phe	0.01	0.01

XBL 786 - 4007

Figure 2A. The concentration dependent absorption spectra of the heme octapeptide at pH 7.0, 20°C.

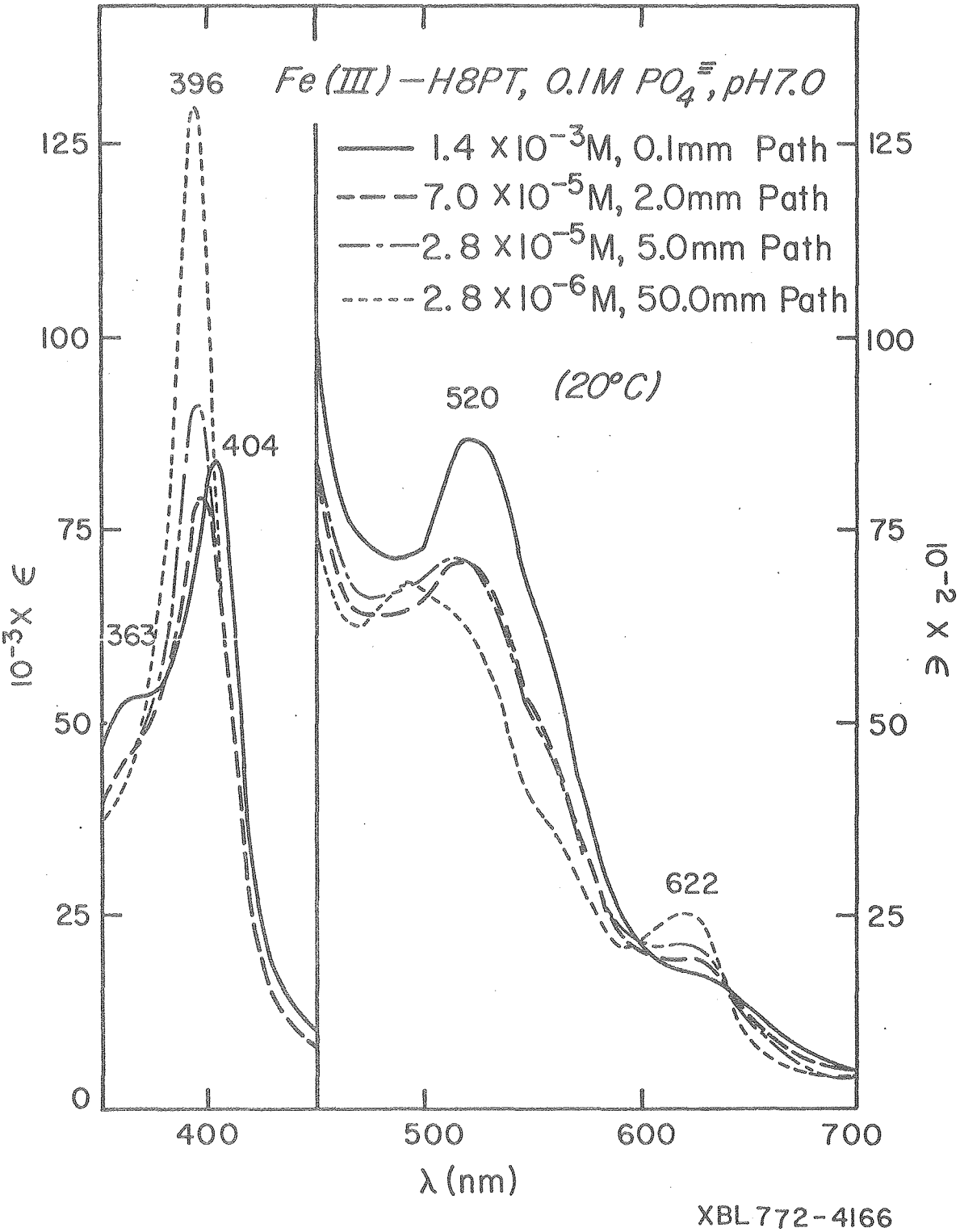
Fe(III)–H8PT, 0.1M $PO_4^{\equiv}$, pH7.0
1.4 x10^{-3}M, 0.1mm Path
7.0 x10^{-5}M, 2.0mm Path
2.8 x10^{-5}M, 5.0mm Path
2.8 x10^{-6}M, 50.0mm Path
(20°C)
396
404
363
520
622
$10^{-3} \times \epsilon$
$10^{-2} \times \epsilon$
λ (nm)
0
25
50
75
100
125
400
500
600
700

XBL 772-4166

Figure 2B. The concentration dependent Soret circular dichroism spectra of the heme octapeptide at pH 7.0, 20°C.

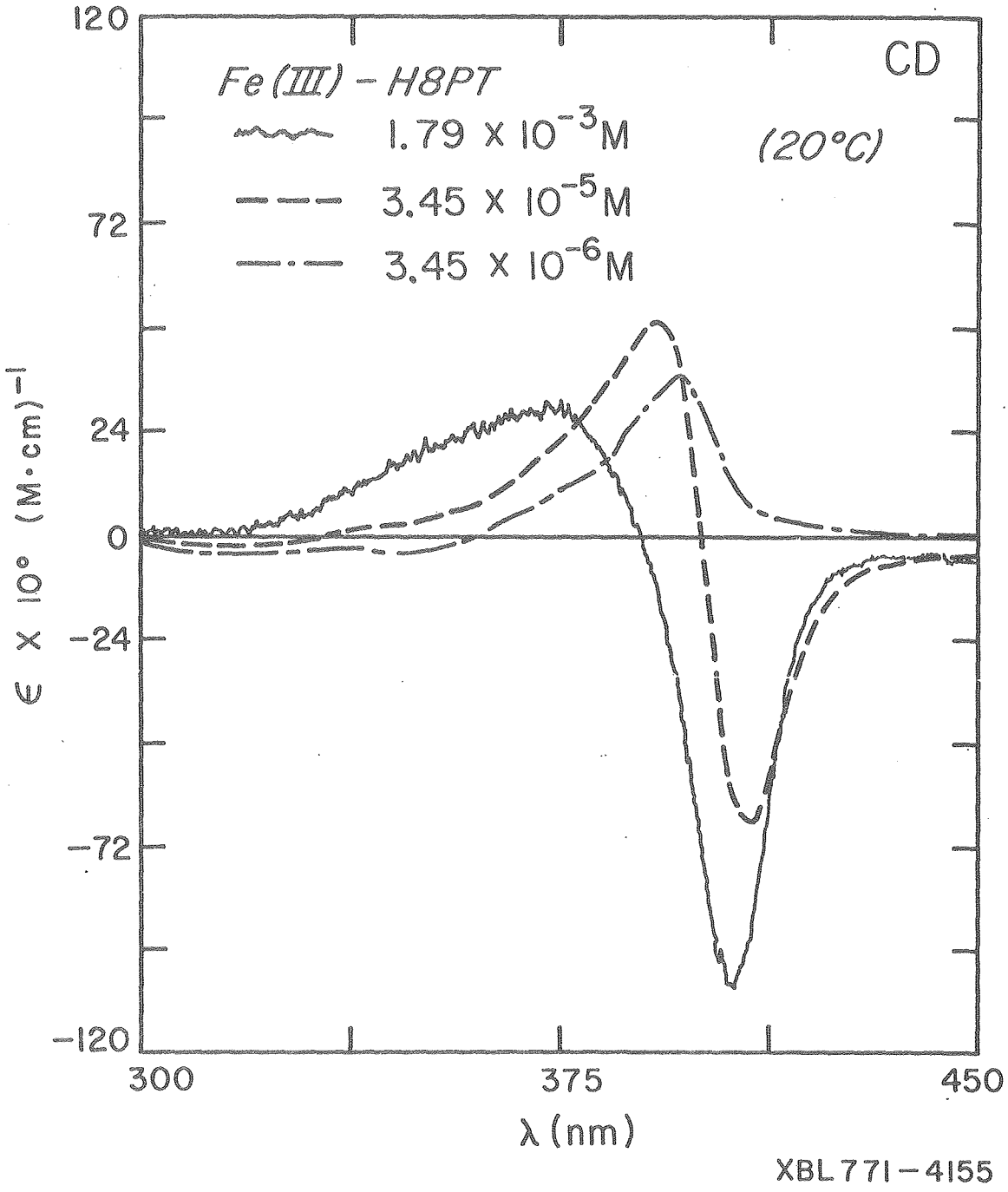
120
72
24
0
-24
-72
-120
300
375
450
λ (nm)
Ψ x 10° (M·cm)⁻¹
CD
Fe(III) - H8PT
1.79 x 10⁻³M
3.45 x 10⁻⁵M
3.45 x 10⁻⁶M
(20°C)
XBL 771-4155

Figure 3A. The concentration dependent absorption spectra of the N-acetylated heme octapeptide at pH 7.0, 20°C.

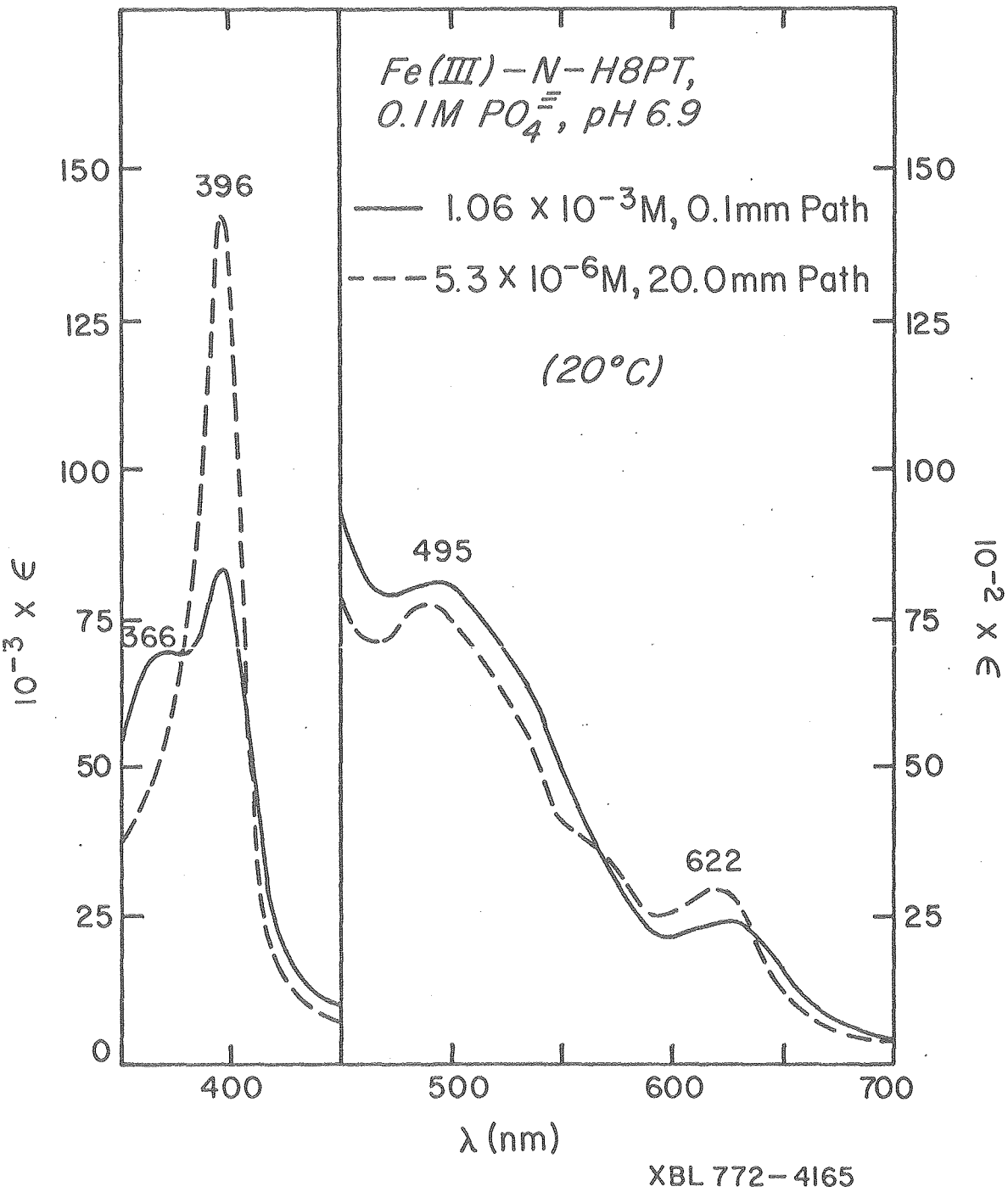
Fe(III)-N-H8PT,
0.1M $PO_4^{\equiv}$, pH 6.9
1.06 x 10^{-3}M, 0.1mm Path
5.3 x 10^{-6}M, 20.0mm Path
(20°C)
396
366
495
622
10^{-3} x ε
10^{-2} x ε
λ (nm)
0
25
50
75
100
125
150
400
500
600
700

XBL 772-4165

Figure 3B. The concentration dependent Soret circular dichroism spectra of the N-acetylated heme octapeptide at pH 7.0, 20°C.

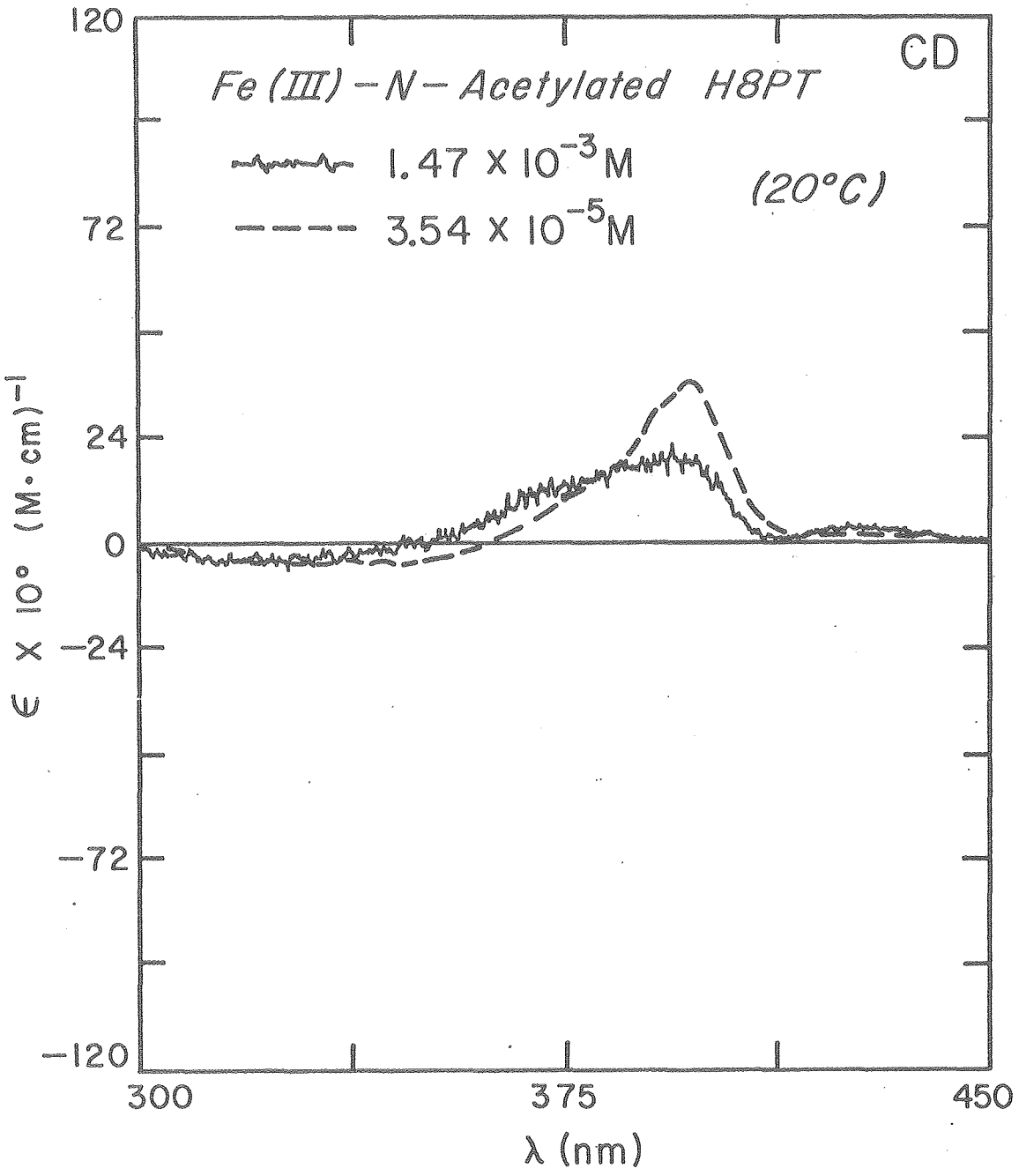
120
72
24
0
−24
−72
−120
CD
Fe (III) – N – Acetylated H8PT
1.47 X 10⁻³ M
3.54 X 10⁻⁵ M
(20°C)
ε X 10° (M·cm)⁻¹
300
375
450
λ (nm)

XBL 771-4154

content of each solution equal. In Fig. 2A, the spectrum of the H8PT at low heme concentration (dotted trace) is of high spin character: The Soret band lies below 400 nm, α, β bands are not well resolved and there is a distinct 625 nm charge transfer band that is believed to arise from a porphyrin π to iron dπ transition. At low heme concentration, where monomeric species are predominant, a sixth axial ligand site is thought to be occupied by a water molecule, a weak field ligand. The spectrum at high concentration (solid trace), on the other hand, exhibits a large amount of low spin character, indicated by the red-shifted Soret band, the well resolved strong β band at 520 nm and reduced intensity of the 625 nm band. The low spin form arises from intermolecular coordination of the heme via the free N-terminal amino group of another peptide, providing a strong field ligand. A split Soret transition with its maximum at 404 nm and a shoulder at 363 nm is due to exciton resonance interaction. As has been discussed previously by Urry (21), a dipolar interaction potential between transition moments in heme aggregates consists of a term describing interactions of the Soret transition in one chromophore with the Soret transitions in other chromophores, and a term resulting from interactions of the Soret transition with all of the other in-plane polarized transitions, such as the visible and charge transfer bands. The former gives rise to exciton splitting of the doubly degenerate Soret transition and the latter to dispersion

force interactions leading to hyper- or hypochromism. Hyper- and hypochromism attending aggregation are associated with increase and decrease respectively of the oscillator strength on a per absorbing unit basis (22). Tinoco (27) and Rhodes (28) have related these phenomena to geometric arrangements of subunits in polymeric systems. The assumption is that the transition under consideration is in the plane of an aromatic chromophore and that the polarizability in that plane is greater than the polarizability perpendicular to the plane. More specifically, the planar aromatic groups in a stacked conformation are expected to give rise to hypochromism and those in a head-to-tail alignment, to hyperchromism. The same conclusion such as above may be made in aggregated heme peptide systems, because the Soret transition is x-y polarized and the dipole strength in-plane is much greater than that out-of-plane. In Fig. 2A is shown the apparent aggregation-dependent hypochromism of the H8PT. This suggests that the H8PT exists in a more stacked configuration than the head-to-tail alignment consistent with the reported results (22). Exciton interactions treated by Kasha (29) predict a blue or red shift of the absorption band position in addition to splitting of the band in the two limiting cases - a parallel stacking or a head-to-tail alignment of transition dipoles, respectively. In other words, hypochromism leads to a blue shift and hyperchromism, to a red shift. In the H8PT case, the

Soret band is split about the position of the monomer transition which suggests an oblique orientation of heme planes.

The effect of exciton interaction is more pronounced in CD spectra because the induced molecular dissymetry results in split Soret transitions with rotational strengths of opposite sign. In Fig. 2B, the Soret CD spectrum at low heme concentration exhibits only a single peak with a maximum at 396 nm while at high concentration, a double CD feature is observed, in good agreement with the reported results (22). The lack of an isosbestic or isoelliptic point in the spectra indicates that the aggregation results in multiple states involving higher degrees of polymerization.

After N-acetylation, as can be seen in Fig. 3A, the visible region of the absorption spectrum remains high spin in character even at high heme concentration. This provides evidence for the removal of ligand-induced aggregation. The Soret band is still split, however, although its maximum occurs at a different wavelength, 396 nm (solid trace). The band maximum is at the monomer position, unlike the free H8PT whose maximum occurs at 404 nm. This suggests the presence of heme interactions that may be different in nature. Fig. 3B shows CD spectra that consist of a single positive peak at both low and high concentration. The decreased ellipticity and the small bandshape changes at high concentration indicate some kind of heme interaction.

The ability of porphyrins to participate in π interactions is widely recognized from both their tendency to aggregate in solution regardless of whether a metal or axial ligand is present, and their interaction with organic donor and acceptor molecules (30-35). In addition, several model compounds forming π donor-acceptor stacking type dimers have been characterized in terms of their spectroscopic and magnetic properties (36). As suggested by Goff and Morgan (8) in their studies of hemin c aqueous solution properties, most probably the N-H8PT molecules are also associated by dihydroxo bridges or bound by π donor-acceptor forces. The latter would require hydrolysis of each Fe(III) to reduce charge at the iron center for closer approach of two hemes. They have shown that the hemin c solution at 4×10^{-6} M gives rise to a split Soret band with one of the maxima occurring at the monomer position, which agrees with our absorption results of the N-H8PT at high concentration. Should such an interaction indeed exist, a weak antiferromagnetic coupling should be observed as a slightly diminished value of the high spin heme iron (S = 5/2) magnetic moment (36). As will be seen in chapter V, our magnetic data are consistent with the view of having π interaction in the N-H8PT at high concentration.

REFERENCES

1. M. Momenteau, M. Rougée and B. Loock. Eur. J. Biochem. 71, 63 (1976).
2. C.K. Chang and T.G. Traylor. Proc. Nat. Acad. Sci. U.S. 70, 2647 (1973).
3. J.P. Collman, R.R. Gagne, C.A. Reed, T.R. Halbert, G. Lang and W.T. Robinson. J. Am. Chem. Soc. 97, 1427 (1975).
4. G.C. Papaefthymiou, R.B. Frankel, S. Foner, S.C. Tang and S. Koch. J. de Physique, Coll C6, Suppl. 12, Tonne 37, 209 (1976).
5. E.H. Abbott and P.A. Rafson. J. Am. Chem. Soc. 96, 7378 (1974).
6. D. Brault and M. Rougee. Biochem. 13, 4591 (1974).
7. S.J. Cole, G.C. Curthoys and E.A. Magnusson. J. Am. Chem. Soc. 92, 2991 (1970).
8. H. Goff and L.O. Morgan. Inorg. Chem. 15, 2062 (1976).
9. H. Tuppy and S. Paléus. Acta Chem. Scand. 9, 353 (1955).
10. H.A. Harbury and P.A. Loach. J. Biol. Chem. 235, 3640 (1960).
11. H.A. Harbury and P.A. Loach. J. Biol. Chem. 235, 3646 (1960).
12. H.A. Harbury, J.R. Cronin, M.W. Fianger, T.P. Hettinger, A.J. Murphy, Y.P. Myer and S.N. Vinogradov. Proc. Nat. Acad. Sci. 54, 1658 (1965).
13. N. Nanzyo and S. Sano. J. Biol. Chem. 243, 3431 (1968).
14. G. Corradin and H.A. Harbury. Biochim. Biophys. Acta 221, 489 (1970).

15. A.M. Arutyunyan and Y.A. Sharonov. J. Mol. Biol. __, 478 (1975).

16. W.W. Wainio and K. Hillman. Bioenergetics 6, 161 (1974).

17. W.W. Wainio, L.M. Krausz and K. Hillman. Biochem. Biophys. Res. Comm. 39, 1134 (1970).

18. H. Goff and L.O. Morgan. Inorg. Chem. 15, 2069 (1976).

19. Y.P. Myer and H.A. Harbury. Annals N.Y. Academy of Sciences, 139, 685 (1967).

20. G.C. Wagner and R.J. Kassner. Biochim. Biophys. Acta 405, 205 (1975).

21. D.W. Urry. J. Am. Chem. Soc. 89, 4190 (1967).

22. D.W. Urry and J.W. Pettegrew. J. Am. Chem. Soc. 89, 5276 (1967).

23. M.T. Wilson and R.J. Ranson. Eur. J. Biochem. 77, 193 (1977).

24. A.M.T. Jehanli, D.A. Stotter and M.T. Wilson. Eur. J. Biochem. 71, 613 (1976).

25. J.C. Sutherland, L.E. Vickery and M.P. Klein. Rev. Sci. Instrum. 45, 1089 (1974).

26. H. Fraenkel-Conrat. Methods in Enzymology 4, 245 (1957).

27. I. Tinoco, Jr. J. Am. Chem. Soc. 82, 4785 (1960).

28. W. Rhodes. J. Am. Chem. Soc. 83, 3609 (1961).

29. M. Kasha. Radiation Res. 20, 55 (1963).

30. D. Mauzerall. Biochemistry 4, 1801 (1965).

31. R.J. Abraham, P.A. Burdidge, A.H. Jackson and D.B. Macdonald. J. Chem. Soc. B. 620 (1966).

32. W.S. Caughey, J.L. York and P.K. Iber, in Magnetic Resonance in Biological Systems, A. Ehrenbert, et al., Ed., Pergamon Press, Oxford, 1967.

33. D.A. Doughty and C.W. Dwiggins. J. Phys. Chem. 73, 423 (1969).

34. C.D. Barry, H.A.O. Hill, B.E. Mann, P.J. Sadler and R.J.P. Williams. J. Am. Chem. Soc. 95, 4545 (1973).

35. R.J. Abraham, G.H. Barnett, E.S. Bretschneider and K.M. Smith. Tetrahedron 29, 553 (1973).

36. H.J. Schugar, G.R. Rossman and H.B. Gray. J. Am. Chem. Soc. 91, 4564 (1969).

CHAPTER IV

ABSORPTION AND MCD SPECTRA OF THE COMPLEXES OF N-H8PT

CHAPTER IV

A. INTRODUCTION

Studies of electronic structure and magnetic properties of hemoproteins are essential to the understanding of their physiological functions. In cytochromes, of particular interest has been the possible role of axial ligands provided by the protein in the regulation of electron transport. Evidence suggests that the magnetic state of the iron, which in part is determined by the chemical nature of the axial ligands, plays an important role in electron transport by affecting the reduction potential of the enzyme (1,2). As discussed in Chapter II, the electronic properties of porphyrin are closely coupled with the magnetic properties of iron in ferric hemoproteins (3-10). Thus, optical measurements are convenient for monitoring subtle changes in the immediate heme environment. Magnetic circular dichroism (MCD) is especially useful for structural studies of hemoproteins because of its ability to discriminate both the oxidation and spin state changes independently of each other (11-20). Our effort has been focused on elucidating the electronic structure of the heme in general through detailed ligand binding effects on the ferric N-H8PT.

Described in this chapter are our initial attempts to prepare the model complex of cytochrome c with the H8PT using organic analogs of methionine sulfur ligand in both aqueous and non-aqueous (dimethyl sulfoxide) solvents. Sulfur

ligands possess weak binding affinities toward ferric ion. Thus, solubility often is a limiting factor for the extent of ligation. Dimethyl sulfide which has a stronger binding affinity towards Fe (III) ion than methionine in dimethyl sulfoxide has been used in hopes of increasing the amount of the ligand bound hemes. Also included are the absorption and MCD spectral measurements on the complexes of the N-H8PT with various external ligands, i.e. fluoride, hydroxide, azide, N-methionine, imidazole and cyanide at neutral pH (except hydroxide), 20°C. These complexes behave generally as predicted by ligand field strength considerations. Imidazole-sulfur coordination is thought to produce a strong field interaction, because cytochrome c exists in the purely low spin state independent of temperature. However, our model system studies show that this appears not to be the case.

Spectroscopic identification of the intrinsic axial ligands of cytochromes whose x-ray structures are not yet known is of particular interest to us. Previous workers have suggested that the inherent sensitivity of the visible MCD spectral band shape to the electronic structure of the heme chromophore bears a great potential for determining the nature of the axial ligands (16). In this regard, our N-H8PT complexes seem to provide excellent model systems for systematic comparative studies. Attempts have been made to elucidate the unknown ligands of cytochromes c_1 (yeast) and

f (spinach). Both cytochromes are known to be of type c. That is, the α band maximum of the reduced form occurs near 550 nm which is 10-20 nm higher in energy than the α band of typical low spin hemoproteins in the reduced state. This is believed to arise from the covalent linkage of the heme group to the protein which breaks the π bond of the two vinyl side chains included in the π system of protoporphyrin IX. The main question is whether methionine coordination is a universal property of all type c cytochromes. The MCD results alone do not provide unequivocal evidence.

B. EXPERIMENTAL

Materials and Methods

The ligand solutions were prepared by dissolving appropriate potassium salts in 0.1 M phosphate buffer at pH 7.0. The stock solution of N-acetylated methionine (3.0 M) was prepared by a slow addition of a solution containing 6.0 M KOH in 0.1 M phosphate buffer to solid N-methionine until it reached neutral pH, followed by adjustment of the final volume with 0.1 M phosphate buffer, pH 7.0. N-methionine amide was used as obtained from Cyclo Chemical Company. N-methionine methyl ester was prepared from methionine methyl ester-HCl salt obtained from Sigma by N-acetylation. The procedure used was as follows. 0.5 g methionine methyl ester-HCl was dissolved in 100 ml pyridine followed by addition of 50% molar excess of acetic anhydride. To this mixture an equivalent amount

of tetraethyl amine was added to pull the equilibrium to the product formation and it was allowed to react for six hours. After rotary evaporation, the oily residue was dissolved in an equal volume of $CHCl_3$, washed with 0.3 M HCl solution three times, washed again with saturated NaCl solution and filtered after the addition of sodium sulfate. The solution was then subjected to rotary evaporation. N-methionine methyl ester was a yellowish oil. Cytochromes c (yeast) and f (spinach) were a generous gift from Dr. J. Siedow, Department of Botany, Duke University, N.C. Dimethyl sulfide and dimethyl sulfoxide were from Baker and used without further purification. Hemin was from Eastman Kodak and used as obtained.

Absorption spectra were recorded on a Cary 118 spectrometer. When necessary, temperature control was made using a Forma-Temp Jr. model 2095 water bath. MCD spectra were obtained on an instrument which is described elsewhere (21). Temperature control was obtained by using jacketed cells.

C. RESULTS

Fig. 1 shows the absorption spectra of ferric cytochrome c and of the ferric H8PT in the presence of N-methionine or dimethyl sulfide (DMS) in 0.1 M phosphate buffer, pH 7.0. The ligand concentrations indicated in the figure are those at which the spectral changes are nearly saturated. The spectrum of cytochrome c is typical of the low spin form, with a

Figure 1. The absorption spectra of ferric cytochrome c and the ferric heme octapeptide in the presence of N-methionine or dimethyl sulfide. The ligand concentrations are those at which the spectral changes are nearly saturated.

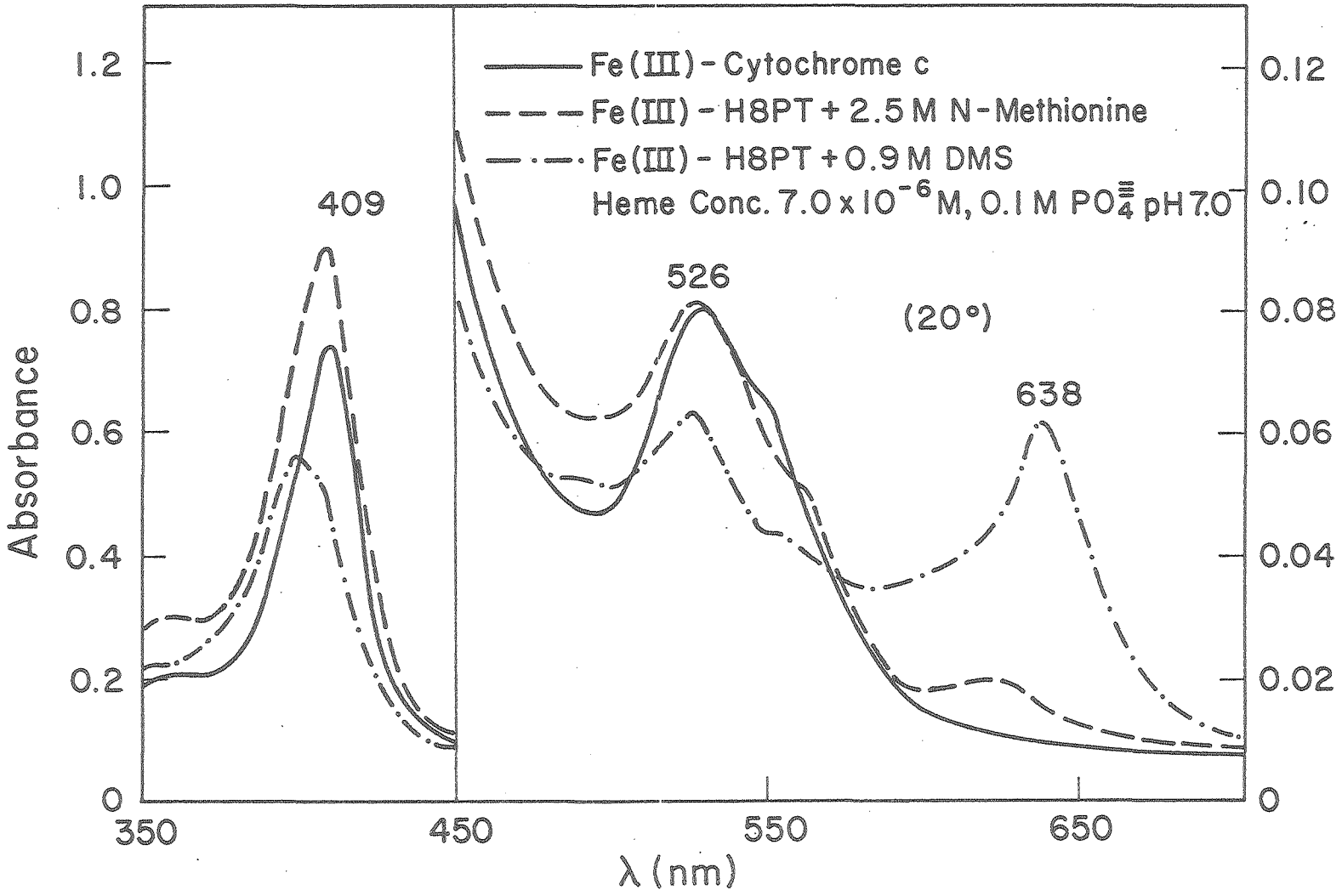
Fe(III) - Cytochrome c
Fe(III) - H8PT + 2.5 M N-Methionine
Fe(III) - H8PT + 0.9 M DMS
Heme Conc. 7.0 x 10⁻⁶ M, 0.1 M PO₄ pH 7.0
409
526
638
(20°)
Absorbance
λ (nm)
1.2
1.0
0.8
0.6
0.4
0.2
0
0.12
0.10
0.08
0.06
0.04
0.02
0
350
450
550
650

XBL 786-3967

Soret maximum at 410 nm and a β maximum at 528 nm. Even though the two axial ligands of the H8PT complex with N-methionine (N-Met-H8PT), are identical to those of cytochrome c, it exhibits a residual of the charge transfer band near 625 nm characteristic of a high spin form in addition to all the low spin features of cytochrome c. This suggests that the N-Met-H8PT complex exists as a thermal mixture of high and low spin forms, as has been found in various hemoprotein derivatives. Although DMS appears to be a good sulfur ligand representing methionine, the spectrum of the DMS-H8PT complex does not exhibit either the low spin, the high spin or the mixed spin spectral features. The Soret intensity is diminished drastically with indications of at least two transitions under the absorption envelope, concomitant with the appearance of a strong new band at 638 nm. The nature of this new band is not clear. Furthermore, the intensities of the 638 nm band and the Soret band decrease as a function of time. Fig. 2 shows the absorption spectra of the ferric H8PT with or without DMS in 80% DMSO/H_2O. The free H8PT in DMSO/H_2O shows some low spin features as indicated by the increase of the β band intensity near 525 nm and the shift of the Soret maximum to lower energy, 402 nm. Most probably, this is due to interaction with the solvent molecules. DMSO is a weak field ligand, but the effective ligand field strength is expected to be greater than that of water owing to its increased electron donating

Figure 2. The absorption spectra of the ferric heme octapeptide with or without dimethyl sulfide in 80% DMSO/H_2O.

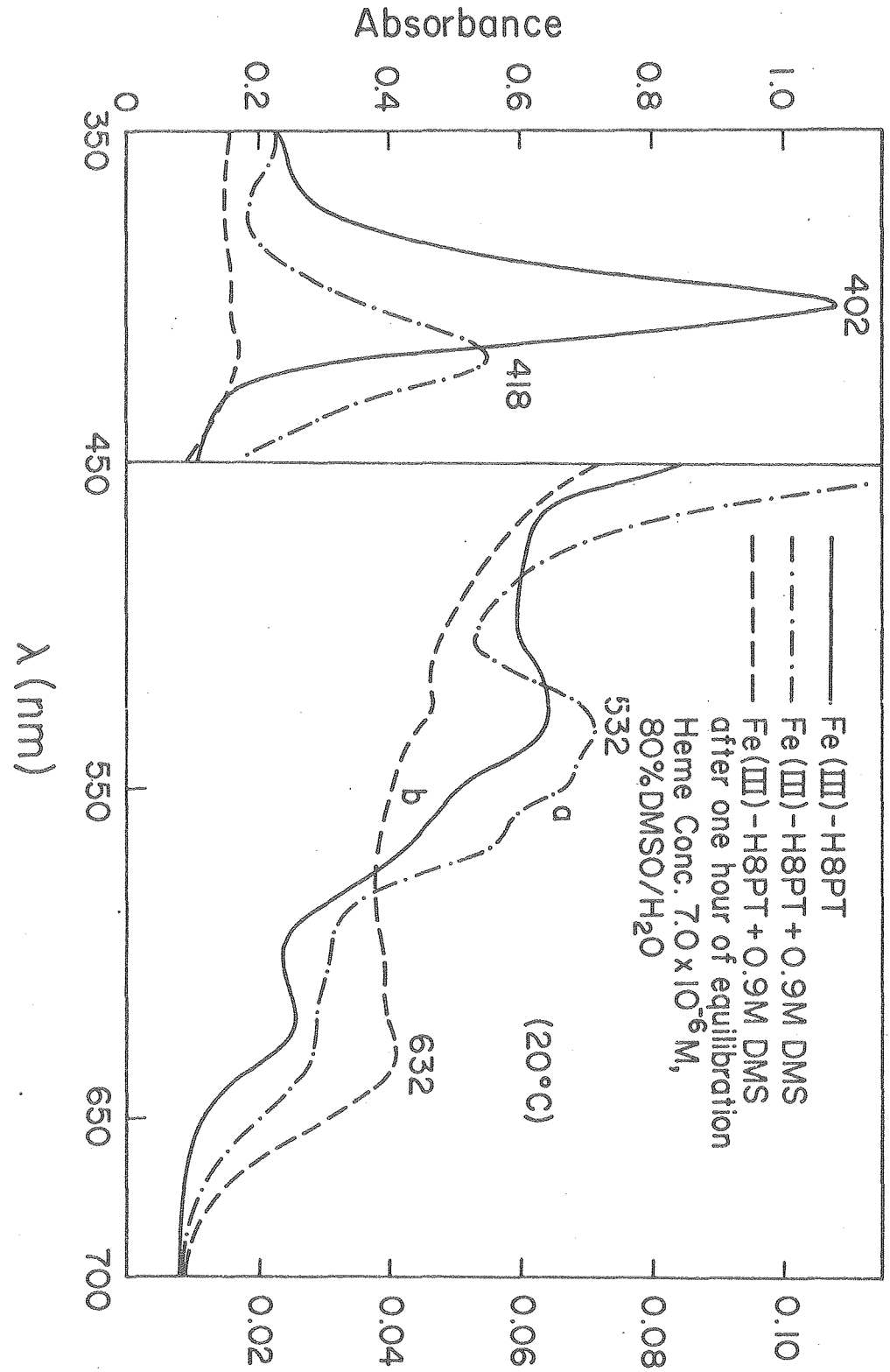
Absorbance
0
0.2
0.4
0.6
0.8
1.0
350
450
550
650
700
λ (nm)
0.02
0.04
0.06
0.08
0.10
402
418
532
632
a
b
Fe(III)-H8PT
Fe(III)-H8PT + 0.9M DMS
Fe(III)-H8PT + 0.9M DMS
after one hour of equilibration
Heme Conc. 7.0 x 10⁻⁶ M,
80% DMSO/H₂O
(20°C)

XBL 786-3971

nature. The two spectra for the DMS-H8PT complex show time dependent behavior. The initial spectrum, Fig. 2(a) appears to reflect the mixed spin form, although the Soret maximum occurs at a much longer wavelength and its intensity is too low. Again, there are indications of having more than one transition in the Soret band. In the final spectrum, Fig. 2(b), which is obtained after one hour of equilibration, the Soret intensity is almost absent and the β band intensity is decreased while the 632 nm band is increased. Reduction of Soret intensity seems to indicate the attack on the porphyrin π system.

The absorption spectra of the N-H8PT in the presence of imidazole, N-methionine or 0.1 M phosphate buffer, pH 7.0 are shown in Fig. 3. The imidazole complex yields a typical low spin hemichrome spectrum, and the aquo complex a high spin spectrum, as predicted from their ligand field strength considerations. The N-Met-N-H8PT complex, however, again gives rise to the mixed spin spectral characteristics. In Fig. 4 are shown the actual spectra recorded during a spectrophotometric titration for N-methionine binding in 0.1 M phosphate buffer, pH 7.0. The spectra are shown with up to 2.0 M N-methionine. The spectra at higher N-methionine concentration are virtually the same as the spectrum at 2.0 M concentration except that the Soret intensity increases slightly and the band maximum exhibits a small blue shift (< 2 nm). There is an isosbestic point at 583 nm and an

Figure 3. The absorption spectra of the N-acetylated heme octapeptide in the presence of N-methionine, imidazole or 0.1 M phosphate buffer at pH 7.0, 20°C. The ligand concentrations are those at which the spectral changes are saturated.

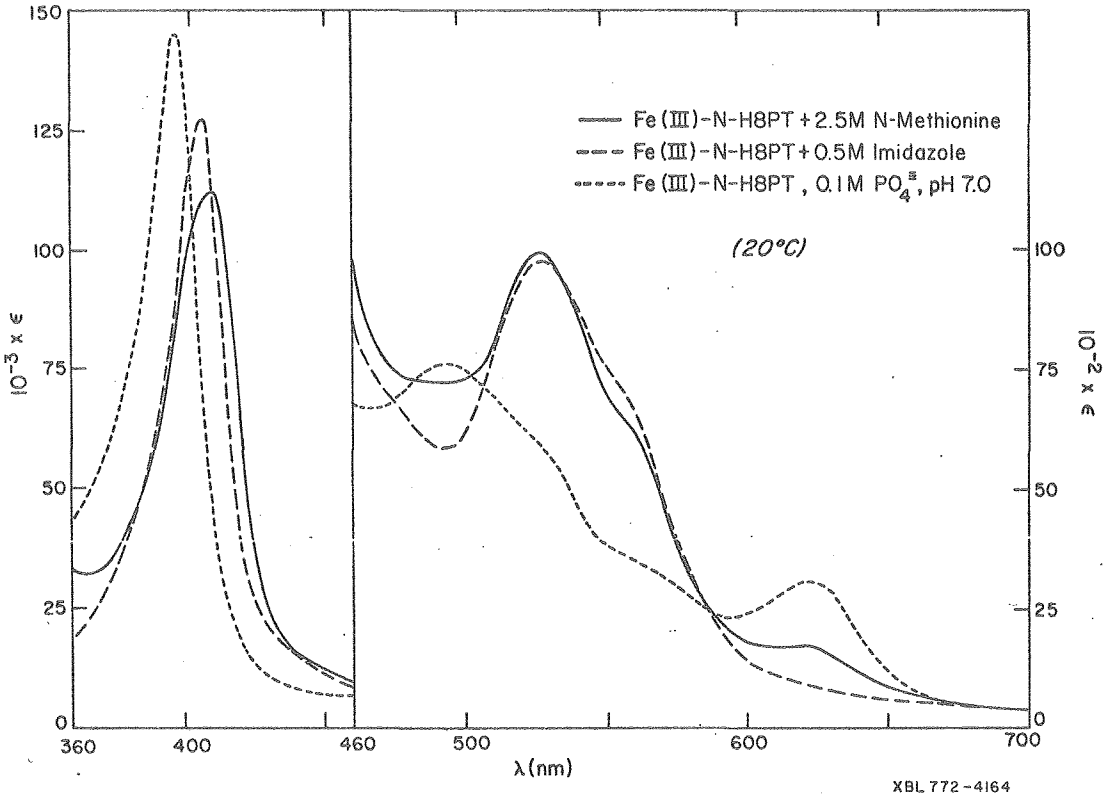
Fe(III)-N-H8PT + 2.5M N-Methionine
Fe(III)-N-H8PT + 0.5M Imidazole
Fe(III)-N-H8PT , 0.1M $PO_4^{\equiv}$, pH 7.0
(20°C)
$10^{-3} \times \epsilon$
$10^{-2} \times \epsilon$
λ(nm)
150
125
100
75
50
25
0
360
400
460
500
600
700
XBL 772-4164

Figure 4. The spectral titration for N-methionine binding to the N-acetylated heme octapeptide. The ligand concentrations from a to f correspond to 0, 0.1, 0.2, 0.5, 1.0 and 2.0 M respectively.

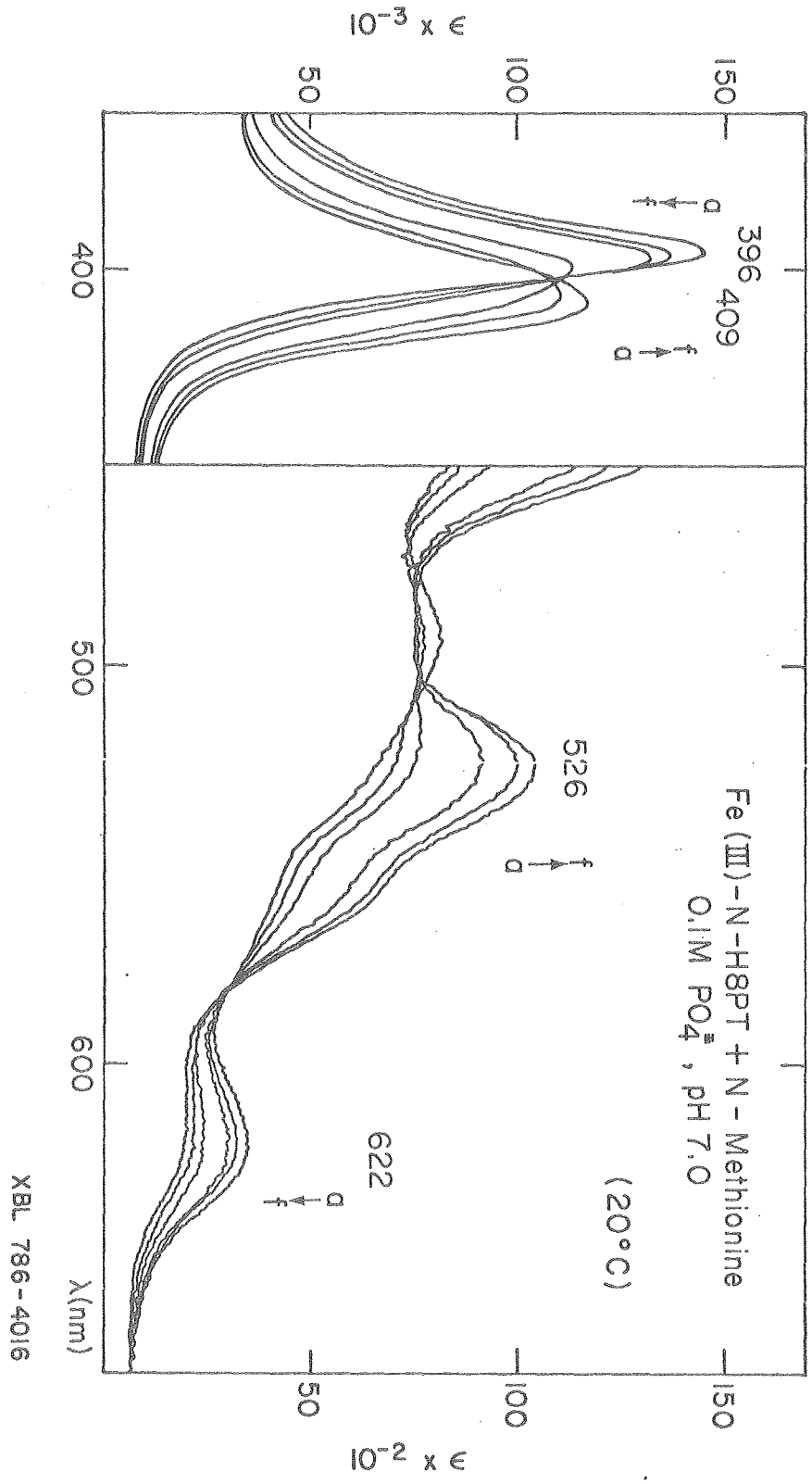
$10^{-3} \times \epsilon$
150
100
50
a
f
396
409
f
a
400
500
600
λ(nm)
526
f
a
622
a
f
Fe (III) - N - H8PT + N - Methionine
0.1M $PO_4^{\equiv}$, pH 7.0
(20°C)
150
100
50
$10^{-2} \times \epsilon$

XBL 786-4016

approximate one near 504 nm, but none appears in the Soret region except at 400 nm below 0.1 M concentration. This may indicate the presence of a third species at high N-methionine concentration or may reflect some unknown solvent or charge effect of N-methionine. The absorbance fractional changes observed at the Soret, β or charge transfer band (Fig. 5) all suggest that at 2.5 M N-methionine the spectral change is nearly saturated. Table I summarizes the absorption spectral data of the ferric N-H8PT complexes with various added ligands at pH 7.0 (except OH^-), 20°C. The extinction coefficient of the N-methionine complex is approximately 20% greater than that of cytochrome c, which has ε_M = 106 x 10^3 $M^{-1}cm^{-1}$. However, its band maxima agree with those of cytochrome c within 2 nm. In general, the position of the Soret maximum consistently shifts to lower energy as a function of increasing ligand field strength. The intensity of 625 nm band also decreases and the position shifts to lower energy.

Fig. 6 shows the Soret MCD spectra of the N-H8PT in the presence of a strong field (Imidazole), weak field (Fluoride) or N-methionine ligand. The fluoride complex shows a relatively weak magnetic ellipticity while the imidazole and N-methionine complexes exhibit strong magnetic ellipticities. A first derivative band shape characteristic of a low spin hemin complex appears to be a Faraday A term but it is actually known to be a superposition of two C terms of

Figure 5. The absorbance fractional change for N-methionine binding to the N-acetylated heme octapeptide against the N-methionine concentration.

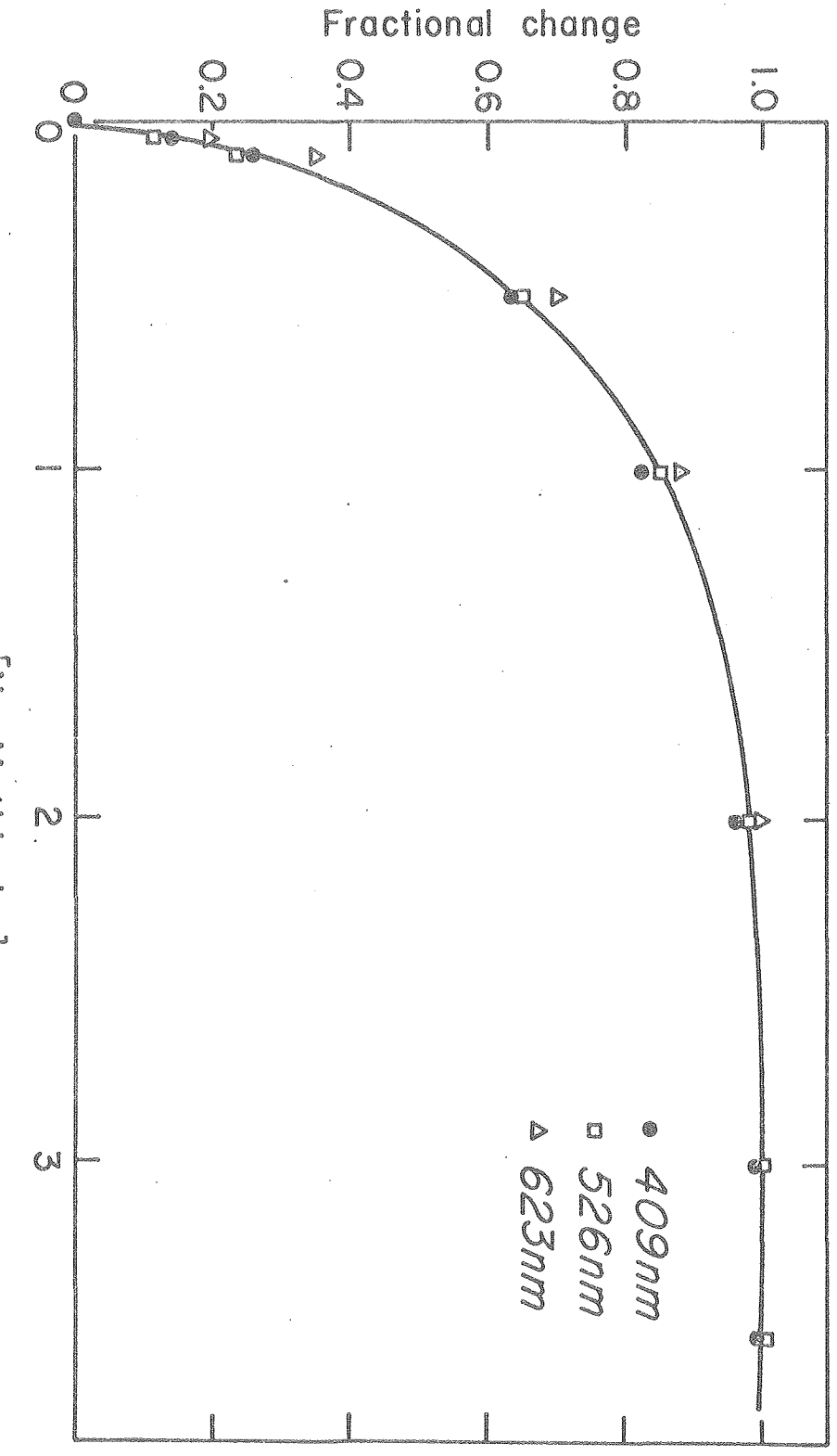

Fe(III) - N-H8PT + N-Methionine, 0.1M $PO_4^{\equiv}$, pH 7.0, 20°C

XBL 772-4172

TABLE I

Absorption Spectra of Fe(III)-N-H8PT Complexes, 0.1m $PO_4^{\equiv}$, PH 7.0

Ligand	Lig. Conc. (M)	Soret, nm (ε_{mM})	β band	α band	CT, nm (ε_{mM})
Fluoride	2.0	393 (146)	485*(7.98)	562 (5.02)	606 (6.19)
Water	---	396 (143)	494*(9.35)	560 (4.40)	623 (3.71)
Hydroxide	pH 11.0	402 (98)	534 (9.01)	566 (7.40)	600 (4.95)
Azide	1.0	406 (127)	533 (11.6)	562 (7.98)	622 (2.00)
N-Methionine	2.5	409 (126)	526 (12.4)	560 (7.63)	622 (2.06)
Cyanide	0.5	409 (121)	532 (12.6)	560 (8.46)	---
Imidazole	1.0	406 (128)	527 (12.8)	560 (8.67)	---
Cytochrome c	---	410 (106)	528 (11.2)	560 (6.9)	---

* Visible Charge transfer band

XBL 786 - 4008

Figure 6. The Soret magnetic circular dichroism spectra of the N-acetylated heme octapeptide in the presence of fluoride, N-methionine or imidazole ligand.

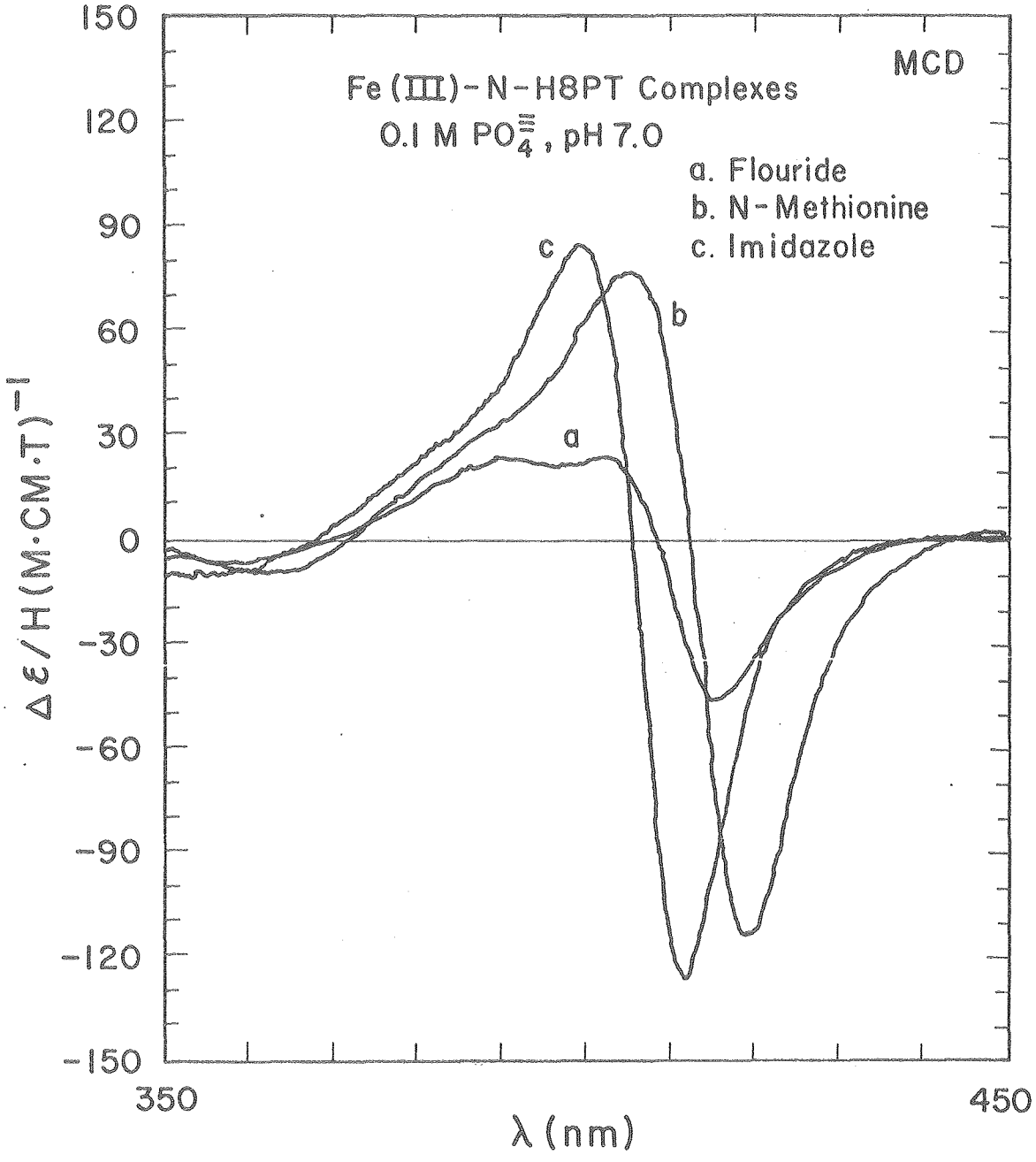
MCD
Fe(III)-N-H8PT Complexes
0.1 M $PO_4^{\equiv}$, pH 7.0
a. Flouride
b. N-Methionine
c. Imidazole
a
b
c
150
120
90
60
30
0
-30
-60
-90
-120
-150
350
450
λ (nm)
$\Delta\varepsilon/H\,(M\cdot CM\cdot T)^{-1}$

XBL 786-3965

opposite polarity, thus paramagnetic in origin (12). Theoretical origins of Faraday A, B and C terms have been discussed in detail in Chapter II. The absorption maximum of each complex (Table I) does not correspond to the corresponding MCD zero crossing, which suggests that there are additional transitions in the Soret region. A Faraday A and/or B term may contribute to the observed MCD intensity. Table II includes the Soret MCD and CD spectral data of the ferric N-H8PT complexes with various ligands at pH 7.0, 20°C. When compared with cytochrome c, the N-methionine complex exhibits larger magnetic ellipticities, consistent with the observed larger extinction coefficient of the Soret transition. In general, however the intensities of both peaks and troughs in the Soret region increase with increasing ligand field strength.

Fig. 7 compares the visible MCD spectrum of the N-Met-N-H8PT complex with those of cytochromes c_1 (yeast) and f (spinach) in both oxidized and reduced states. In the oxidized state, a strong transition with a zero crossing near 557 nm indicates an MCD A term associated with Q_{0-0} transition (α band). Between the Q_{0-1} (β band) and Soret transitions, more detailed features that arise from overlap of several weak C terms are not resolved in the absorption spectra. The weak C terms in that region are thought to be associated with the visible charge transfer transition (CT_2, Fig. 7, Chapter II) whose position and intensity are a sensitive function of the chemical nature of the axial ligands.

TABLE II

Magnetic Circular Dichroism and Circular Dichroism Spectra of Fe(III)-N-H8PT Complexes, 0.1M $PO_4^{\equiv}$, PH 7.0

Ligand	MCD Peak nm ($\Delta\varepsilon$/H)	Zero Crossing nm	MCD Trough nm ($\Delta\varepsilon$/H)	CD max nm ($\Delta\varepsilon$)
Fluoride	403 (22)	408	416 (-46)	394 (9)
Water	392 (36)	398	405 (-43)	397 (17)
Hydroxide	398 (30)	405	412 (-36)	403 (11)
Azide	401 (61)	407	413 (-85)	406 (13)
N-Methionine	406 (77)	412	419 (-113)	414 (14)
Cyanide	402 (84)	409	416 (-120)	405 (20)
Imidazole	400 (85)	406	412 (-127)	408 (13)
Cytochrome c	402 (75)	409	416 (-102)	--- ----

XBL 786 - 4009

Figure 7. The visible magnetic circular dichroism spectra of the N-methionine complex of N-H8PT, cytochrome f and cytochrome c_1.

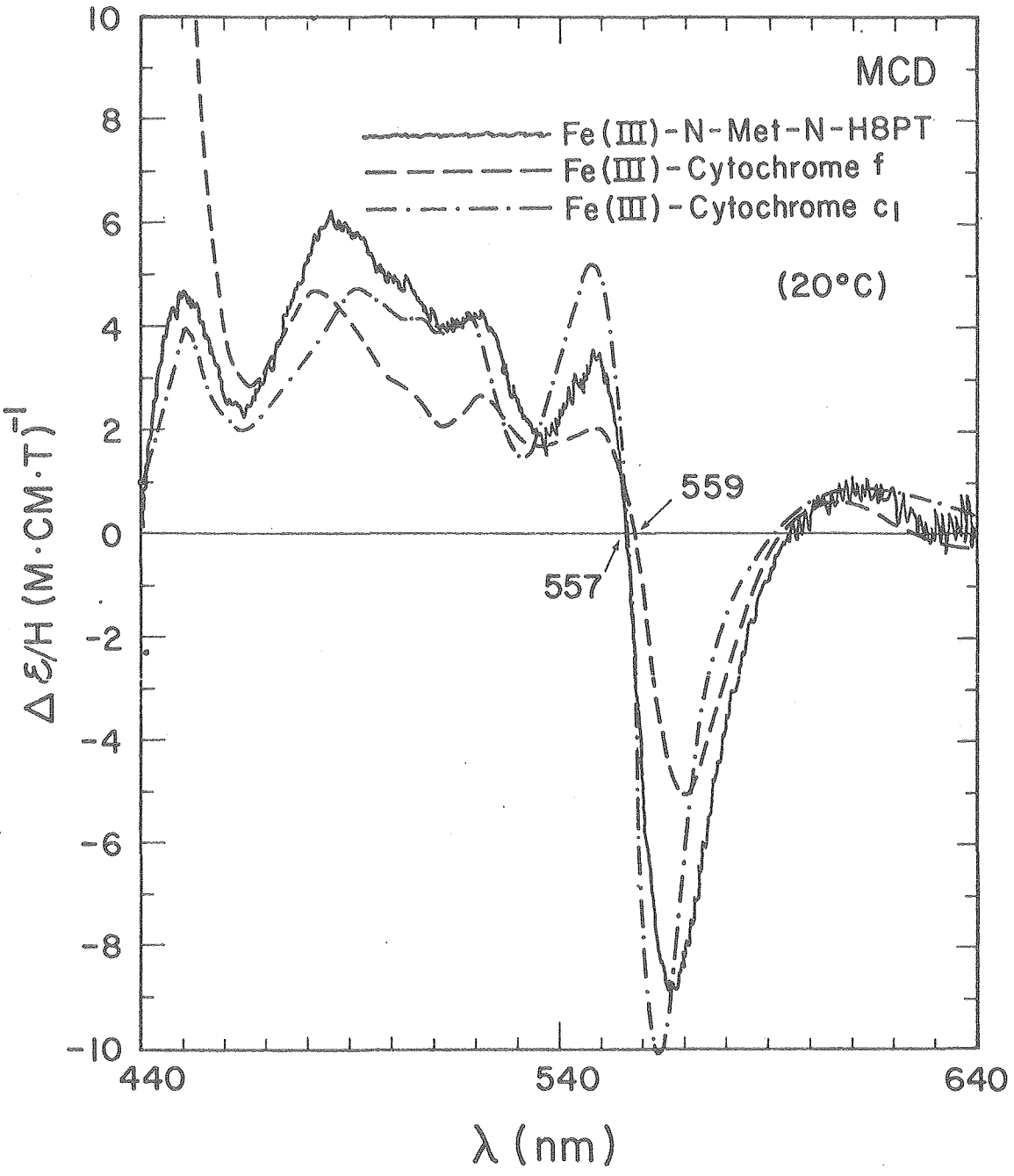
MCD
Fe(III)-N-Met-N-H8PT
Fe(III)-Cytochrome f
Fe(III)-Cytochrome c1
(20°C)
559
557
10
8
6
4
2
0
-2
-4
-6
-8
-10
440
540
640
λ (nm)
Δε/H (M·CM·T)⁻¹

XBL 786-3966

Therefore, they probably reflect the nature of the axial ligands as well as the local heme environment. The N-Met-N-H8PT complex shows better resolved spectral features than the room temperature spectrum of cytochrome c, in fact it looks closer to the low temperature spectrum (16). In the reduced state, a strong A term dominates the spectrum, while weak vibronic transitions appear at the high energy side. In both oxidation states striking spectral similarities are found between the N-Met-N-H8PT complex and cytochrome c_1, although the relative intensities of the bands are different. This suggests that the axial ligands of cytochrome c_1 are probably histidine and methionine residues. Differences in intensity may reflect subtle differences of the local heme environment. In the spectrum of ferric cytochrome f, not only are the band intensities much weaker and not well resolved, but the zero crossing is red shifted by 2 nm. Even in the reduced state the spectrum of cytochrome f is rather distinct from that of the N-Met-N-H8PT complex. Nevertheless, if the whole spectrum is blue shifted by 2 nm, a reasonable agreement is observed between cytochrome f and the N-Met-N-H8PT complex. The appearance of a weak MCD A term near 630 nm with a negative trough in the oxidized state is probably associated with the near IR charge transfer band characteristic of the high spin state (16,22,23). At 630 nm cytochrome c shows a positive MCD with $\Delta\varepsilon/H$ about 0.6, while the acid form of cytochrome c (pH 1.8) where chloride

ion is thought to replace the methionine ligand exhibits $\Delta\varepsilon/H = -2.0$ (results not shown) (16). In the N-Met-N-H8PT complex, there is only an indication of the presence of an A term. At 630 nm, zero MCD is observed.

D. DISCUSSION

Interpretation of the absorption spectral results of the N-methionine or DMS complex of the ferric N-H8PT deserves careful attention. Although it appears that the model system of cytochrome c, the N-Met-N-H8PT complex exists as a thermal mixture of high and low spin forms at room temperature, absorption evidence alone is not conclusive. One of the serious problems is associated with the weak binding of sulfur ligands toward the ferric form. As shown in Fig. 5, a very large molar excess of N-methionine is required for saturation of the absorbance change. Therefore, it is not clear whether incomplete N-methionine binding is responsible for the residual of the high spin component at 2.5 M ligand concentration. The percentage of N-methionine ligation as a function of ligand concentration can be estimated from analysis of the spectral titration curves shown in Fig. 4. If we assume that only one N-methionine per heme binds to iron the equilibrium expression may be written in terms of the extinction coefficients as shown in Fig. 8 where ε_o is the extinction coefficient in the absence of N-methionine,

Figure 8. A plot of ε versus $(\varepsilon-\varepsilon_o)$/[N-methionine] at 409 nm where ε_o is the extinction coefficient of the N-H8PT at zero N-methionine and ε, at any ligand concentration. The slope corresponds to -1/Q where Q is the equilibrium quotient for one N-methionine binding per heme.

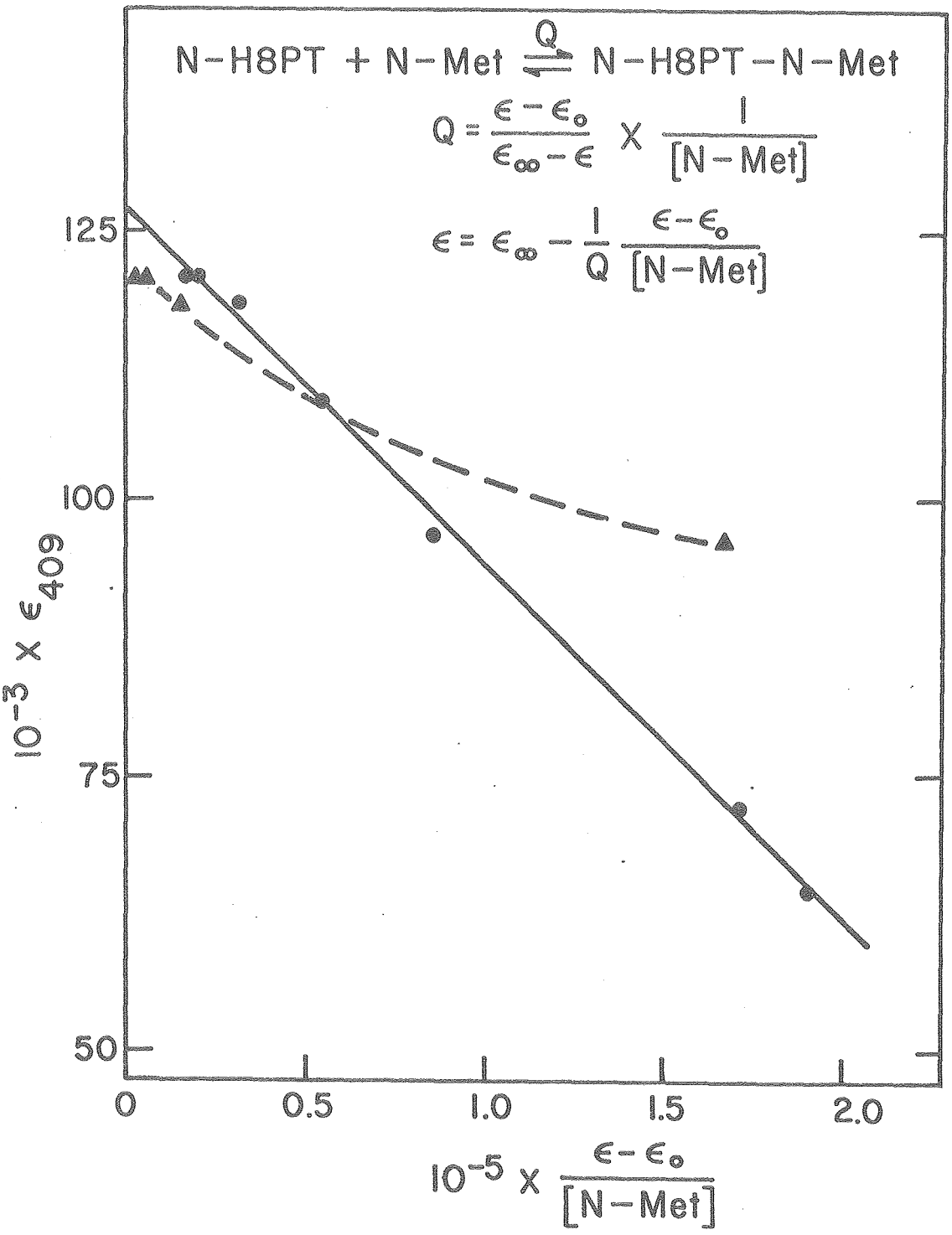
N-H8PT + N-Met ⇌ N-H8PT-N-Met
Q
$Q = \frac{\epsilon - \epsilon_o}{\epsilon_\infty - \epsilon} \times \frac{1}{[N-Met]}$
$\epsilon = \epsilon_\infty - \frac{1}{Q} \frac{\epsilon - \epsilon_o}{[N-Met]}$
125
100
75
50
$10^{-3} \times \epsilon_{409}$
0
0.5
1.0
1.5
2.0
$10^{-5} \times \frac{\epsilon - \epsilon_o}{[N-Met]}$

XBL 772-4171

ε at any ligand concentration, and ε_∞ at complete ligation (24). In Fig. 8, a plot of ε versus $\varepsilon-\varepsilon_o$/[N-methionine] results in a straight line. The observed value of ε_∞ is found to be 126 x 10^3 $M^{-1}cm^{-1}$ and the equilibrium quotient for N-methionine binding (N-Met + N-H8PT $\rightleftharpoons$ N-Met-N-H8PT), Q, 3.2. From these values we could estimate that at 2.5 M ligand concentration approximately 90% of ligand is bound at room temperature. A similar analysis in the visible region (at 526 nm) also shows 90% ligand binding at 2.5 M concentration. The intensity of 625 nm band is clearly too large to account for 10% of the high spin N-H8PT, however. If the intensity of 625 nm band is taken to reflect the amount of the high spin form present, then the intensity of the N-Met-N-H8PT complex corresponds to about 35% high spin state assuming that the fluoride complex is purely high spin. It is possible that there is some bis-N-Met-N-H8PT complex formed. Practically no steric hinderance exists in the peptide to protect the imidazole coordination at the fifth site although replacement of the tightly bound imidazole ligand is not energetically favorable. Fig. 9 compares the absorption spectra of the bis-N-Met-hemin complex with the N-Met-N-H8PT complex in both oxidized and reduced states at pH 7.0, 20°C. The reduced bis-N-Met-hemin complex exists in the low spin state as evidenced by the well resolved and strong α, β band intensity while the oxidized form appears to exist in the high spin state or mixed spin state. The change of the spin state upon reduction is not understood. It may reflect

Figure 9A. The absorption spectra of the bis-N-methionine complex of hemin in the oxidized and reduced states.

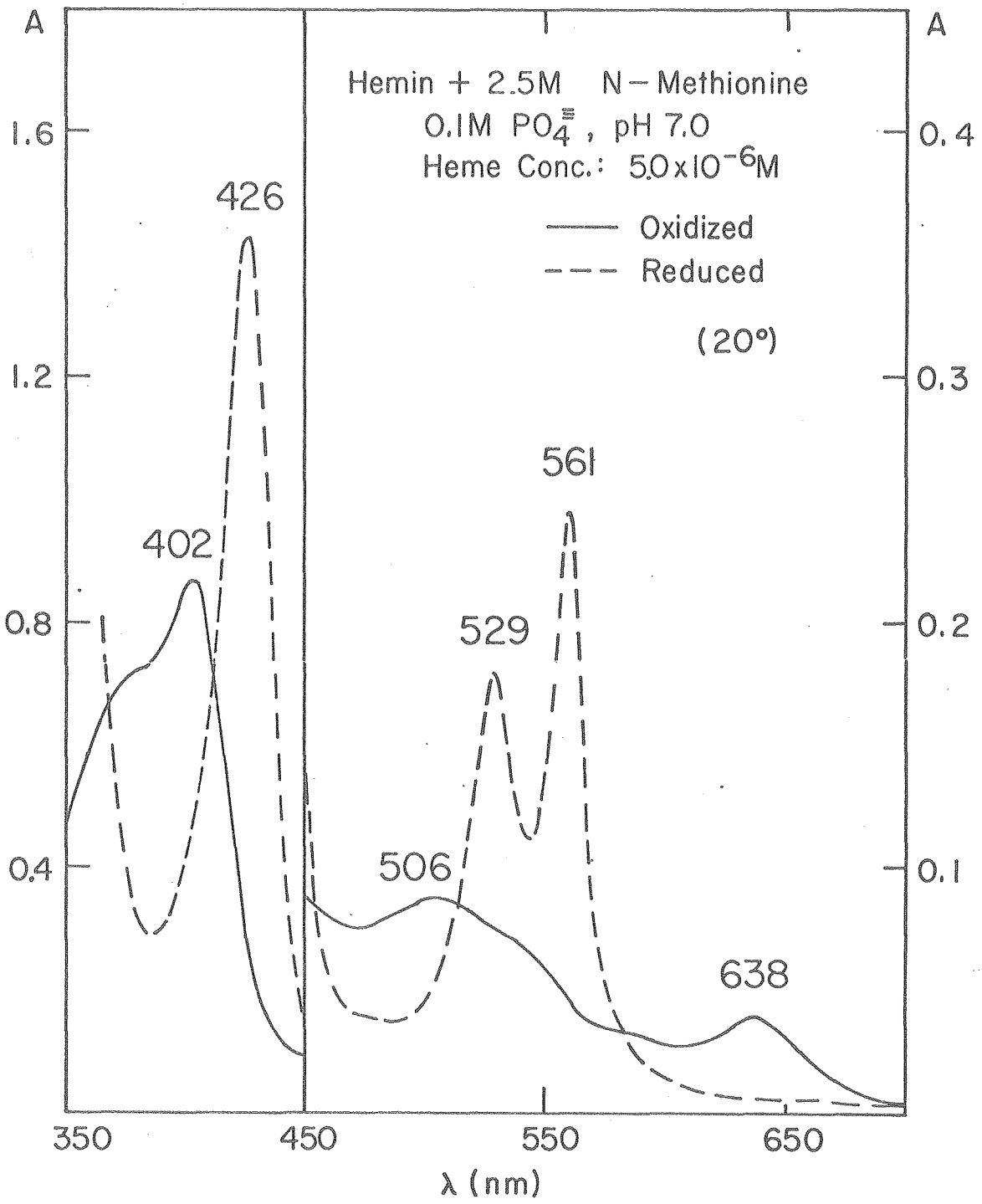
A
A
Hemin + 2.5M N-Methionine
0.1M $PO_4^{\equiv}$, pH 7.0
Heme Conc.: 5.0×10^{-6}M
Oxidized
Reduced
(20°)
426
561
402
529
506
638
1.6
1.2
0.8
0.4
0.4
0.3
0.2
0.1
350
450
550
650
λ (nm)

XBL 786-4018

Figure 9B. The absorption spectra of the N-methionine complex of N-H8PT in the oxidized and reduced states.

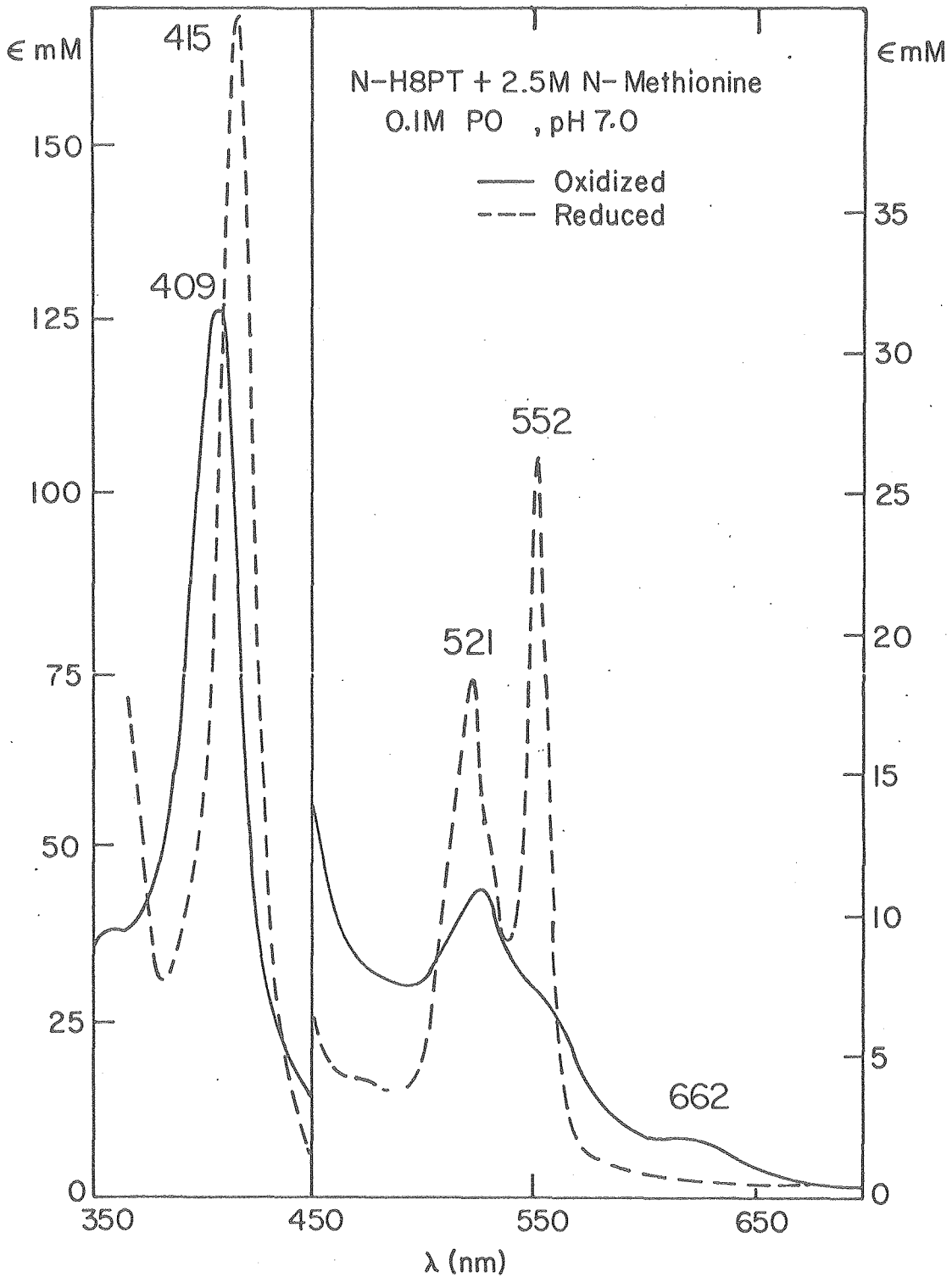
ε mM
ε mM
415
409
552
521
662
N-H8PT + 2.5M N-Methionine
0.1M PO , pH 7.0
Oxidized
Reduced
150
125
100
75
50
25
0
35
30
25
20
15
10
5
0
350
450
550
650
λ (nm)

XBL 786-4017

the fact that in the oxidized form only one methionine per heme is bound due to its weak binding nature toward the ferric form. If indeed the bis-N-Met-N-H8PT complex is responsible for the residual of the near IR charge transfer band which accounts for 35% high spin form at room temperature, then at least 25% heme must be bis-N-methionine coordinated. If this is true, then we would certainly expect to observe deviation from linearity in Fig. 7 at high ligand concentrations, because two independent equilibrium quotients will be involved. However, all of the points fall nicely on a straight line. Furthermore, in the reduced state where the intensity of the α band is believed to be very sensitive to the chemical nature of the axial ligands, the α/β band ratio of the N-Met-N-H8PT complex (1.42) falls right in the middle between that of the bis-Im-heme c complex (1.62) and that of the bis-N-Met-heme c complex (1.12) (24). The position of the Soret, α and β bands of the N-methionine complex also agree with those of cytochrome c within ± 2 nm. In addition, iron-sulfur interaction is indicated by the presence of a 695 nm band, a charge transfer transition from iron to sulfur, although it is not resolved in Fig. 3 owing to the small extinction coefficient (< 800). A test is made of the number of absorbing species in the N-Met-N-H8PT complex solution using the graphical method of Coleman, Varga and Mastin (CVM). A CVM plot (Fig. 10) is shown as the absorbance differences between various N-methionine concentrations (j) and no N-methionine (o) obtained at several wavelengths (i) against

Figure 10. The Coleman, Varga and Mastin (CVM)* plot: the absorbance differences between various N-methionine concentrations (j) and zero N-methionine (o) obtained at several wavelengths (i) are plotted against the corresponding absorbance differences at the reference wavelength, 526 nm. The i's correspond to 396, 409, 560 and 622 nm.

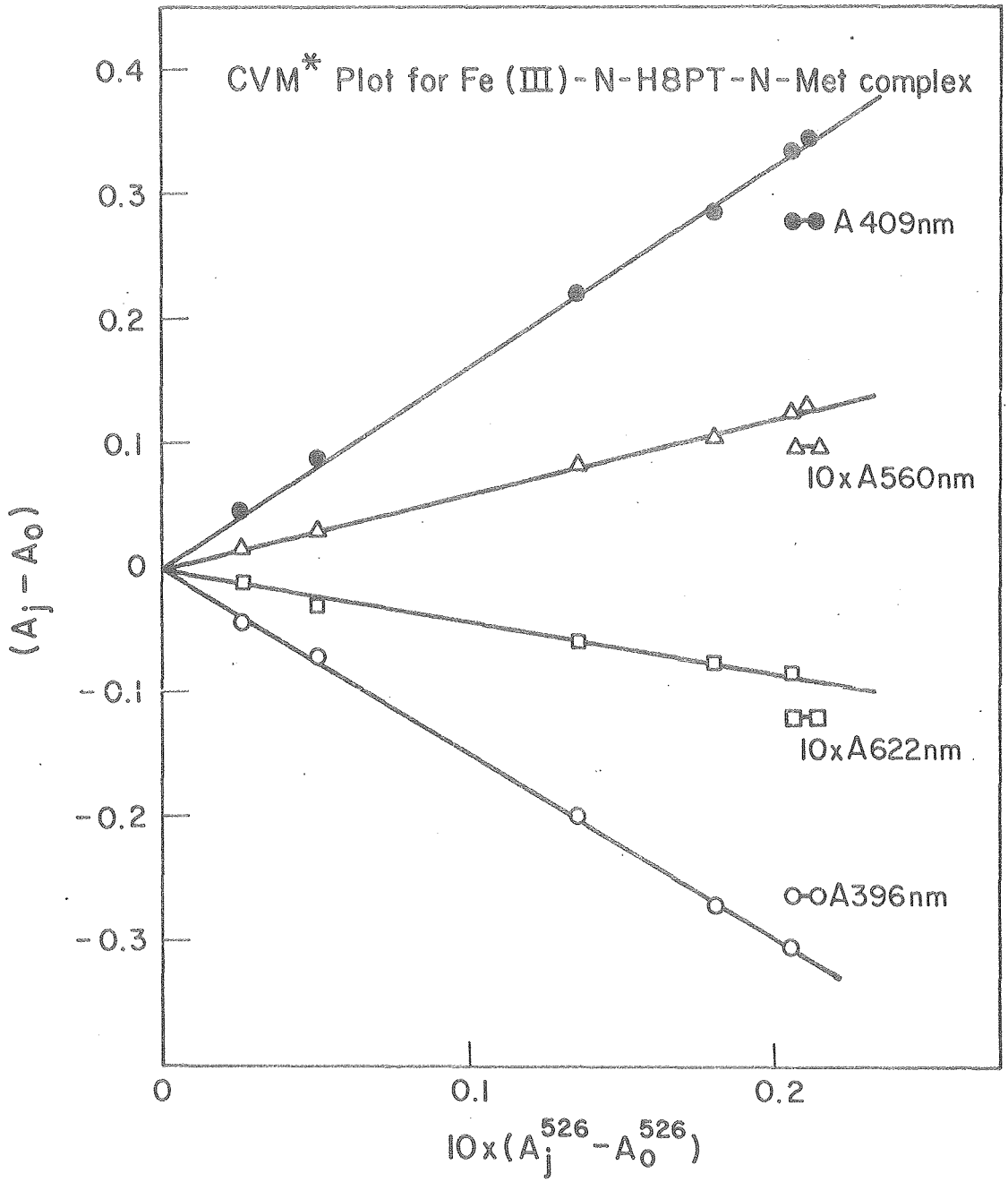
CVM* Plot for Fe (III) - N-H8PT-N-Met complex
A 409nm
10x A560nm
10x A622nm
A396nm
0.4
0.3
0.2
0.1
0
-0.1
-0.2
-0.3
(Aj - Ao)
0
0.1
0.2
10x(Aj526 - Ao526)

XBL786-3969

the corresponding absorbance differences at the reference wavelength, the β band maximum (526 nm). All of the points fall in straight lines which intersect at the origin. This clearly indicates that there are only two absorbing species in solution and that bis-N-Met-N-H8PT complex formation is not significant. Thus, we believe that the absence of an isosbestic point in the Soret region is due to the solvent effect of N-methionine at high concentration.

Other ligands that may compete with sulfur binding are the free carboxyl group of N-methionine, which is known to be a relatively weak field ligand. However, the use of N-methionine amide as well as N-methionine methyl ester yields virtually identical spectra at the saturating ligand concentration (results not shown). In the case of N-methionine methyl ester, the Soret maximum occurs at a shorter wavelength, near 404 nm, but this may be because a different solvent medium (50% ethylene glycol/H_2O) has been used to increase solubility. An analysis of the titration curve for N-methionine methyl ester binding in 50% EG/H_2O at room temperature at the Soret band maximum also yields approximately 90% ligand binding at 2.5 M ligand concentration. DMS, in addition to being a good organic sulfur ligand representing methionine, lacks the free carboxyl group. It has stronger binding affinity and is more soluble than N-methionine in 80% DMSO/H_2O. However, the resulting spectra of the DMS-H8PT complex in both aqueous and 80% DMSO/H_2O (Figs 1 and 2) do not resemble that of

cytochrome c. The origin of the intense band near 638 nm is not clear. If it is a charge transfer transition of porphyrin π to iron $d\pi$ type, the intensity of the 638 nm band should be weaker than that of the 625 nm band in the N-methionine complex. This is probably because the charge transfer band borrows intensity via configuration interaction from the visible $\pi \rightarrow \pi^*$ transition (Q_{0-0}), the extent of which depends on the energy separation between the two transitions. The drastically reduced Soret intensity and its peculiar time-dependent behavior suggests that attack has been made on the porphyrin π system (Fig. 2). Cyclic organic sulfur ligands, such as tetrahydrothiophene or p-dithiane, also do not exhibit spectral features characteristic of cytochrome c (results not shown). Furthermore, the solubility of these ligands is limited even in non-aqueous medium. Thus, we believe that the organic sulfur ligands cannot be substituted for N-methionine and that an aqueous solvent medium most closely reflects the environment of the heme in the active cytochromes.

The MCD studies of ferric heme and hemoproteins have established that the origin of the Soret MCD spectra is predominantly paramagnetic, i.e., the ground state is spin degenerate, in contrast to the optical spectra where the porphyrin $\pi \rightarrow \pi^*$ transition dominates (15,25). Low spin complexes are found to exhibit much stronger MCD than high spin complexes. This may be explained on the basis of

spin-orbit coupling, although rigorous theoretical treatment has not been done. A first derivative Soret MCD band shape in low-spin ferric heme complexes appears to be a Faraday A term, but temperature-dependent MCD has shown it to be a superposition of two closely spaced C terms of opposite sign (25,26). The mechanism that is consistent with the observed MCD involves spin-orbit interaction between the circular orbital motion of a porphyrin π electron and the non-zero spin density at the paramagnetic iron (25). It is evident that the spin-orbit coupling must be important in the excited state, because the porphyrin π^* orbital is doubly degenerate. Weak MCD in high spin complexes is believed to reflect the difference in the extent of spin-orbit coupling, presumably owing to the out-of-plane high spin iron position. Because C term effect arises from the paramagnetism of iron, the Soret MCD intensity is intrinsically very sensitive to the spin state of iron. In fact, in ferrimyoglobin complexes the intensity is found to be linearly proportional to the percentage of low spin form. The MCD spectral results shown in Table II indicate that in general, the magnitude of Soret magnetic ellipticities of the ferric N-H8PT complexes is in good accord with the values of the corresponding hemeprotein derivatives. However, the fluoride complex exhibits a much stronger MCD than the ferrimyoglobin-fluoride complex ($\Delta\varepsilon/H = \pm 6$). The observed intensity is not due to a low spin contaminant, because the absorption spectrum recorded after each MCD measurement indicates fluoride complexation. In addition, the spectral band shape

is distinct. Its MCD zero crossing is red shifted by more than 10 nm from the Soret absorption maximum. Careful temperature dependent MCD measurements will be useful for further analysis. The N-methionine complex also exhibits a strong MCD, even larger than that of cytochrome c. This is not due to narrower band width of the N-methionine complex. Thus, this effect is not consistent with the absorption data if the observed intensity is taken to represent the amount of low spin form. A large Soret MCD may simply be associated with the large extinction coefficient found in the N-methionine complex (Table I). In our model complexes it may also be that Faraday A and/or B term contribution turns out to be rather significant due to the different local environment at the heme site.

The visible MCD spectra consist of an A term associated with the Q_{0-0} transition and overlap of weak C terms associated with the visible charge transfer transition [$a_{1u} \rightarrow e_g(d\pi)$] (16). Because the position and intensity of the visible charge transfer band are known to be sensitive to the electronic structure of the porphyrin π system via configuration interaction (30), the detailed MCD spectral features in that region probably reflect the chemical nature of the axial ligands. However, as can be seen in the low spin derivatives of cytochrome c (Fig. 11), for example, only subtle differences are found in their band extrema, intensities and zero crossing (16). Cytochrome c is known to undergo a low spin to low spin transition with a pK value of 9.3, so that

Figure 11. The visible magnetic circular dichroism spectra of ferric cytochrome c at pH 7.0, pH. 11.0 and in the presence of imidazole ligand all of which are of low spin type.

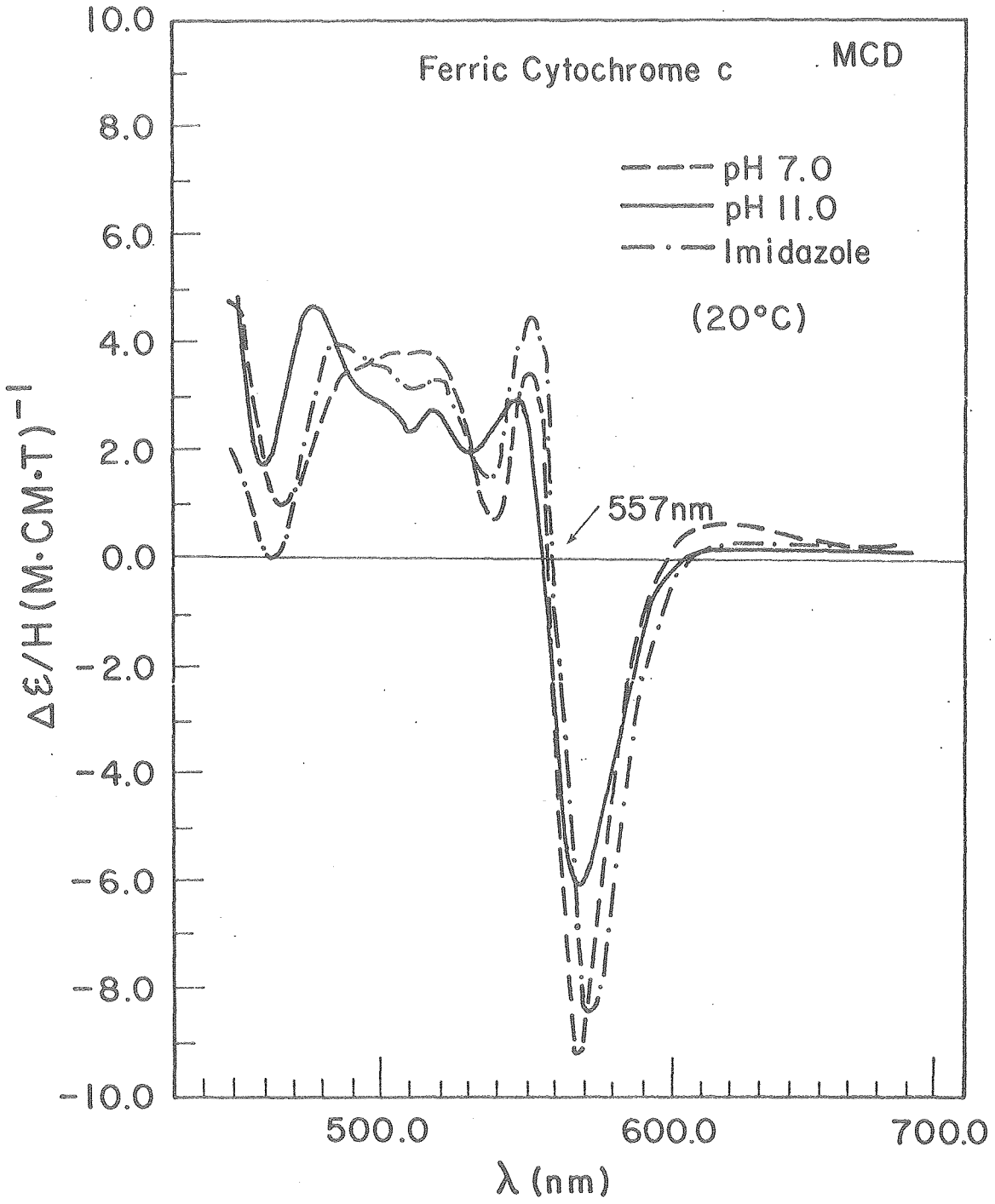
Ferric Cytochrome c
MCD
pH 7.0
pH 11.0
Imidazole
(20°C)
557nm
10.0
8.0
6.0
4.0
2.0
0.0
-2.0
-4.0
-6.0
-8.0
-10.0
500.0
600.0
700.0
λ (nm)
Δε/H (M·CM·T)⁻¹

XBL 786-3963

at pH 11.0 lysine is probably the sixth axial ligand (27-30). In the lysine complex the main distinction seems to be that the 480 nm band is blue shifted by 4-5 nm while the A term trough is decreased in intensity. In the bis-imidazole complex, on the other hand, the intensity ratio of 550/480 band is greater than 1.0 and the 480 nm band appears broader in addition that its minimum extends to zero MCD. In view of these observations it seems reasonable to assume that methionine acts as one of the axial ligands in cytochrome c_1 (Fig. 7). This is also consistent with the absorption evidence of having the 690 nm band, which is believed to be iron to sulfur charge transfer transition (31). The assignment of the unknown ligand in cytochrome f is difficult. The intensity of the A term trough is weak and the 480 nm band is blue shifted, as in the case of cytochrome c at pH 11.0, which suggests lysine coordination. However, the spectral features are also in reasonable agreement with those of N-Met-H8PT complex. The absence of a 690 nm band appears to favor lysine coordination. Furthermore, the low temperature EPR spectrum of cytochrome f exhibits g_z = 3.51 which compares well with the lysine complex g_z value of 3.40 (unpublished results). Further investigation of the redox properties and pH dependent variations of the optical and MCD spectra will provide complementary information regarding the nature of the ligand in cytochrome f. Temperature dependent MCD studies by Yoshida, et al. (23) on the band appearing near 630 nm

with a weak trough ($\Delta\varepsilon/H = -2.0$) in aquo-ferrimyoglobin and hemoglobin have shown that the A and B terms dominate that region, which is consistent with the view that the near IR charge transfer transition is porphyrin π to iron $d\pi$ and is characteristic of a high spin form. However, the N-Met-N-H8PT complex shows no MCD trough in that region although a small decrease of the MCD intensity is observed. This is not consistent with what we find in the absorption spectrum where the intensity of the charge transfer band corresponds to about 35% high spin state (Fig. 3).

REFERENCES

1. C.S.G. Phillips and R.J.P. Williams. Inorganic Chemistry Vol. II, 312 (1966).

2. J.E. Falk and D.D. Perrin, in "Haematin Enzymes", J.E. Falk , R. Lemberg and R.K. Morton, Eds., Pergamon Press, Oxford, p. 56 (1961).

3. D.W. Smith and R.J.P. Williams. Struc. and Bonding 7, 1 (1969).

4. T. Iizuka and T Yonetani. Advan. in Biophys. 1, 157 (1970).

5. D.W. Smith and R.J.P. Williams. Biochem. J. 110, 297 (1968).

6. J. Beetlestone and P. George. Biochemistry 3, 707 (1964).

7. P. Day, D.W. Smith and R.J.P. Williams. Biochemistry 6, 3747 (1967).

8. M. Kotani. Adv. Chem. Phys. VII, 159 (1964). J. Duchesne Ed.

9. A.S. Brill and R.J.P. Williams. Biochem. J. 78, 246 (1961).

10. P. George, J. Beetlestone and J.S. Griffith. "Haematin Enzymes" (1961).

11. Y.A. Sharonov and N.A. Sharonova. FEBS Letters 27, 221 (1972).

12. B. Briat, D. Berger and M. Leliboux. J. Chem. Phys. 57, 5606 (1972).

13. L.E. Vickery Proc. First Taniguchi Int. Sym. Biophys. Katada, Japan, (1975).

14. L. Vickery, T. Nozawa and K. Sauer. J. Am. Chem. Soc. 98, 343 (1976).

15. J. True and J.J. Hopfield. J. Chem. Phys. 63, 613 (1975).

16. L. Vickery, T. Nozawa and K. Sauer. J. Am. Chem. Soc. 98, 351 (1976).

17. T. Nozawa, N. Kobayashi and M. Hatano. Biochim. Biophys. Acta. 427, 652 (1976).

18. A.M. Arutjunjan, A.A. Konstantinov and Y.A. Sharonov. FEBS Letters 46, 317 (1974).

19. P.M. Dolinger, M. Kielezewski, J.R. Trudell, G. Barth, R.E. Linder, E. Bunnenberg and C. Djerassi. Proc. Natl. Acad. Sci. U.S. 71, 399 (1974).

20. G.T. Babcock, L.E. Vickery and G. Palmer. J. Biol. Chem. 251, 7907 (1976).

21. J.C. Sutherland, L.E. Vickery and M.P. Klein. Rev. Sci. Inst. 45, 1089 (1974).

22. S. Yamamoto, T. Nozawa and M. Hatano. Polymer 15, 330 (1974).

23. S. Yoshida, T. Iizuka, T. Nozawa and M. Hatano. Biochim. Biophys. Acta. 405, 122 (1975).

24. H. Goff and L.O. Morgan. Inorganic Chem. 15, 2069 (1976).

25. L.A. Livshitz, A.M. Arutyunyan and Y.A. Sharonov. J. Chem. Phys. 64, 1276 (1976).

26. H. Kobayashi. Adv. Biophys. 8, 191 (1975).

27. R.K. Gupta, S.H. Koenig. Biochem. Biophys. Res. Commun. 45, 1134 (1971).

28. R.A. Morton. Can. J. Biochem. 51, 465 (1973).

29. W.E. Blumberg, J. Peisach, B. Hoffman, E. Stellwagen,

E. Margoliash, L. Marchang, J. Tulloss and B. Feinberg. Fed. Proc. 32, 469 (1973).

30. L.A. Davis, A. Scheifer and G.P. Hess. J. Biol. Chem. 249, 2624 (1974).

31. L.S. Kaminsky, Y.L. Chiang and T.E. King. J. Biol. Chem. 250, 7280 (1975).

CHAPTER V

PARAMAGNETIC SUSCEPTIBILITY AND ESR SPECTRA OF THE COMPLEXES OF N-H8PT

CHAPTER V

A. INTRODUCTION

In the preceding chapter, the discussion has been mainly focused on the electronic structure of the heme in the ferric N-H8PT complexes. From the absorption and MCD spectral measurements, some semi-empirical correlations of the magnetic properties of iron with the electronic structure of porphyrin have been developed (1-10). More quantitative conclusions had to be postponed, however, because the observed intensity and position of the bands that are sensitive to the structural changes of the local heme environments are not from pure electronic transitions. Many overlapping bands are known to appear in the visible region, and the transitions are known to be mixed via configuration interaction (6). For example, it is uncertain whether the presence of the residual 625 nm band in the absorption spectrum of the N-Met-N-H8PT complex is indeed due to thermal spin equilibrium between high and low spin states. It may alternatively arise from the thermal mixture of two chemically distinct species, one with the high spin ground state and the other with the low spin ground state, each with no thermal spin equilibrium. In addition, the possible presence of an intermediate spin ground state ($S = 3/2$) or quantum mechanical admixture of spins (see Chapter II) can not be excluded. Our object in this chapter is to present evidence to verify the spectral observations by direct measurement of paramagnetic susceptibility and electron spin resonance (EPR), the two complementary techniques for

monitoring the magnetic behavior of iron in hemeproteins. As has been discussed in Chapter II, the existence of thermal spin equilibrium is common in ferric hemoprotein derivatives (3,5,11-14). The thermodynamic parameters involved in such a spin transition can be determined from the temperature dependence of the paramagnetic susceptibility near the room temperature region. On the other hand, the ground spin state can be easily revealed by the low temperature EPR spectrum or by the direct measurement of susceptibility at low temperature. However, the interpretation of the susceptibility measurements may be complicated owing to non-Curie behavior arising from spin-orbit interaction in both high and low spin states. (For details, see Chapter II.) Low temperature EPR is a remarkably powerful tool for the structural studies of hemeproteins. Its inherent sensitivity is capable of differentiating chemically distinct species found in slightly different local heme environments. In addition, the anisotropy of g tensors not only reflects the local symmetry of the ferric ion but also contains information regarding the extent of mixing of the excited states into the ground state via spin-orbit interaction (2,15-19). Furthermore, the existence of a quantum-mechanically admixed spin ground state is distinguishable (20-22). The limitation of the EPR technique is in the high temperature region where the EPR spectra of hemeproteins are not measurable, owing to very efficient spin-lattice relaxation mechanisms.

Thus, susceptibility measurements in the high temperature region become essential for a unique interpretation of the observed magnetic behavior.

The room temperature magnetic measurements of the ferric N-H8PT complexes with various external ligands at pH 7.0 have been carried out by the NMR method of Evans (23-25). The use of this technique over the conventional Gouy balance method has three additional advantages: 1) It requires less than 0.2 ml solution at concentrations of a few mM; 2) The temperature control is easily monitored; and 3) The measurement is simple and fast. The percentage of the low spin state estimated in each complex under the assumption of thermal spin equilibrium is found to be consistent with both the optical and MCD spectral results. Furthermore, in the N-Met-N-H8PT complex, the temperature dependence of the effective magnetic moment (-5 to 40°C) yields linearity between ℓn K vs 1/T for a high spin $\rightleftharpoons$ low spin transition. Corresponding ΔH° and ΔS° values are found to be -7.46 kcal/mole and -25.94 e.u. after correcting for the thermodynamic contribution due to temperature dependent ligand binding. The EPR spectra obtained at 11°K indicate a low spin ground state with $g_z = 2.91$, $g_y = 2.31$ and $g_x = 1.51$ for the N-Met-N-H8PT complex and a high spin ground state with $g_\perp = 6.03$ and $g_\parallel = 2.01$ for the aquo complex of the N-H8PT. The possibility of having a third species with a high spin ground state, in the N-Met-N-H8PT solution, such as the bis methionine

complex, is excluded also by the EPR evidence. From the observed g values of the N-Met-N-H8PT complex we estimate that the axial distortion corresponds to 1200 cm^{-1} while rhombic distortion corresponds to 780 cm^{-1} within the $^2T_{2g}$ set. These values differ significantly from the values found in native cytochrome c (19). A possible change in Fe-S chemical bonding is suggested as a model to account for the electronic structural difference found in the model complex of cytochrome c.

B. EXPERIMENTAL

Materials

The ligand solutions were prepared as described in Chapter IV, and typical heme concentrations used for both magnetic and EPR measurements were in the range of 1 to 2 mM. Ferrimyoglobin was from Sigma and was used after it was fully oxidized by the addition of ferricyanide followed by filtration on a Bio-Gel P-2 column.

Methods

NMR spectral measurements were carried out on a Varian A-60 NMR spectrometer with a V-6040 NMR variable temperature controller. The sample cells were precision-made coaxial tubes from Wilmad Glass Co. Inc. (Cat No. 517). EPR spectral measurements were recorded on a Varian E-9 EPR spectrometer in an X-band region with a cryostat probe (Air Products Corp.).

Paramagnetic Susceptibility Measurement

The method is the NMR technique developed by Evans (23). It is based on the principle that the position of a given proton resonance of a molecule is dependent on the bulk susceptibility of the medium in which the molecule is found. The mass susceptibility, χ_i (Eq. 1), is directly related to the difference of the proton resonance lines of a reference material in the presence and absence of the paramagnetic species.

$$\chi_i = \frac{3\Delta f}{2\pi f_o m} + \chi_o + \chi_o \frac{d_{solv} - d_{soln}}{m} \qquad (1)$$

where m is the concentration of the paramagnetic substance in $g \cdot ml^{-1}$; f_o, the frequency of the spectrometer; Δf, the shift in frequency of a reference molecule; χ_o, the mass susceptibility of the solvent; and d_{solv} and d_{soln}, the densities of solvent and solution, respectively. In our experiment 3% acetone solution in 0.1 M phosphate buffer at pH 7.0 was placed in the annular section of the cell and the identical solution containing the N-H8PT complexes in the order of mM concentration was placed in the inner tube. Fig. 1 shows the NMR spectra of 3% acetone in the presence of fluoride (weak field ligand), N-methionine or imidazole (strong field ligand) complex of the N-H8PT. The heme concentration of each solution was about 1.5 mM. The peak at low field is the acetone resonance from the buffer solution and the small peak at high field with variable

Figure 1. The NMR spectra of acetone in the presence of ferric N-H8PT complexes with imidazole N-methionine or fluoride.

PARAMAGNETIC NMR SHIFTS BY Fe(III)-N-H8PT COMPLEXES

3% Acetone in 0.1M $PO_4^{\equiv}$, pH 7.0, 25°C

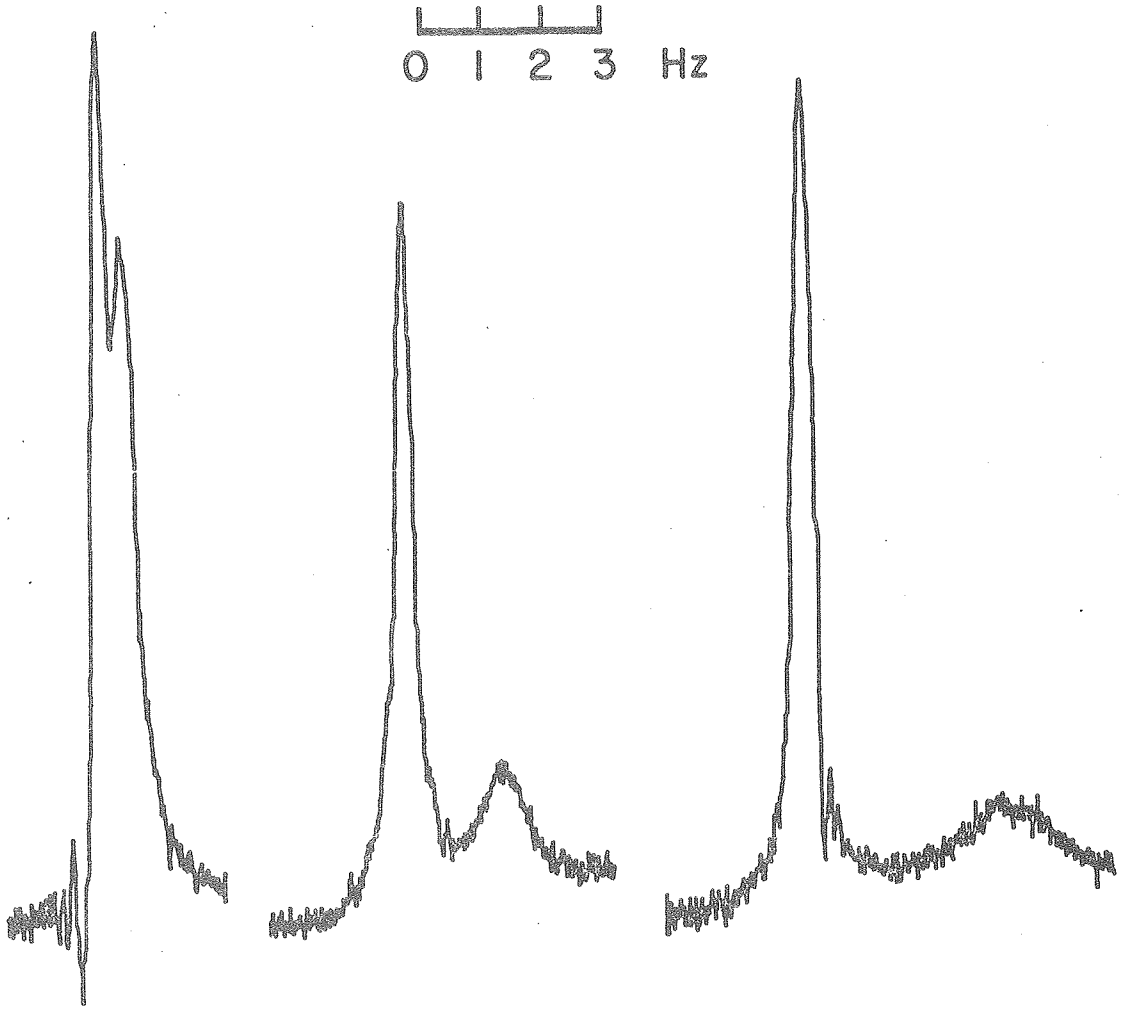

XBL772-4167

signal intensity arises from the sample solution. As can be seen, the magnitude of the frequency shift decreases as a function of ligand field strength. The molar susceptibility, χ_M (Eq. 2), was obtained by multiplication of χ_g by the molecular weight of the heme peptide.

$$\chi_M = \frac{3\Delta f}{2\pi f_o M} \times 10^3 + \chi_o^M \qquad (2)$$

where M is the concentration of the heme peptide in mole$\cdot\ell^{-1}$. The $(d_{solv}-d_{soln})$ term was neglected since only dilute solutions were used. The value of χ_o^M was taken to be the molar susceptibility of water (-13×10^{-6} erg $G^{-2}M^{-1}$). χ_M was then corrected for the diamagnetic contribution of the heme peptide. Diamagnetic susceptibility of a molecule may be written:

$$\chi_{mol}^{dia} = \sum_i n_i\chi_i + \Sigma\varepsilon \qquad (3)$$

where the molecule contains n_i atoms of atomic susceptibility (i.e. per gram atom), χ_i and ε represent "constitutive" corrections which take account of such factors as the existence of π-bonds (26). Much work on this additivity of atomic susceptibilities is due to Pascal, thus the quantities are commonly referred to as Pascal's constants. Using the table given by Selwood (27), the diamagnetic contribution of the N-H8PT was estimated to be -742×10^6 erg $G^{-2}M^{-1}$. The effective magnetic moment, μ_{eff} was obtained by the following relation

$$\mu_{eff}^2 = \frac{3kT}{N\beta^2} \chi_M^{corr} \qquad (4)$$

where β is the Bohr magneton and N, Avogadro's number. Complexes giving rise to intermediate values of μ_{eff} between the high and low spin forms can be analyzed on the basis of thermal equilibrium. At equilibrium

$$\underset{(1-\alpha)}{\text{high spin}} \overset{K}{\rightleftharpoons} \underset{(\alpha)}{\text{low spin}} \qquad (5)$$

where α is a fraction of low spin component (% low spin) and K is the equilibrium constant. μ_{eff} is given by

$$K = \alpha/(1 - \alpha) \qquad (6)$$

$$\mu_{eff} = \alpha\mu_{LS}^2 + (1 - \alpha)\mu_{HS}^2 \qquad (7)$$

where subscripts LS and HS indicate purely low spin and purely high spin states, respectively. α was determined using the values of μ_{LS}^2 and μ_{HS}^2 as 5 and 35 in units of Bohr magneton, respectively. The dependence of μ_{eff}^2 on temperature permits evaluation of ΔH° and ΔS° for a high spin ⇌ low spin transition from the Van't Hoff equation.

$$\ell n\ K = -\frac{\Delta H^\circ}{R}\left(\frac{1}{T}\right) + \frac{\Delta S^\circ}{R} \qquad (8)$$

Nickel chloride ($NiCl_2$) solution which has χ_g of 34×10^{-6} at 20°C was used to calibrate the NMR spectrometer. The concentration of nickel was determined gravimetrically by precipitation with dimethylglyoxime (28). Peak separation between the methyl and hydroxyl proton lines of methanol was

used to monitor the temperature of the probe. The validity of the technique was tested with ferrimyoglobin derivatives. The diamagnetism correction for myoglobin was determined by measuring the frequency shift of the ferrous myoglobin-cyanide complex (s = 0).

Analysis of Thermal Spin Equilibrium

According to the method of analysis derived by Iizuka and Kotani (12), the observed $\Delta H°$ and $\Delta S°$ values for a high spin $\rightleftharpoons$ low spin transition can be explained in terms of the energy difference between the two spin states and of the effective statistical weight factor associated with the transition. If the high and low spin states are populated according to Boltzmann statistics, the fraction of the low spin state, α, is given by

$$\alpha = \frac{\omega_L e^{-E_L/RT}}{\omega_L e^{-E_L/RT} + \omega_H e^{-E_H/RT}} \qquad (9)$$

where E_L and ω_L are the energy and the effective statistical weight for the low spin state, respectively, and E_H and ω_H are the corresponding values for the high spin state. If only the spin degree of freedom is considered, ω_H/ω_L would be 3, because the spin degeneracies $(2s + 1)$ are 6 and 2 for the high and low spin states. In a real molecular system, however, it is important that other degrees of freedom associated with the spin degeneracy change are taken into consideration. Thus, a new parameter γ is introduced such

that $\omega_H/\omega_L = 3\gamma$. If ε is defined as the energy difference between the high and low spin states ($\varepsilon = E_H - E_L$), α and the equilibrium constant, K, are given by

$$\alpha = [1 + 3\gamma e^{-\varepsilon/kT}]^{-1} \tag{10}$$

$$K = \alpha/(1 - \alpha) = (3\gamma)^{-1} e^{\varepsilon/kT} \tag{11}$$

By substituting Eq. (11) into Eq. (7), and assuming that ε and γ are independent of temperature, the following relation is obtained for the enthalpy and entropy terms:

$$\Delta H^\circ = -N\varepsilon \tag{12}$$

$$\Delta S^\circ = -Nk \ln 3\gamma \tag{13}$$

where N is Avogadro's number and k is the Boltzmann constant. Now, if the effective magnetic moment is expressed in terms of ε and γ, by substituting Eq. (10) for Eq. (6),

$$\mu_{eff}^2 = \frac{\mu_L^2 + 3\gamma \cdot e^{\mp\varepsilon/kT} \cdot \mu_H^2}{1 + 3\gamma \cdot e^{\mp\varepsilon/kT}} \tag{14}$$

The - sign of ε/kT corresponds to $\varepsilon > 0$ and the + sign, $\varepsilon < 0$. In the case of $\varepsilon > 0$, the low spin state is the ground state; i.e., μ_{eff}^2 approaches μ_L^2 at the low temperature limit and $\mu_{eff}^2 \simeq \mu_L^2 + 3\gamma \cdot \mu_H^2/(1 + 3\gamma)$, which approaches γ_H^2 at the high temperature limit (if $\gamma << 1$). The temperature at which $\Delta G^\circ = 0$, the characteristic temperature, T_c, may be physically significant, because at $T = T_c$, $\alpha = 1/2$ and $\mu_{eff}^2 = (\mu_L^2 + \mu_H^2)/2$ only if $\varepsilon > 0$ and $\gamma >> 1$ or $\varepsilon < 0$ and $\gamma << 1$.

C. RESULTS

Figure 2 compares the percentage of the low spin state in ferrimyoglobin derivatives as determined by the NMR method with the literature values measured using a Gouy balance or optical method at room temperature (3,5). A straight line with a slope of 1 that intersects at the origin is evidence of good agreement between the two methods. Table I summarizes the effective magnetic moments and estimated % low spin (Eq. 6) of the ferric N-H8PT complexes at pH 7.0, 25.0°C. In general, these results are as predicted by ligand field strength considerations. The fluoride and aquo complexes exhibit slightly reduced magnetic moments compared with those expected from the spin only value for the high spin state, i.e. 5.9 μ_B. However, the reduced value of μ_{eff} for the aquo complex, 5.4 μ_B, is comparable to the reported values for the acid pH H11PT and H8PT, which range from 4.8 to 5.3 μ_B (29). At pH < 3.0, all of the N-terminal amino groups are protonated so that they do not induce aggregation. Nevertheless, the observed magnetic moments of the H11PT and H8PT are smaller than the high spin value. This has been attributed to weak anti-ferromagnetic coupling between the heme centers via π donor-acceptor type interactions (30,31). As has been discussed in Chapter IV, the aquo complex of the N-H8PT at high heme concentration also seems to participate in π donor-acceptor type interactions: the absorption spectral results show that the Soret transition is split, with one of the maxima at the monomer position (Fig. 3A, Chapter IV) which is distinct

Figure 2. The percentage of low spin states for ferrimyoglobin derivatives determined by the NMR method is compared with the literature values (3,5).

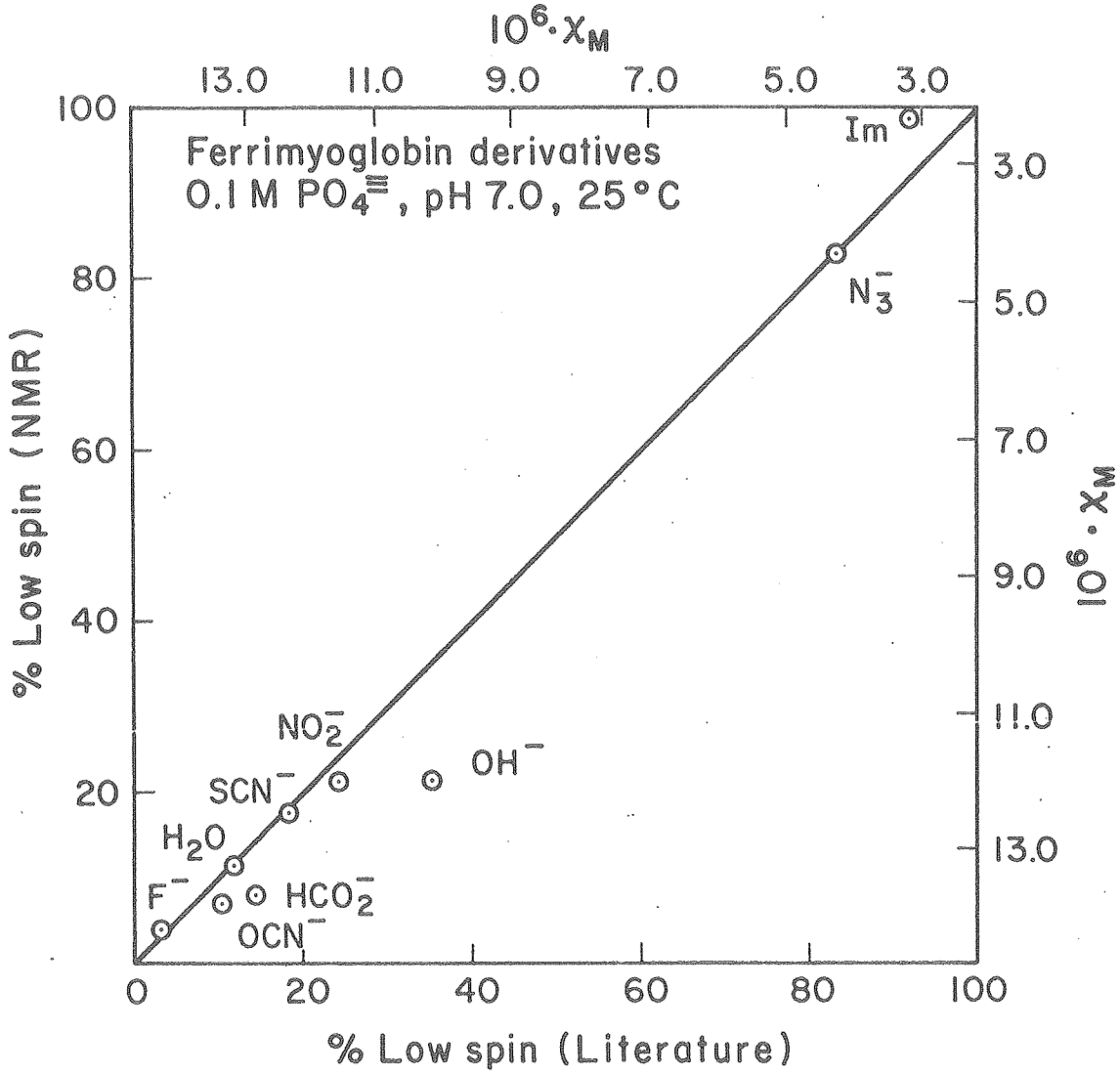
$10^6 \cdot \chi_M$
13.0
11.0
9.0
7.0
5.0
3.0
Ferrimyoglobin derivatives
0.1 M $PO_4^{\equiv}$, pH 7.0, 25°C
Im
N_3^-
NO_2^-
SCN^-
OH^-
H_2O
F^-
HCO_2^-
OCN^-
% Low spin (NMR)
% Low spin (Literature)
0
20
40
60
80
100
$10^6 \cdot \chi_M$

XBL 786-3970

TABLE I

PARAMAGNETIC SUSCEPTIBILITY OF Fe (III) - N-H8PT COMPLEXES MEASURED BY NMR AT 25°C

Ligand	Heme Conc. (mM)	Δf	$\chi_M^{Corr} \times 10^3$	μ_{eff}	% Low Spin
Fluoride	1.84	2.75	12.62	5.48	16
Water	1.85	2.70	12.34	5.42	19
Hydroxide	1.49	1.30	7.67	4.28	56
Azide	2.37	1.30	5.10	3.49	76
N-Methionine	2.11	1.60	6.79	4.02	63
Cyanide	1.82	0.60	3.35	2.83	90
Imidazole	1.72	0.40	2.58	2.48	96
Cytochrome c*	----	----	----	2.30	100

XBL 786 - 4011

from exciton resonance splitting. In fact, the observed magnetic moment is consistent with the view of having weak anti-ferromagnetic coupling. The reduced magnetic moment of the fluoride complex is most likely due to the same effect. The absorption spectrum of the fluoride complex that has been used for the magnetic measurement shows a single Soret peak but its band width is broad and the position is blue shifted to 388 nm. Furthermore, the near IR charge transfer band is also broadened and occurs near 610 nm, which is red shifted by about 5 nm. This suggests that fluoride is not ligated completely, and some of the aquo complex still undergoes π donor-acceptor type interaction.

The N-Met-N-H8PT complex shows μ_{eff} of 4.0 μ_B, much larger than the expected low spin value of native cytochrome c (2.3 μ_B). The temperature dependence of μ^2_{eff} for the N-methionine complex yields a linear relation between ℓn K and 1/T, where K is the equilibrium constant for a high spin (S = 5/2) $\rightleftharpoons$ low spin (S = 1/2) transition (Fig. 3). Corresponding ΔH° and ΔS° values are found to be -8.0 kcal/mole and -25.2 e.u., respectively. However, the analysis of the spectrophotometric titration for N-methionine binding has shown that, at room temperature, 10% of the N-H8PT remains ligand unbound at 2.5 M ligand concentration (Chapter IV). Thus, the observed ΔH° and ΔS° values include thermodynamic contributions from temperature-dependent ligand binding.

Figure 3. A plot of ℓn K versus 1/T for a high spin to low spin transition in the N-methionine complex of N-H8PT as determined by the NMR method.

THERMODYNAMICS OF SPIN TRANSITION IN Fe(III)-N-H8PT-N-METHIONINE COMPLEX

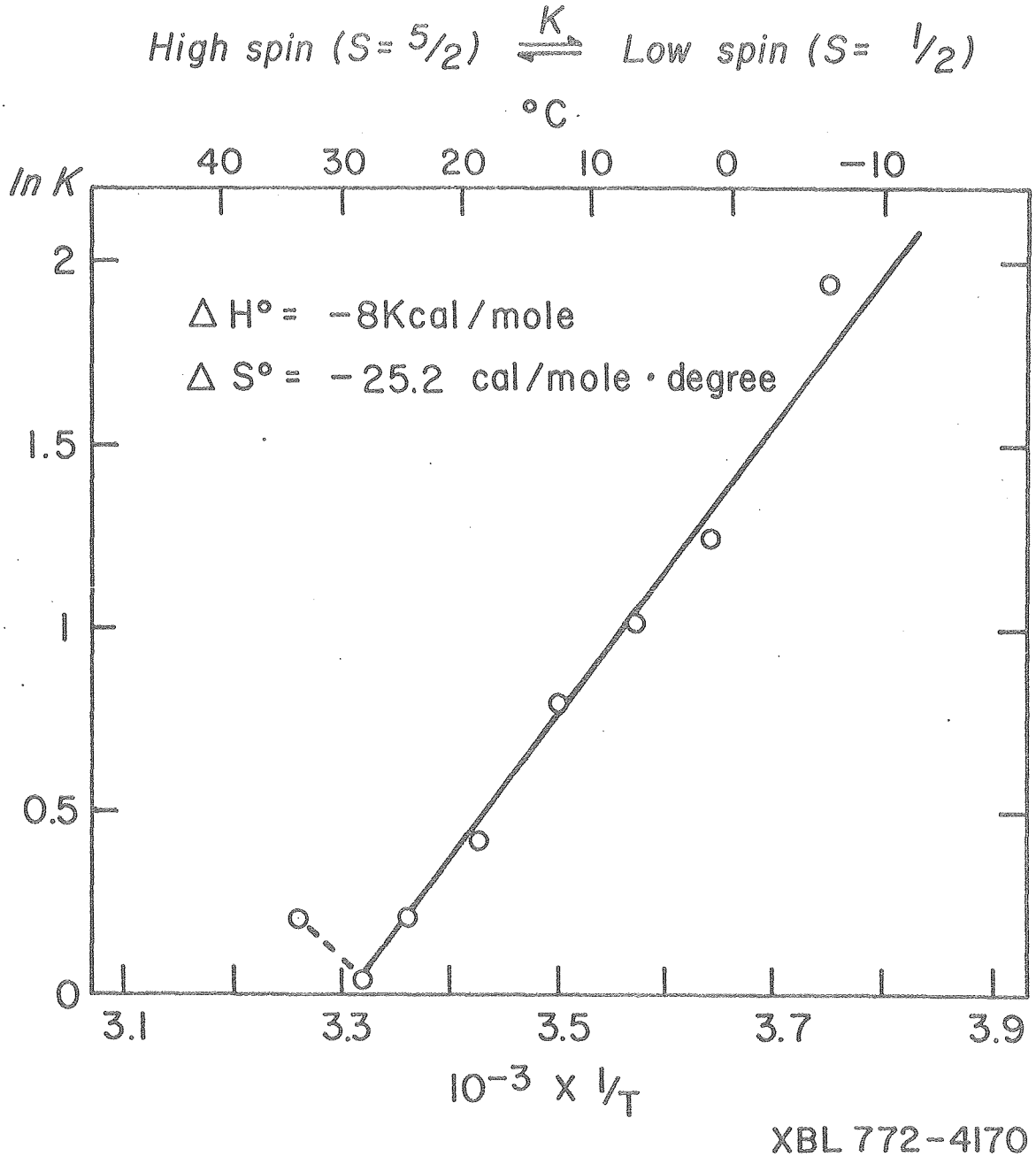

However, this effect is expected to be rather small because the equilibrium quotient for N-methionine binding is a small number (Q = 3.2) and already 90% ligand is bound at 2.5 M N-methionine concentration at room temperature. Fig. 4 shows a plot of ℓn Q versus 1/T where each value of Q is determined from the titration curve at each temperature, as in Fig. 8, Chapter IV. Corresponding ΔH° and ΔS° values are found to be -0.44 kcal/mole and 0.74 e.u. The azide complex of ferrimyoglobin yields ΔH° = -3.75 kcal/mole and ΔS° = -10.7 e.u. as measured by the NMR method (results not shown). These values agree very well with the reported values of ΔH° = -3.75 kcal/mole and ΔS° = -9.6 e.u. confirming the validity of the temperature dependent magnetic measurements by NMR.

Figure 5 shows the approximately linear dependence of the Soret absorption maximum on the percentage of the low spin form of the ferric N-H8PT complexes. Such linearity has been observed in ferrimyoglobin and ferrihemoglobin complexes (32). It can be explained on the basis of the position of iron with respect to the porphyrin plane. The existing x-ray evidence supports the movement of iron out of the heme plane towards the proximal histidine ligand in the high spin ferrimyoglobin complex (33,34). Then, destabilization of the porphyrin π^* orbital due to doming effect of the heme plane may explain the blue shifted Soret transition. If we assume

Figure 4. A plot of ℓn Q versus 1/T where Q, the equilibrium quotient for N-methionine binding, is determined from the titration curve as given in Fig. 8 of Chapter IV.

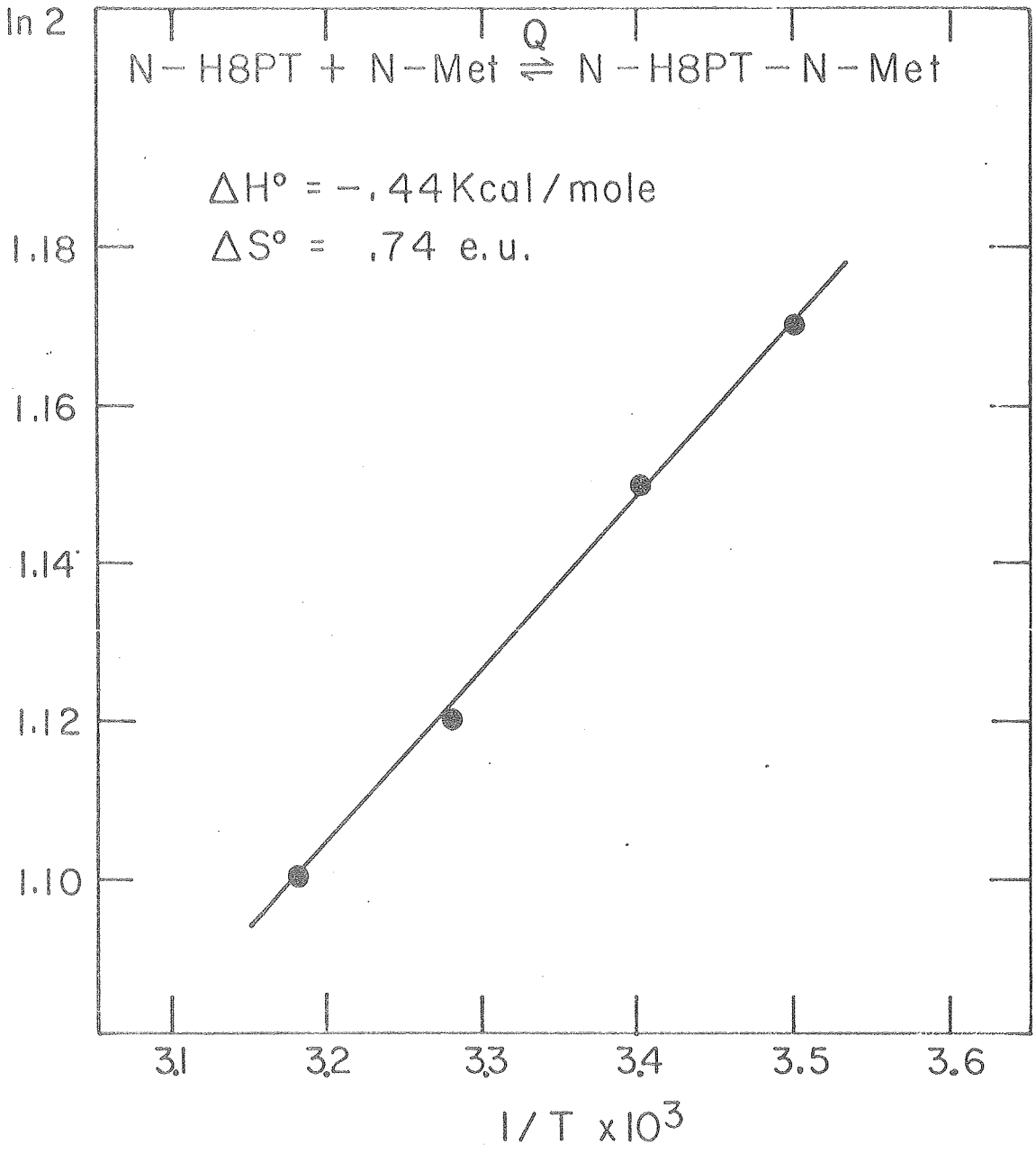
ln 2
N-H8PT + N-Met ⇌ N-H8PT-N-Met
Q
ΔH° = -.44 Kcal/mole
ΔS° = .74 e.u.
1.18
1.16
1.14
1.12
1.10
3.1
3.2
3.3
3.4
3.5
3.6
1/T x10³

XBL 786-4001

Figure 5. A plot of the position of the Soret absorption maximum versus the percent low spin form for various N-H8PT complexes as determined by the NMR method.

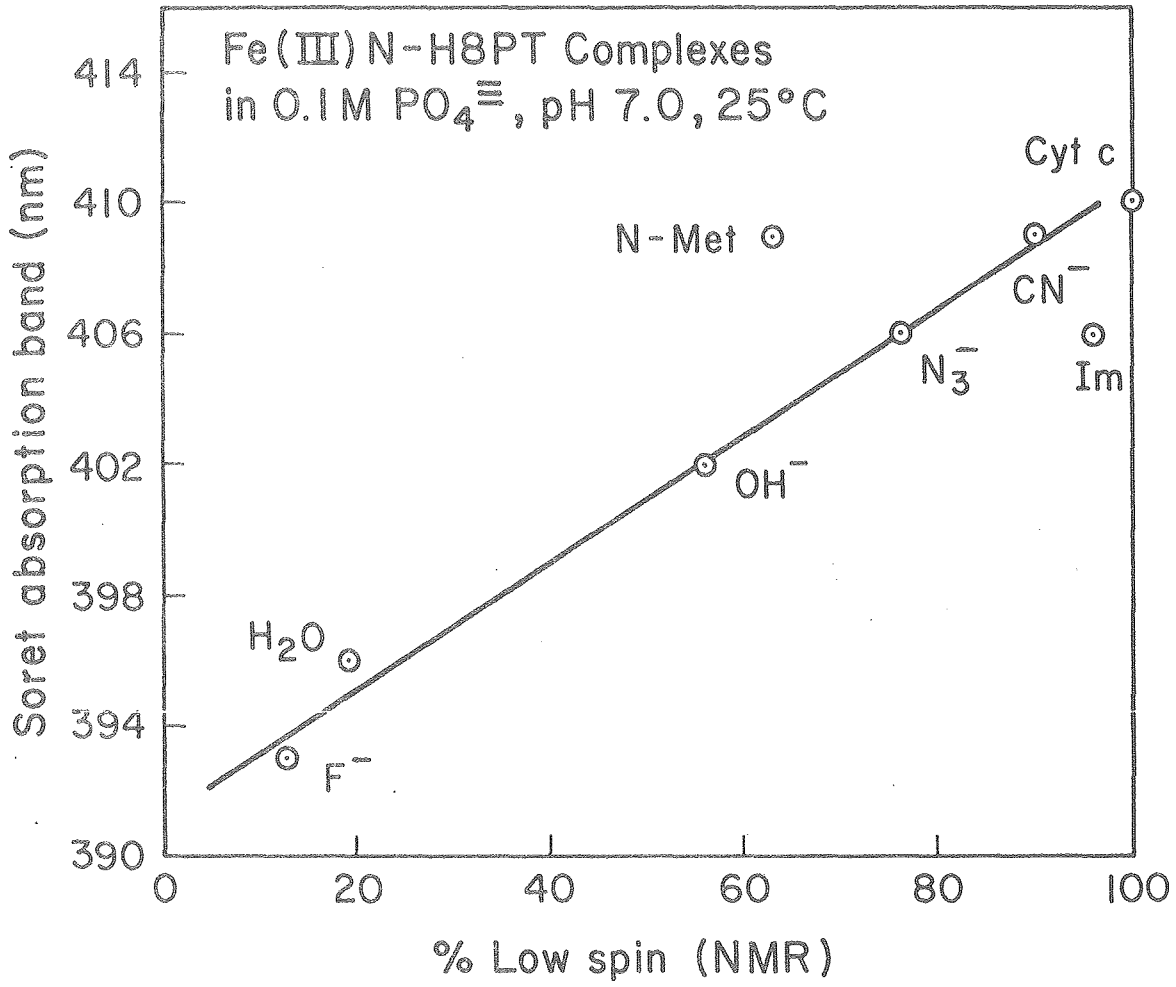
Fe(III) N-H8PT Complexes
in 0.1 M $PO_4^{\equiv}$, pH 7.0, 25°C
Soret absorption band (nm)
414
410
406
402
398
394
390
0
20
40
60
80
100
% Low spin (NMR)
Cyt c
N-Met
CN^-
N_3^-
Im
OH^-
H_2O
F^-

XBL 786-3964

that the Soret band results from direct overlap of pure high and low spin bands, we expect to observe an approximate linear correlation between the position of the Soret transition and % low spin (35). Except for the imidazole and N-methionine complexes, we do observe such a correlation. The intensity of the β band is believed to be low spin in origin (see Chapter II). Williams, et al. (5), have demonstrated that the true β band intensity obtained by curve resolving the spectra into Gaussian bands depends linearly on susceptibility. Even without such extensive treatment, the observed β band intensity of the N-H8PT complexes still exhibits a linear dependence on % low spin (Fig. 6). Deviations are found for the aquo- and N-methionine complexes. Briat, Berger and Leliboux (12, Chap IV have established from the temperature dependent Soret MCD measurement of cytochrome b_2 (down to liquid helium temperature) that the origin of the Soret MCD intensity is predominantly paramagnetic and low spin in nature. This suggests that a linear relation exists between the Soret MCD intensity and % low spin. Fig. 7 shows such linearity even for the model complexes. The hydroxide, azide and N-methionine complexes, however, do not fall on the straight line. Although the reason for this discrepancy is not clear, it is assumed that additional transitions occur in the Soret region of such complexes.

Fig. 8 shows the EPR spectra of the ferric H8PT, N-H8PT, N-Met-N-H8PT complex and cytochrome c at pH 7.0, 15°K. The spectrum of the aggregated ferric H8PT shows both high and low spin signals. The low spin signal exhibits g_z = 3.17,

Figure 6. A plot of the β band intensity at 528 nm versus the percent low spin form for various N-H8PT complexes as determined by the NMR method.

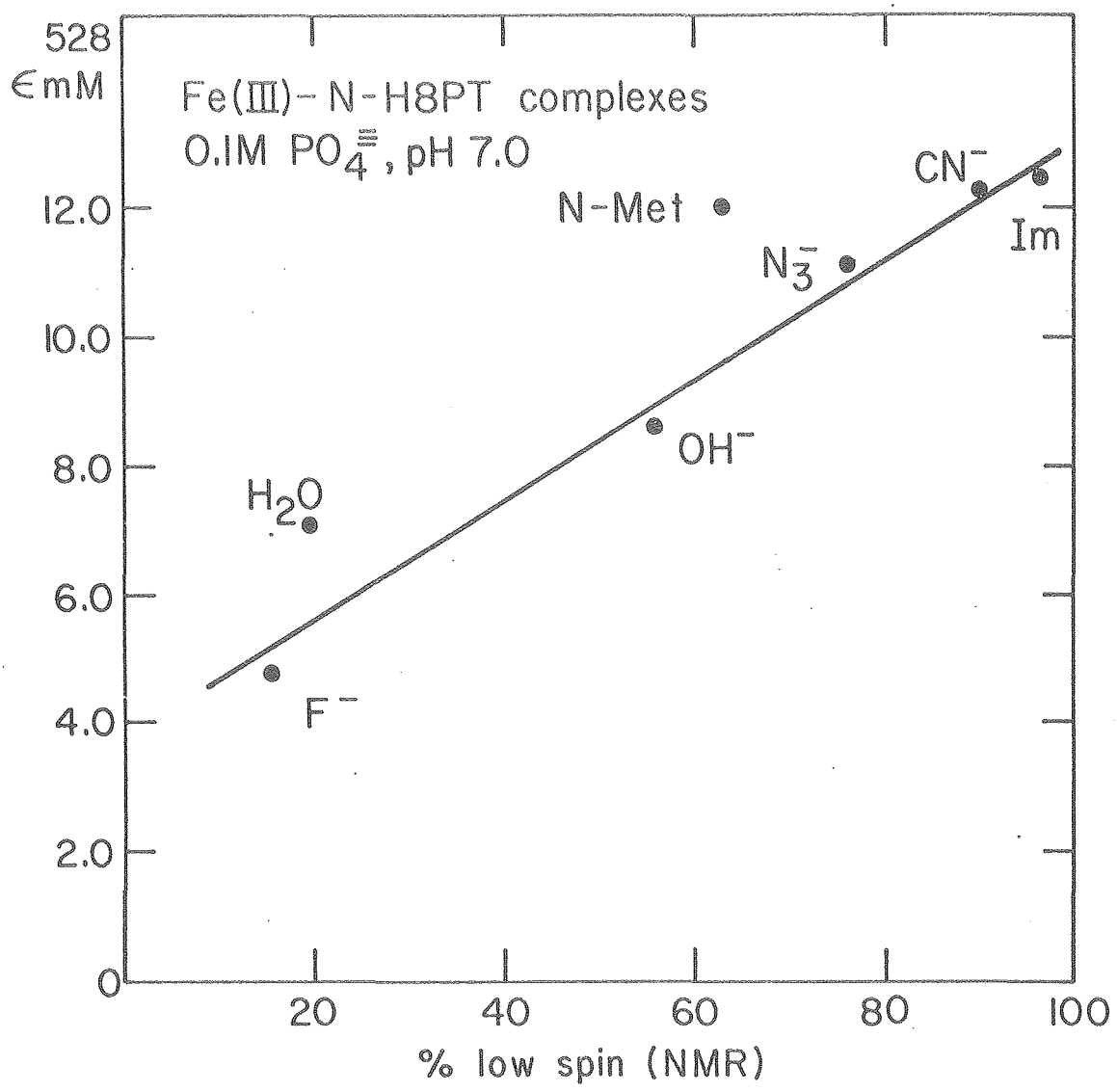
528
∈mM
Fe(III)-N-H8PT complexes
0.1M $PO_4^{\equiv}$, pH 7.0
12.0
10.0
8.0
6.0
4.0
2.0
0
N-Met
CN^-
Im
N_3^-
OH^-
H_2O
F^-
20
40
60
80
100
% low spin (NMR)

XBL 786-4006

Figure 7. A plot of the Soret magnetic circular dichroism trough intensity versus the percent low spin form for various N-H8PT complexes as determined by the NMR method.

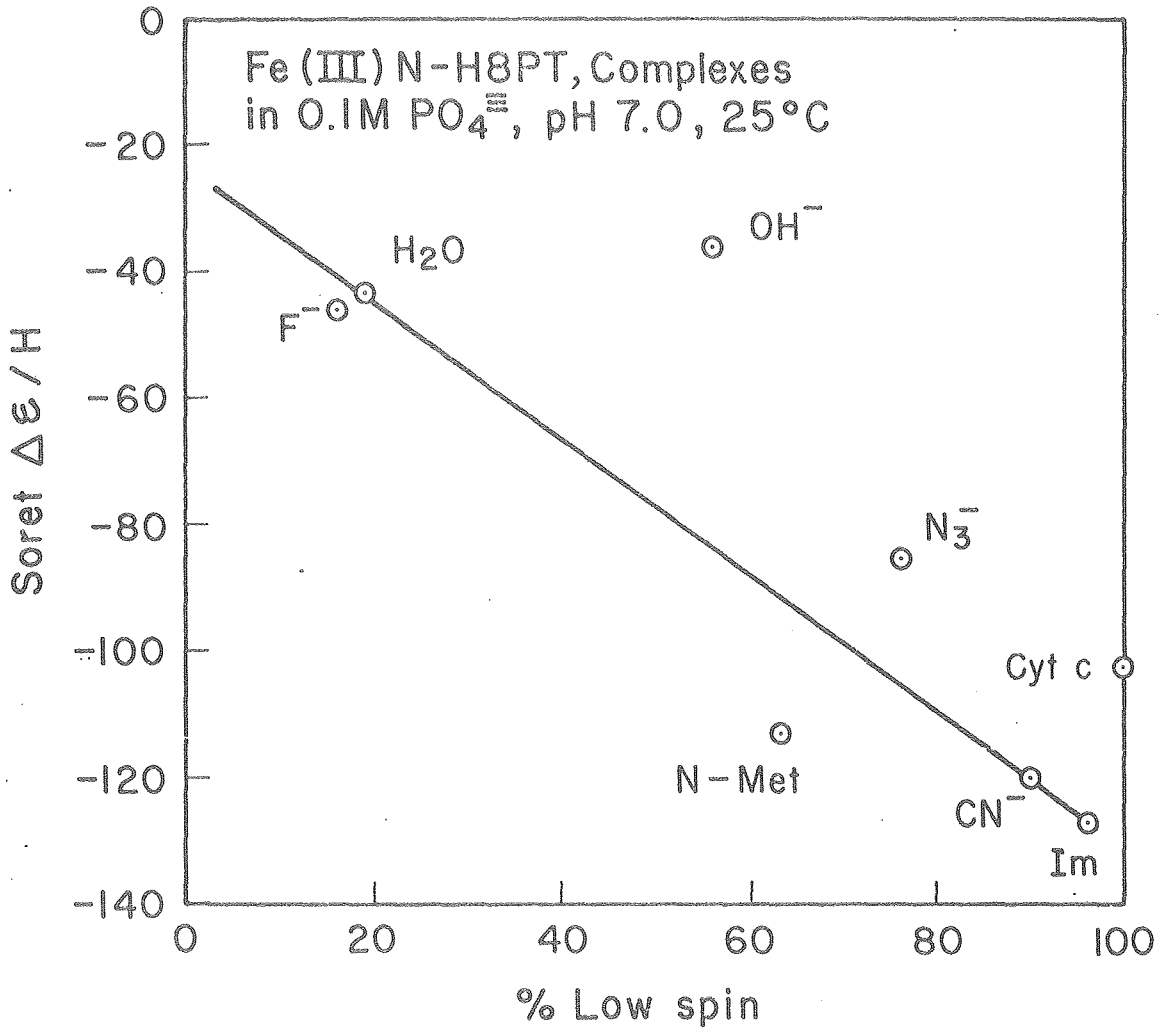
Fe (III) N-H8PT, Complexes
in 0.1M $PO_4^{\equiv}$, pH 7.0, 25°C
Soret Δε/H
% Low spin
0
-20
-40
-60
-80
-100
-120
-140
0
20
40
60
80
100
H_2O
OH^-
F^-
N_3^-
Cyt c
N-Met
CN^-
Im

XBL 786-3962

Figure 8. The electron spin resonance spectra of the aggregated H8PT, N-acetylated H8PT, N-methionine complex of N-H8PT and cytochrome c in a ferric state. Microwave frequency, 9.26 G Hz., Microwave power, 10 mW, modulation frequency, 10 Gauss and temperature, 15°K.

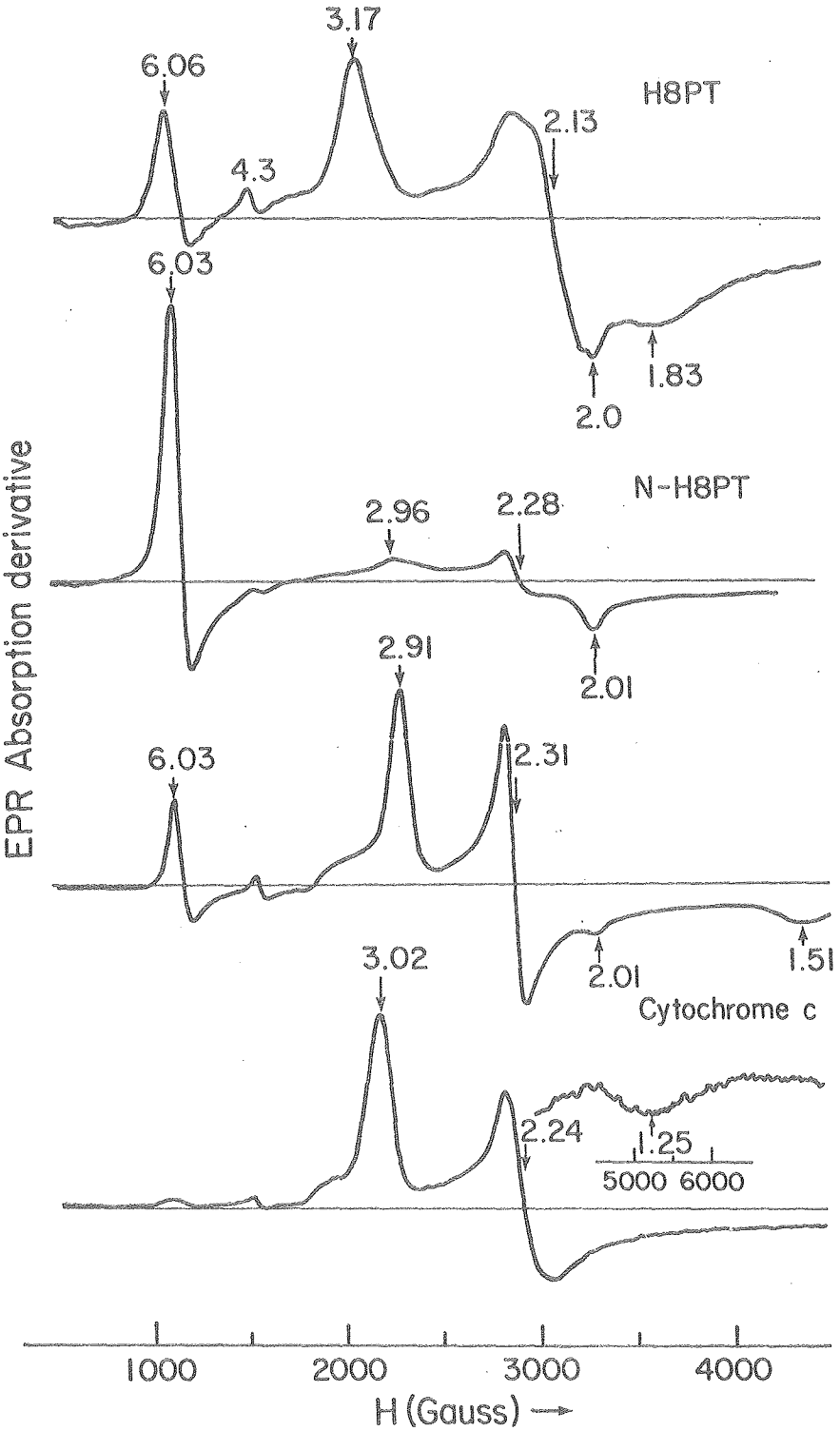
3.17
6.06
H8PT
2.13
4.3
6.03
1.83
2.0
N-H8PT
2.96
2.28
2.91
2.01
6.03
2.31
2.01
1.51
Cytochrome c
3.02
2.24
1.25
5000 6000
EPR Absorption derivative
1000
2000
3000
4000
H (Gauss) →

XBL 786-3968

g_y = 2.13 and g_x = 1.83, and is rather broadened, indicating the presence of multiple low-spin heme components. This is expected because a higher degree of aggregation is known to exist at high heme concentration, as evidenced by the lack of isosbestic and isoelliptic points (Fig. 2, Chapter IV).

The broadened low-spin type spectrum has also been observed with the aggregated ferric H11PT, which exhibits g values at 3.03, 2.16 and 1.46 (36). The aquo complex of the ferric N-H8PT exists in the high spin ground state with $g_\perp$ = 6.03 and $g_\parallel$ = 2.01. There is a small amount of the low spin form with g_z = 2.95 and g_y = 2.32 (g_x not resolved). This is probably the hydroxide complex of the N-H8PT. In fact the N-H8PT at pH 11.5 shows g_z = 2.95, g_y = 2.28 and g_x = 1.93. The slightly reduced magnetic moment of the ferric N-H8PT may, in part, have been due to the hydroxide form. The N-Met-N-H8PT complex exists in the low spin ground state with g_z = 2.91, g_y = 2.31 and g_x = 1.51, which are quite different from the g values of cytochrome c (g_z = 3.03, g_y = 2.24 and g_x = 1.25). The abscence of an apparent $g_\perp$ signal between 4 and 6 clearly excludes the possibility of having the intermediate spin (S = 3/2) or quantum-mixed spin (between S = 5/2 and S = 3/2) ground state (22). However, a minor high spin component with $g_\perp$ = 6.03 coexists at 11°K where thermal population of spins is not possible. The shape of this high spin signal corresponds to a single component, which must be a chemically distinct species from the N-Met-N-H8PT

complex. We believe that it is the ligand-free form of the N-H8PT, because the position of the g_1 signal is identical to that of the aquo complex. Should this be the case, and if we assume that the room temperature ratio of the N-methionine bound to the unbound is independent of temperature, then the high spin component would correspond to about 10% of the total heme concentration (see Chapter IV). We estimate the minor high spin component to be 12% by direct comparison of the doubly integrated area of the g_1 signal using the aquo complex of the N-H8PT of known heme concentration as a standard (results not shown).

D. DISCUSSION

The room temperature magnetic measurements have demonstrated that there is a close correlation between the electronic properties of porphyrin and magnetic properties of iron even in the model complexes. For example, a linear dependence of the Soret band position as a function of % low spin has been shown in Fig. 5. The energy of the Soret transition which reflects the energy level of the porphyrin π^* orbital depends not only on the position of iron with respect to the heme plane but also on the extent of π interaction between the ligand and porphyrin ring. In fact, the N-methionine and imidazole complexes that deviate from linearity contain π ligands; imidazole is a good π donor ligand, while N-methionine is a π acceptor ligand. Furthermore, the specific protein conformation of each heme protein exerts a tension to

constrain the ligand into a certain geometry. In our N-H8PT complexes practically no such steric restriction exists. This may be one of the reasons why the Soret band position of all N-H8PT complexes is blue-shifted compared to corresponding hemoglobin and myoglobin derivatives (6). The different extent of solvation in the N-H8PT complexes may also contribute to the shifted Soret band position. As discussed in Chapter II, the Soret MCD spectra of hemoproteins are extremely useful for the assignment of oxidation and spin state changes independently of each other. In the oxidized state, the Faraday C term which dominates the Soret region arises from spin-orbit interaction of the non-zero spin density of $d\pi$ electrons with porphyrin π orbital motion. If mixing of $d\pi$ with porphyrin π orbitals is considered, the wavefunctions should be the product wavefunctions between the two. Then the Soret transition for the low-spin heme corresponds to $^2E_g \rightarrow {}^2E_u$, while for the high spin heme it is $^6A_{1g} \rightarrow {}^6E_u$. Obviously, spin-orbit interaction is important in the low spin case where the ground state symmetry shows orbital degeneracy. It has been shown by Serber (37) that without spin-orbit coupling the spin magnetic moment alone does not contribute to magnetic optical activity, because after summing over all multiplet components the net effect from the spin magnetic moment vanishes. Because the high spin ground state is orbitally non-degenerate and is split only

by the second order spin-orbit coupling, it would exhibit weak MCD C term effects. The empirical observation for ferrimyoglobin derivatives has shown that the intensity of Soret MCD is directly proportional to % low spin state. Our N-H8PT complexes provide additional evidence in support of this semi-empirical finding (Fig. 7).

The behavior of the N-Met-N-H8PT complex is atypical in every case examined. This reflects the uniqueness of chemical bonding and perhaps the difference in the geometry of the bound N-methionine with respect to the heme plane. How do we account for this in terms of the observed magnetic properties? According to the analysis of the thermal equilibrium of spins given by Iizuka, et al.(12), the enthalpy term (ΔH°) corresponds to the energy difference (ε) between the high and low spin states, while the entropy term (ΔS°) corresponds largely to the change of other degrees of freedom (γ) associated with spin degeneracy change. The observed energy difference is 2638 cm^{-1} for the N-Met-N-H8PT complex. The positive sign is consistent with the low spin ground state but its magnitude is apparently much greater than kT even at room temperature. Table II summarizes the thermodynamic data for ferrimyoglobin, hemoglobin and peroxidase derivatives in the literature (11-13). In fact, most derivatives exhibit energy differences much greater than the room temperature kT ($\simeq$ 200 cm^{-1}). Nevertheless, they all exhibit thermal equilibrium of spins at room temperature.

TABLE II

THERMODYNAMIC PARAMETERS OF THE HIGH SPIN (s = 5/2) LOW SPIN (s = 1/2) TRANSITION FOR Fe(III)-MYOGLOBIN, Fe(III)-HEMOGLOBIN, Fe(III)-PEROXIDASE and Fe(III)-N-H8PT COMPLEXES

COMPLEX	GROUND STATE	ε (cm^{-1})	γ	ΔH^o ($cal \cdot mole^{-1}$)	ΔS^o (e.u.) ($cal \cdot mole^{-1} \cdot degree^{-1}$)	T_c (^oK)
$Mb(Fe^{3+}) \cdot H_2O$	High	-1270	$3.05 \cdot 10^{-3}$	+3640	+9.39	388
$Mb(Fe^{3+}) \cdot OCN^-$	High	-1061	$8.53 \cdot 10^{-4}$	+3034	+11.9	254
$Mb(Fe^{3+}) \cdot N_3^-$ (crystal)	Low	+1280	$5.33 \cdot 10^{1}$	-3660	-10.2	361
$Mb(Fe^{3+}) \cdot N_3^-$	Low	+1310	$4.01 \cdot 10^{1}$	-3740	-9.58	391
$Mb(Fe^{3+}) \cdot Im$	Low	+3783	$4.12 \cdot 10^{6}$	-10820	-32.7	331
$Hb(Fe^{3+}) \cdot H_2O(II)$	Low	+211	0.227	-608	+0.765	---
$Hb(Fe^{3+}) \cdot OCN^-$	Low	+249	0.328	-712	+0.0142	---
$Hb(Fe^{3+}) \cdot OH^-$	Low	+655	4.20	-1886	-5.07	372
$Hb(Fe^{3+}) \cdot N_3^-$	Low	+1770	$3.02 \cdot 10^{2}$	-5094	-13.62	374
$CCP(Fe^{3+}) \cdot H_2O$*	High	-1230	$5.59 \cdot 10^{-4}$	+3510	+12.8	274
$CCP(Fe^{3+}) \cdot OH^-$*	Low	+1830	$2.58 \cdot 10^{4}$	-5220	-22.5	232
N-H8PT·N-Met	Low	+2638	$1.60 \cdot 10^{5}$	-7560	-25.9	292

*CCP, cytochrome c peroxidase.

The data for Fe(III)-myoglobin, Fe(III)-hemoglobin and Fe(III)-peroxidase were taken from Iizuka and Kotani, Iizuka and Kotani, and Iizuka et al., respectively.

XBL 786 - 4010

For this to be true, the entropy term must be very large to compensate for the large enthalpy change. Such a compensation effect has been demonstrated for ferrimyoglobin and hemoglobin derivatives by Iizuka, et al. (13), as shown in Fig. 9. As expected, γ is found to be proportional to ε, such that the characteristic temperature, T_c, at which $\Delta G^\circ = 0$ (i.e., where the ratio of high spin to low spin state is 1) falls near room temperature. Surprisingly, the N-met-N-H8PT complex also exhibits such a compensation effect (Fig. 9). In other words, the transition from the low spin to high spin state is not favored energetically but is favored by the entropy difference. This suggests that the entropic driving force which may be associated with the movement of iron in and out of the heme plane, surface charge effects, conformational rearrangement or solvent interactions is not in the protein conformation but must be an intrinsic property of the electronic structure of the heme. Interestingly, both imidazole and azide complexes of cytochrome c do not exhibit any thermal equilibrium of spins between 20°K and 300°K (38). This leads us to speculate that perhaps the hemeproteins with the low spin ground state, such as cytochromes involved in electron transport, do not exhibit thermal equilibrium of spins; while those with the high spin ground state do, even if the strong field axial ligands are coordinated. The hemes of cytochromes are already hexacoordinated and

Figure 9. A plot of ΔS° versus ΔH° for a high spin to low spin transition for various complexes of ferrimyoglobin and hemoglobin, and the N-methionine complex of N-H8PT.

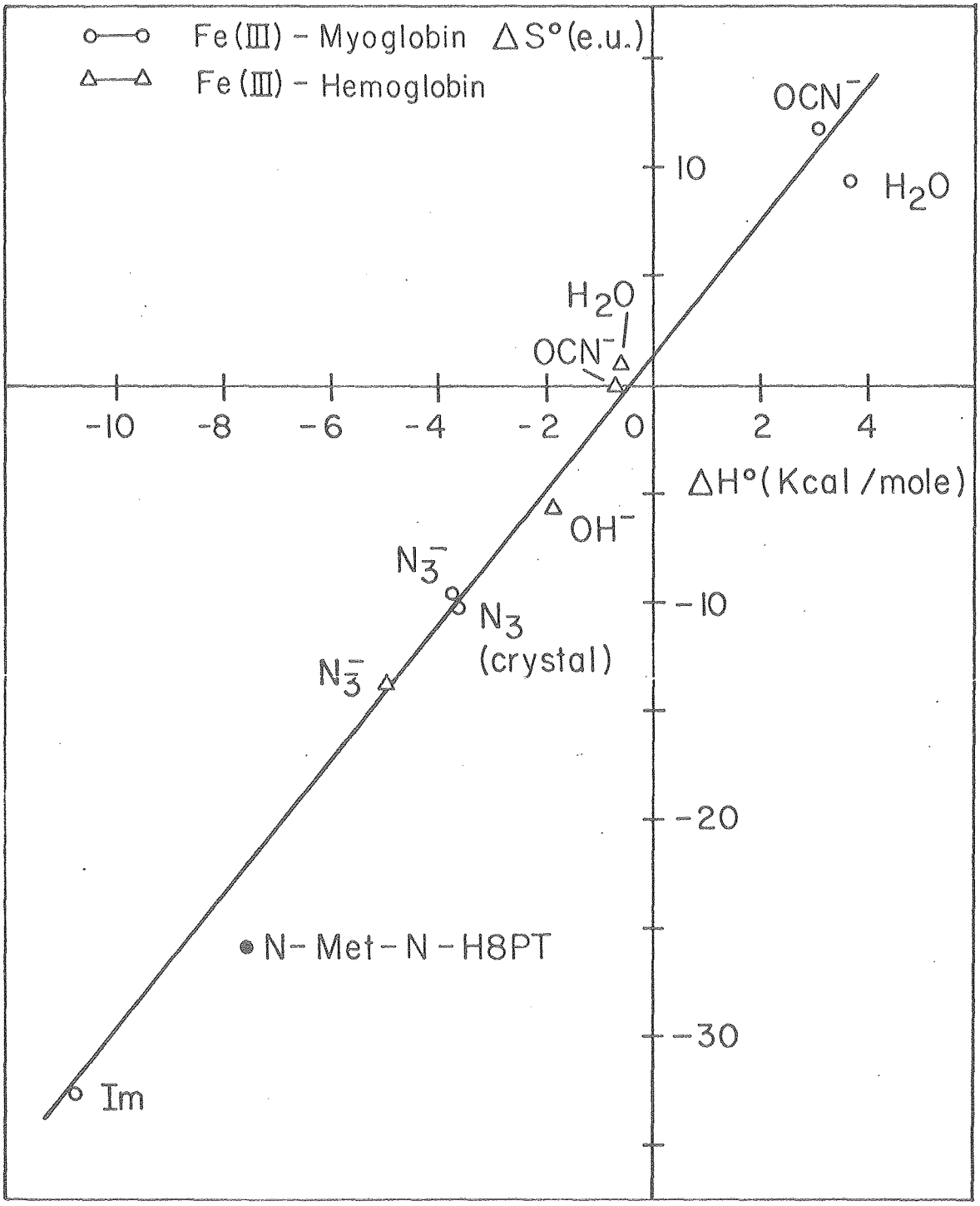
Fe(III) - Myoglobin ΔS°(e.u.)
Fe(III) - Hemoglobin
OCN⁻
H₂O
H₂O
OCN⁻
-10
-8
-6
-4
-2
0
2
4
ΔH°(Kcal/mole)
10
-10
-20
-30
OH⁻
N₃⁻
N₃
(crystal)
N₃⁻
N-Met-N-H8PT
Im

XBL 786-4002

exist in such a stable state that they may not want to lose the ligand to undergo a spin state change. This may be true because the physiological function of cytochromes do not require axial ligand substitution, but transfer electrons by changing the redox state of iron. On the other hand hemeproteins with a high spin ground state, such as hemoglobin, myoglobin, peroxidase and cytochrome a_3, all require O_2 binding and subsequent spin state change to trigger the catalytic reactions. Cytochrome P450 is an exception. Although cytochrome P450 also requires O_2 binding for its catalytic reaction, the resting enzyme is found to be in the low spin state. However, it does undergo spin state change upon substrate binding by some unknown mechanism (34-41). O_2 binding is believed to follow the substrate binding step, which is consistent with our thermodynamic point of view (42,43). In this regard it seems reasonable to assume that the hemes with a high spin ground state have an intrinsic ability to compensate for the large energy involved in the spin state change accompanied by ligand binding. Indeed, such a mechanism is a desirable one, because then only a small free energy change is necessary for ligand binding on and off at physiological temperature.

The uniqueness of the N-Met-N-H8PT complex has also been observed in the low temperature EPR spectrum. It exhibits a very different anisotropy of g values from that of native cytochrome c. The EPR spectrum of low spin hemes

arises from the lowest Kramers doublet (^2E_g), as indicated in Fig. 12, Chapter II. Although the ground state is no longer orbitally degenerate, due to axial and rhombic crystal fields, it still contains the residual orbital magnetic moment due to mixing of the upper Kramers doublet states via spin-orbit interaction. It is this spin-orbit interaction which induces anisotropy of g tensors. By examining the ground state wave-function, which is a linear combination of the three states in $^2T_{2g}$ (Fig. 12, Chapter II) one can actually calculate the energy separations within the $^2T_{2g}$ set (15). Taylor (19) has carried out extensive calculations on this using spin-orbit coupling constant (λ), axial (Δ) and rhombic (V) distortion parameters. He has found that the axial splitting, Δ/λ, corresponds to $B - (A/2)$, and the rhombic, V/λ, to A where A is defined as $g_x/(g_z+g_y) + g_y/(g_z-g_x)$ and $B = g_x/(g_z+g_y) + g_z/(g_y-g_x)$. If λ is assumed to be 400 cm^{-1}, the values of Δ and V correspond to 1020 cm^{-1} and 600 cm^{-1}, respectively in the case of cytochrome c. This is somewhat different from the reported values by Blumberg (16). Interestingly, the axial distortion is much greater in the N-Met-N-H8PT complex (1200 cm^{-1}) than in cytochrome c (Fig. 10). The extent of rhombicity which is defined as the ratio of rhombic to axial distortion, V/Δ, is also different between the two. While the axial distortion reflects the crystal field strength determined by the electron density at the iron, the rhombic distortion reflects the geometry of the bound ligand with respect to the heme plane; i.e., the extent of π interaction between the ligand and heme. In view of this, we propose a model involving a change of

Figure 10. The energy splittings of the axial and rhombic distortions in the $^2T_{2g}$ set for cytochrome c and the N-methionine complex of N-H8PT.

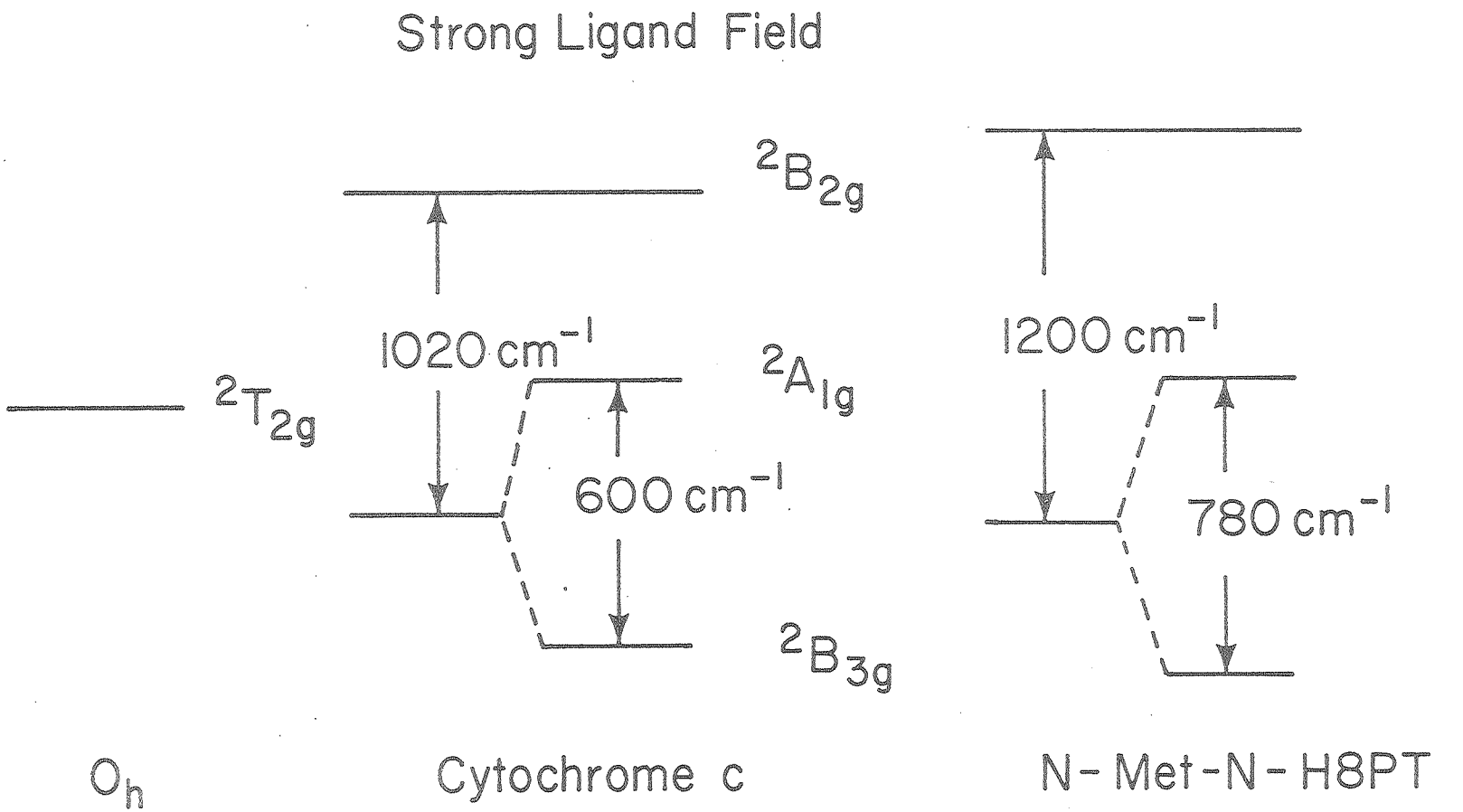
Strong Ligand Field
$^2B_{2g}$
1020 cm^{-1}
$^2A_{1g}$
$^2T_{2g}$
600 cm^{-1}
$^2B_{3g}$
1200 cm^{-1}
780 cm^{-1}
O_h
Cytochrome c
N-Met-N-H8PT

XBL787-4072

Fe-S distance in the N-Met-N-H8PT complex. The greater axial distortion indicates stronger orbital overlap between the axial ligands and the iron. If we assume that the Fe-N distance remains constant, then shortening the Fe-S bond length would certainly account for the observed effect. The change in axial chemical bonding is closely correlated with the redox properties of hemeproteins. If there is a stronger orbital overlap, the ferric form will become more stabilized because of greater electron density at the iron. This may result in a shift of the mid-point reduction potential, E_m, to a lower value. Indeed, the E_m of horse heart cytochrome c is + 250 mV while that of N-Met-N-H8PT complex is - 50 mV (44). Thus, we believe that with a given spin state and axial coordination, one of the ways of controlling a wide variation of mid-point potential is through the change in the extent of orbital overlap between the axial ligands and iron and in the geometry of the bound axial ligands. Our model is consistent with the view proposed by R.J.P. Williams (45) that an approximate 0.1 Å shortening of the Fe-S bond would correspond to a decrease in redox potential of approximately 400 mV. This is evidenced by the NMR chemical shifts of the axial ligand resonances arising from ring current shifts of the heme group.

REFERENCES

1. A.S. Brill and R.J.P. Williams. Biochem. J. 78, 246 (1961).

2. M. Kotani. Adv. Chem. Phys., VII, 159 (1964). J. Duchesne, ed.

3. J. Beetlestone and P. George. Biochemistry 3, 707 (1964).

4. P. George, J. Beetlestone and J.S. Griffith. Rev. of Mod. Phys. p.441 (1964).

5. P.W. Smith and R.J.P. Williams. Biochem. J. 110, 297 (1968).

6. D.W. Smith and R.J.P. Williams. Structure and Bonding 7, 1 (1970).

7. L. Vickery. Proceedings of the First Taniguchi International Symposium on Biophysics, Katada, Japan, 1975.

8. J. Treu and J.J. Hopfield. J. Chem. Phys. 63, 613 (1975).

9. H. Kobayashi. Adv. Biophys. 8, 191 (1975).

10. M.A. Livshitz, A.M. Arutyunyan and Y.A. Sharonov. J. Chem. Phys. 64, 1276 (1976).

11. T. Iizuka, M. Kotani and T. Yonetani. Biochim. Biophys. Acta 167, 257 (1968).

12. T. Iizuka and M. Kotani. Biochim. Biophys. Acta 181, 275 (1969).

13. T. Iizuka and M. Kotani. Biochim. Biophys. Acta 194, 351 (1969).

14. T. Iizuka and T. Yonetani. Advan. Biophys. 1, 157 (1970).

15. G.M. Harris Loew. Biophys. J. 10, 196 (1970).

16. W.E. Blumberg and J. Peisach, "Probes of Enzymes and Hemoproteins", Vol. II, p. 215, in "Probes of Structure and Function of Macromolecules and Membranes", (B. Chance, T. Yonetani and A.S. Mildvan Eds.) Academic Press, New York. (1971).

17. J. Peisach, W.E. Blumberg. ibid, p. 231 (1971).

18. T.L. Bohan, J. of Mag. Res. 26, 109 (1977).

19. C.P.S. Taylor. Biochim. Biophys. Acta 491, 137 (1977).

20. M.M. Meltempo, T.H. Moss and M.A. Cusanovich. Biochim. Biophys. Acta 342, 290 (1974).

21. M.M. Meltempo. J. Chem. Phys. 61, 2540 (1974).

22. M.M. Meltempo and T.H. Moss. Quarterly Reviews of Biophysics 9, 181 (1976).

23. D.F. Evans. J. Chem. Soc. p. 2003 (1959).

24. J.L. Deutsch and S.M. Poling. J. Chem. Educ. 46, 167 (1969).

25. K.D. Bartle, B.J. Dale, D.W. Jones and S. Maricic. Biochem. Educ. 3, 48 (1975).

26. F.E. Mabbs and D.J. Machin. P. 4, "Magnetism and Transition Metal Complexes", Chapman and Hall, London, 1973.

27. P.W. Selwood. p. 91 "Magnetochemistry", Interscience Publishers, 1956.

28. A.I. Vogel. "A Textbook of Quantitative Inorganic Analysis, including Elementary Instrumental Analysis" p. 479, Wiley, New York, 1961.

29. A.M.T. Jehanli, D.A. Stotter and M.T. Wilson. Eur. J. Biochem. 71, 613 (1976).

30. H.J. Schugar, G.R. Rossman and H.B. Gray. J. Am. Chem. Soc. 91, 4564 (1969).

31. H. Goff and L.O. Morgan. Inorganic Chemistry 15, 2062 (1976).

32. G. Schoffa. Adv. Chem. Phys. VII, p. 182 (1964).

33. D.F. Koenig. Acta Crystallogr. 18, 663 (1965).

34. M.F. Perutz. Nature, Lond. 228, 726 (1970).

35. W. Scheler, G. Schoffa and F. Jung. Biochem. Z. 229, 232 (1957).

36. D.V. DerVartanian. Biochem. Biophys. Res. Comm. 41, 932 (1970).

37. R. Serber. Phys. Rev. 41, 489 (1932).

38. M. Ikeda-Saito and T. Iizuka. Biochim. Biophys. Acta 393, 335 (1975).

40. T. Sugiyama, R. Miura and T. Yamano. "Iron and Copper Proteins" (K.T. Yasunobu, H.F. Mower and O. Hayaishi, eds.) Plenum Press, New York. p.290 (1976).

41. M. Katagiri, O. Takikawa, H. Sato and K. Suhara. Biochem. Biophys. Res. Commun. 77, 804 (1977).

42. J.D. Lambeth, D.R. McCaslin and H. Kamin. J. Biol. Chem. 251, 7545 (1976).

43. R.W. Estabrook, A.G. Hildebrandt, J. Barron, K.J. Netter and K. Leibman. Biochem. Biophys. Res. Commun. 42, 132 (1971).

44. H.A. Harbury, J.R. Cronin, M.W. Fanger, T.P. Hettinger, A.J. Murphy, Y.P. Myer and S.N. Vinogradov. Proc. Natl. Acad. Sci. US 54, 1658 (1965).

45. R.J.P. Williams. FEBS Letters 79, 229 (1977).